(18)

EXPERIMENTAL AND ANALYTICAL STUDIES OF TRANSIENT DISTORTION OF WELDS

by

Eko Kuswantoro

B.Sc. in Mechanical Engineering, Northeastern University
Boston, 1993

SUBMITTED TO THE DEPARTMENT OF OCEAN ENGINEERING IN PARTIAL FULFILLMENT OF THE REQUIREMENTS FOR THE DEGREE

OF

MASTER OF SCIENCE IN OCEAN ENGINEERING

at the
MASSACHUSETTS INSTITUTE OF TECHNOLOGY
June 1995

Signature of Author _____
Department of Ocean Engineering
June 1995

Certified by _____
Koichi Masubuchi
Thesis Supervisor

Accepted by _____
Douglas A. Carmichael
Chairman, Committee for Graduate Studies

EXPERIMENTAL AND ANALYTICAL STUDIES OF TRANSIENT DISTORTION OF WELDS

by

Eko Kuswantoro

Submitted to the Department of Ocean Engineering in June 1995 in partial fulfillment of the requirements for the degree of Master of Science in Ocean Engineering.

Abstract

Due to non-uniform heating, weldment distorts. The distortion starts as soon as the welding starts and continues through cooling. At the end, the distortion remains in the weldment. In general, the transient metal movement during the welding is very different from that during the cooling period.

This thesis is written to present results of experimental and analytical studies on transient distortion behaviors of several types of weldments during welding and subsequent cooling.

In the experimental study, several high frequency laser sensors were used with a data acquisition system to measure and record transient vertical movement at several points on the surfaces of the weldments. Results of the experimental study have been obtained successfully.

In the analytical study, a finite element method developed by ADINA, Inc. was used to simulate the welding of the weldments. In particular, ADINA-T was used to calculate the transient temperature changes of the weldments, and ADINA was used to calculate the transient vertical movement of the weldments. Then, ADINA-PLOT was used to post-process all the results calculated in ADINA-T and ADINA. Results of the analytical study also have been obtained successfully.

To verify the accuracy of the finite element method, the results from ADINA-PLOT were compared with the experimental results. Good agreements have been obtained.

Last but not the least, summary and discussion of the results of the study are presented.

Thesis supervisor: Koichi Masubuchi
Title: Kawasaki Professor of Engineering

Acknowledgment

I would like to express my sincere gratitude to Prof. Masubuchi for his supervision and support during the course of this research.

Also, I need to say special thanks to Mr. Umekuni for his invaluable involvement and help. The same quality of special thanks goes to Mr. Zona for his expertise and generous help in welding the specimens.

To all my friends in the Welding System Group, including Mr. Yamamoto, Mr. Hsiao, Mr. Shimizu, Mr. Liang, Ms. Atmadja, and Ms. Middaugh, I really thank for their warm friendships.

Finally, my most special thanks goes to my Mom and Dad who have been very supportive during my study at MIT. With their prayers every night, I have been able to successfully finish my graduate study on time.

Table of Content

Abstract....(2)
Acknowledgment....(3)
Table of Content....(4)
1. Introduction....(6)
1.1. Distortion Types....(8)
1.2. Distributions of Stress and Temperature during Welding....(9)
1.3. Transient Distortion during and after Welding....(11)
1.4. Method of Reducing Distortion Due to Butt Welding....(12)
1.5. Approaches....(13)
1.6. Objectives of the Thesis....(14)
1.7. Outline of the Thesis....(15)
2. Experimental Approach....(16)
2.1. Experimental Equipments....(16)
2.1.1. GTA Welding Machine....(16)
2.1.2. Laser Sensors and Data Acquisition System....(17)
2.2. Specimens....(19)
2.2.1. Dimensions....(19)
2.3. Locations of Measurement Points....(24)
2.3.1. Locations of Measurement Points for Specimen 1....(24)
2.3.2. Locations of Measurement Points for Specimen 2....(26)
2.3.3. Locations of Measurement Points for Specimen 3, 4, 5, 6....(27)
2.3.4. Locations of Measurement Points for Specimen 7....(28)
2.4. Experimental Results....(30)
2.4.1. Experimental Results of Specimen 1....(30)
2.4.2. Experimental Results of Specimen 2....(36)
2.4.3. Experimental Results of Specimens 3 through 6....(40)
2.4.4. Experimental Results of Specimen 7....(42)
3. Analytical Approach....(44)

3.1. ADINA-T Analysis.....(44)
3.1.1. Mesh Design.....(45)
3.1.2. Specimens with Slits Vs Specimens without Slits.....(51)
3.1.3. Welding Arc Heat Input Distribution.....(52)
3.1.4. Initial Conditions.....(55)
3.1.5. General Heat Transfer Formulas.....(55)
3.1.6. Heat Conduction.....(58)
3.1.7. Boundary Conditions.....(60)
3.2. ADINA-T Results.....(61)
3.3. ADINA Analysis.....(76)
3.3.1. Mesh.....(76)
3.3.2. Initial Conditions.....(77)
3.3.3. Boundary Conditions.....(77)
3.3.4. Load.....(78)
3.3.5. Material Properties.....(78)
3.4. ADINA Results.....(81)
4. Comparisons between Experimental and Analytical Results.....(104)
5. Summary and Discussion of Results.....(113)
6. References.....(117)

Chapter 1

Introduction

Today, many structures are fabricated using welding technologies. The structures range from large ones such as ships, rockets, etc. to small ones such as minute radio and television components. Welded structures have several advantages compared to riveted structures. According to Masubuchi [14], the advantages are as follows:

1. High joint efficiency.

   The joint efficiency, which is defined as a ratio between fracture strength of a joint and fracture strength of the base plate, of a sound butt weld can be as high as 100%. For a riveted joint, it is very difficult to achieve 100% efficiency.

2. Water and air tightness.

   This is one of many reasons why submarines and other marine structures employ welding in their fabrications.

3. Weight reduction.

   By using welding, weight of a hull structure can be reduced up to 20%.

4. No limit on thickness.

5. Reduction in fabrication cost and time.

   By pre-fabricating in a plant and assembling later on a site, fabrication time and cost of a welded structure are reduced significantly.

Nevertheless, since nothing is perfect, welding also has several disadvantages. The disadvantages are as follows:

1. Difficulty in arresting a crack.

   It is very difficult to stop a crack that is already propagating in a welded joint. In a riveted joint, the crack propagation will stop at the end of plate. Riveting has been used as a mean to stop or prevent cracks in these cases.

2. Many weld defects.

The welding process can produce many serious defects, including porosity, slag inclusion, and cracks.

3. Limited to certain materials.

   Some materials are very difficult to weld, including aluminum and high strength steel. If they are welded, there will be weld defects in them.

4. Residual stress and distortion.

   Due to local heat input of welding arc, welding can create residual stress and distortion. This residual stresses may equal the yield stress and the distortion can result in a mismatch in the welded structure.

In terms of residual stress and distortion, there have been many studies conducted to understand and control the creation of residual stress and distortion. According to Masubuchi [14], study on the subjects has been ongoing since 1930's. Around 1940's, Naka pioneered the study of weld shrinkage in Japan. His work included both experimental and analytical studies. He simplified a mathematical model of welding into a one dimensional problem.

To date, most of the studies have dealt only with final values of the stresses and distortion. The final values of the stresses and distortion are the stresses and distortion that remain in the welded structure after cooling process has completed.

However, the stress and distortion start to build up as soon as the welding starts. As soon as the welding starts, there is non-uniform temperature distribution in the welded structure. In turn, the non-uniform temperature distribution creates an incompatible strain distribution in the welded structure. Finally, the incompatible strain distribution leads to the thermal stress and distortion in the welded structure. In addition, the distortion during the welding tends to be totally different from the distortion during the cooling. For example, during bead on edge welding of a rectangular plate, the plate bends downward. After the welding, i.e. during cooling, the plate bends upward. To fully understand how residual stress and distortion occur due to welding, it is important to closely and sequentially study the welding and cooling processes.

1.1. Distortion Types

According to Masubuchi [14], there are various types of distortion due to the welding. They are as follows:

a. Transverse shrinkage.
   Shrinkage that is perpendicular to the weld line.
b. Angular change (transverse distortion).
   This type of distortion occurs close to the weld line and is caused by non uniform temperature distribution in the thickness direction.
c. Rotational distortion.
   Angular distortion that occurs in the plane of the plate due to thermal expansion.
d. Longitudinal shrinkage.
   Shrinkage that is parallel to the weld line.
e. Longitudinal bending distortion.
   Distortion that is in the plane along the weld line and perpendicular to the plate.
f. Buckling distortion.
   Instability that occurs in a thin plate due to thermal compressive stress.

Shown in Figure 1.1 are the various types of distortion described above.

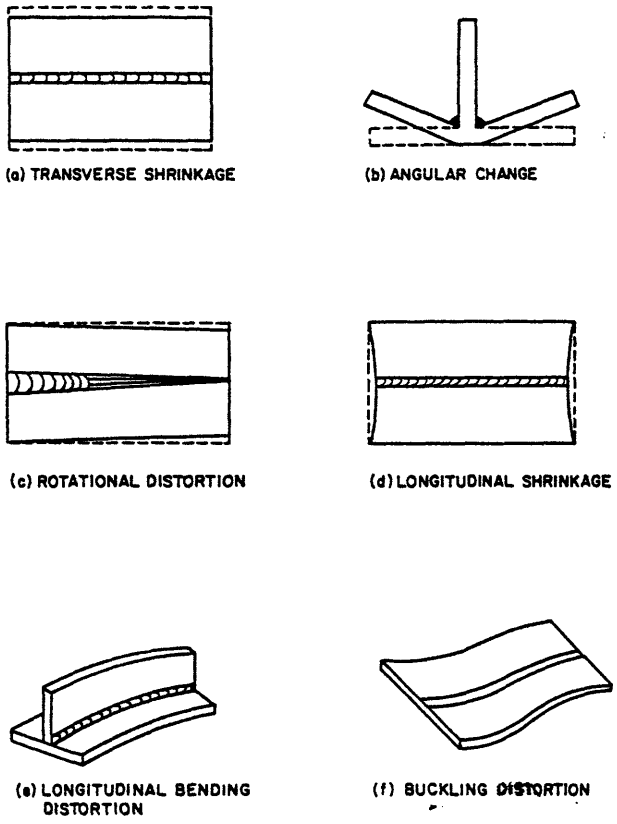

Figure 1.1. Various types of distortion

1.2. Distributions of Stress and Temperature during Welding

Shown in Figure 1.2 are bead-on-plate welding together with distributions of stress and temperature at several cross sections of the plate. The welding arc is currently located at point O.

As shown in Figure 1.2b, at the A-A cross section, which is ahead of the welding arc, the temperature is zero. At the B-B cross section, which crosses the welding arc, the temperature distribution is very steep. At the C-C cross section, which is behind the welding arc, the temperature distribution is less steep. Finally, at the D-D cross section, which is relatively far behind the welding arc, the temperature is zero again.

As shown in Figure 1.2c, at the A-A cross section, the thermal stress in the x direction, σ_x, is zero. At the B-B cross section, the thermal stress right

underneath the welding arc is zero because the molten metal does not support any load. Meanwhile, the expansion of the region near the molten metal is constrained by the surrounding lower temperature region creating a compressive thermal stress that can be as high as the yield stress. To balance this thermal stress, the thermal stress in the region far from the molten metal must be tensile. At the C-C cross section, the thermal stress near the weld line is tensile because the region cools down and shrinks. As the distance from the weld line increases, the thermal stress becomes compressive and then tensile again. At the D-D cross section, the thermal stress at the weld line is tensile, while far from the weld line, the thermal stress is compressive. The thermal stress as shown at the D-D cross section is a typical residual stress distribution.

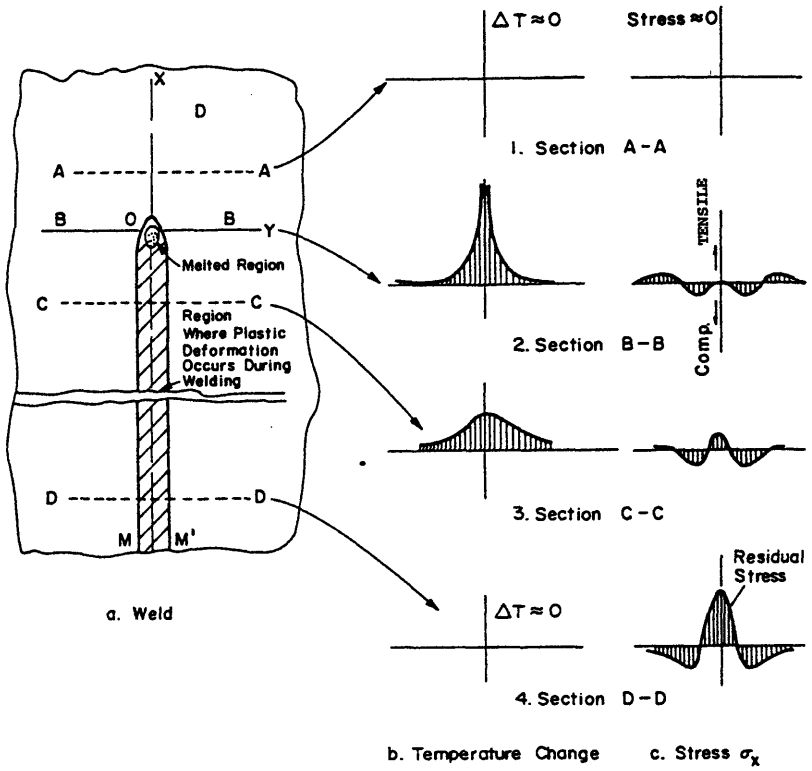

Figure 1.2. Bead on Plate Welding and Distribution of Stress and Temperature

1.3. Transient Distortion During And After Welding

Shown in Figure 1.3 is transient distortion behavior of bead on edge welding on a rectangular plate. During the welding, the upper part of the plate reaches a much higher temperature than the lower part of the plate. As a consequence, the upper part of the plate expands more than the lower part of the plate. Thus, an incompatible strain distribution is created in the plate. This condition causes the plate to bend downward as shown in the upper left corner of Figure 1.3.

After the welding is completed, the cooling process starts. During cooling, the upper part of the plate shrinks, bending the plate upward. If the material of the plate behaves elastically during the distortion, the plate will bend upward until it reaches its original straight shape as shown in curve B'. If the material of the plate behaves non-elastically during the welding, the plate will bend upward as shown in curve B and at the lower right corner of Figure 1.3.

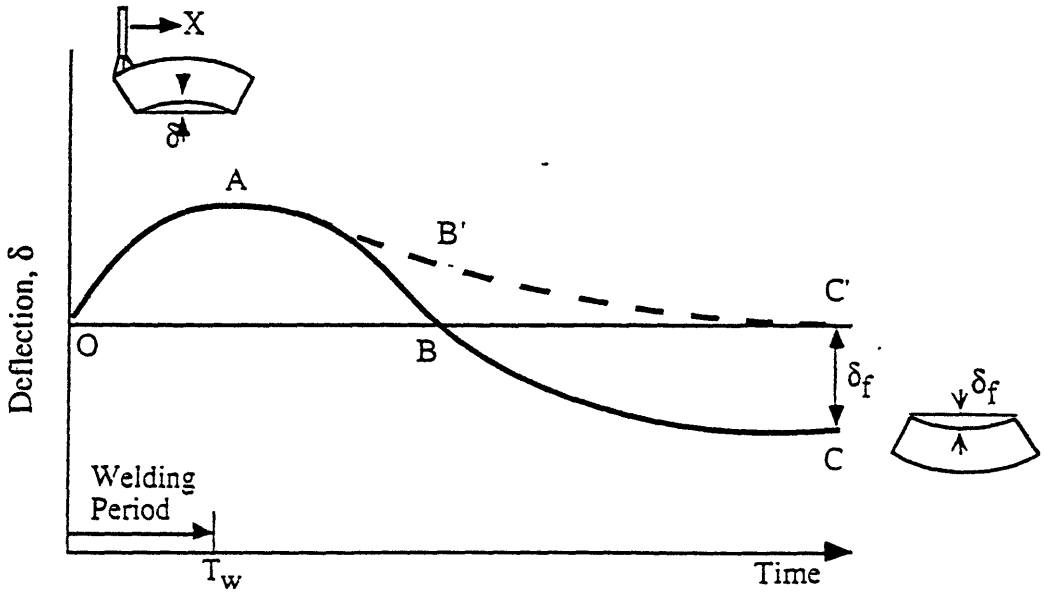

Figure 1.3. Transient distortion behavior of bead on edge welding

1.4. Method of Reducing Distortion Due to Butt Welding

Figure 1.4 shows butt welding applied to two rectangular plates. The phenomena described in section 1.3 above causes the unwelded portion of the plates to bend away from each other, as shown by the arrow directions. Masubuchi [14] calls this type of distortion "rotational distortion."

A common solution to this problem is the use of tack welds. However, tack welds introduce other problems, including additional cost and tim and weld defects.

To solve the problem, Chang [8], Park [16] and Miyachi [15] of MIT suggested the application of side heating to the plates during the welding as shown in Figure 1.4.

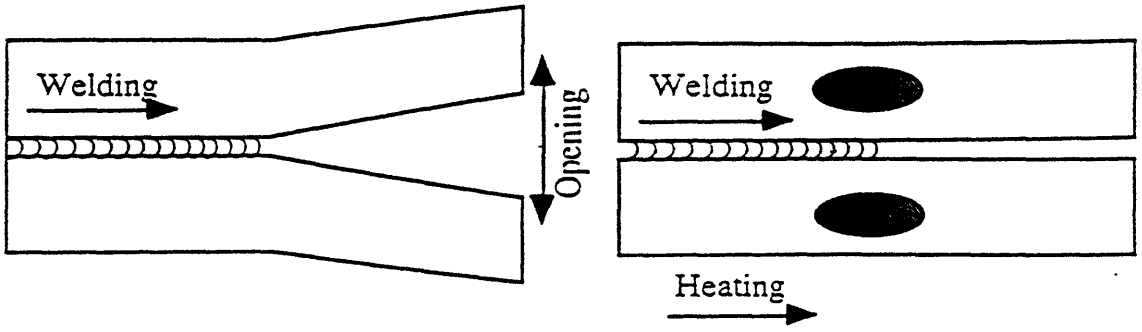

Figure 1.4. Side heating on butt welding

This side heating creates additional thermal stress that counteracts the forces created by the butt welding. Fortunately, the side heating does not introduce additional residual stress to the plates.

1.5. Approaches

There are basically two approaches that can be used to solve the problem, i.e. experimental and analytical approaches. In the experimental approach, results are obtained from direct measurement. In the analytical approach, results are obtained from calculations using a mathematical model of the problem. Quite often, the mathematical model is so complicated that a computer is needed.

In terms of the residual stress and distortion, most of the early studies were approached experimentally. The specimens investigated were relatively simple.

Then, with the development of computers, the studies began to use analytical approaches. However, the early mathematical models were too simple and did not have the capability to accept the fact that material properties are non linear. As early as the 1970's, finite element method has been used in studies related to welding simulation. The advantage of using finite element is that it accepts the fact that material properties are non linear.

In this study, the finite element method developed by ADINA, Inc. [1,2,3,4,5] was used. In particular, ADINA-T was used to calculate transient temperature changes of the specimens, and ADINA was used to calculate transient vertical movements of the specimens. Then, the results calculated in ADINA-T and ADINA were processed for plotting in ADINA-PLOT.

In this study, the experimental approach is necessary to verify the accuracy of the finite element analyses. To get accurate results in the experimental approach, measurement equipment must be capable of measuring the very small changes that occur on experimental specimens during observation periods. In addition, to get comprehensive results, the measurement equipment must also be able to measure changes at any point on the experimental specimens. For these reasons, six high frequency non contact laser sensors together with a data acquisition system were used to measure and record transient vertical movements of six measurement points

on each surface of all the experimental specimens. As mentioned above, the laser sensors have high frequency so that they can measure accurately the vertical movements of the measurement points, both during and after the welding. Additionally, since there is no contact between the laser sensors and the surfaces of the specimens, laser sensors can be used to measure the vertical movements of the measurement points located in very high temperature regions, such as in the vicinity of the welding arc.

1.6. Objectives of the Thesis

The thesis reports the results of experimental and analytical studies on transient distortion resulting from welding several types of specimens.

The first two specimens simulate structures commonly used in ships. Specifically, they are called panel structures. It is known that welding fabrication of panel structures creates distortion in the panel structures. Due to the distorted shapes of the panel structures, many ships have been damaged by water pressure and other compressive stress. Therefore, it is very important to learn how the distortion occurs in the panel during and after welding. The transient distortion behavior of the panels were investigated entirely by using the laser sensors and the data acquisition system described above. No computer simulation was done for these two specimens.

Specimens 3 through 6 simulate a rail track. Fabrication of the rail track is seen as two cantilever beams welded together at one of their ends. During the fabrication, the rail track distorts causing difficulty in the fabrication. There are two variables being investigated here: First is the effect of a slit, and second is the effect of width. These specimens were investigated experimentally and analytically.

The last specimen, i.e. specimen 7, was investigated experimentally by Goktug [11]. The objective of his investigation was to see the effect of a slit on a non- constraint plate that had undergone bead-on-point welding. No

analytical investigation had been done on the specimen. For this reason, specimen 7 has been included in this thesis.

With these results, it is hoped that better understanding of the distortion process due to welding will be achieved, especially in the seven types of weldments being studied,.

1.7. Outline of the Thesis

The thesis is organized as follows:

1. Experimental Approach.
   In this section, details on the experimental investigation are described. Included here are characteristics of experimental equipments, specimens' dimensions and the locations of measurement points on the specimens, descriptions of welding processes applied to the specimens, and the experimental results.
2. Analytical Approach.
   In this section, details on the analytical investigation are described. Included here are procedures of heat transfer analysis in the ADINA-T program, analytical results from the ADINA-T program, procedures of thermal stress and distortion analysis in ADINA program, and analytical results from the ADINA program.
3. Comparison between Experimental and Analytical Results.
   In this section, a comparison between the experimental and analytical results is presented. The comparison section of the thesis is presented to prove that the analytical investigation in the ADINA-T and ADINA programs are accurate and dependable.
4. Summary and Discussion of Results.
   This section is to summarize and discuss briefly all important points learned from the experimental and analytical studies of the distortion of the specimens.

Chapter 2

Experimental Approach

The objectives of the experimental approach, especially true for specimens 3 through 7, are to get very dependable transient vertical movement behaviors for comparison with the results of the analytical approach. For specimens 1 and 2, since there were no analytical investigations, results were obtained only from the experimental investigation.

2.1. Experimental Equipment

In this section, characteristics of all the experimental equipments used in the experimental approach are described in detail, including reasons why they have been chosen. The experimental equipment is as follows:

1. Gas Tungsten Arc (GTA) welding machine.
2. Laser sensor and data acquisition system.

2.1.1. GTA Welding Machine

In real applications, there are several welding methods commonly used to fabricate large structures. The welding methods are as follows:

1. Shielded metal arc welding.
2. Submerged arc welding.
3. Gas shielded arc welding which includes GTA and gas metal arc weldings.
4. Vertical automatic welding.

To closely simulate the real application, the welding method to be used in the experimental investigation must be chosen from the above choices. Given the

above choices, GTA welding was selected because GTA welding is the only possible welding method that does not require a filler metal. A filler metal was not used in order to simplify the subsequent finite element analysis. In addition, GTA welding is also the cleanest welding method available.

Table 2.1 describes GTA welding's characteristics.

Polarity	Direct Current Straight Polarity
Current	150 Amperes
Voltage	13 Volts
Shielding Gas	Argon
Filler Metal	None

Table 2.1. Characteristics of the GTA welding

2.1.2. Laser Sensor and Data Acquisition System

As previously mentioned, the distortion measurement equipment must measure accurately the transient vertical movement of the specimens during welding and cooling. In addition, performance should not be affected by the extreme heat from the welding arc. For these reasons, six high frequency laser sensors produced by Keyence Corporation, model LB-081, were chosen as the distortion measurement equipment.

The laser sensors are high accuracy measurement devices which operate under FUZZY logic control circuit to stabilize the moving targets. They can measure the transient vertical movement of the specimens during the welding and cooling very accurately. Also, performance is not affected by the extreme heat from the welding arc because no contacts are required between the laser sensors and the surfaces of the specimens. It means that the laser sensors

can be used to measure the transient vertical movement at almost any point, including points located in the weld line. Furthermore, they can easily be set to a reference point by AUTO ZERO function.

Shown in table 2.2 is a list of the laser sensors' characteristics.

Maker	KEYENCE Corporation
Sensor Head Model	LB-081
Controller Model	LB-1101
Light Source	Semiconductor Laser Wave Length = 780 nm
Reference Distance	80 mm
Measuring Range	$\pm$ 15 mm
Linearity	0.25% of F.S.
Resolution	8 μm
Response Frequency	36 Hz

Table 2.2. Characteristics of the laser sensors

At the Welding Systems Laboratory of MIT, the laser sensors are interfaced with a 486 PC compatible microcomputer via an analog to digital converter. The heart of the system is a 16 channel, 12 bit A/D board manufactured by Metrabyte Corporation. The system is controlled by custom software written in C and developed at the Welding Systems Laboratory of MIT.

2.2. Specimens

As mentioned before, basically the specimens can be classified into five categories. They are as follows:

1. Single T specimen (specimen 1).
2. Double T specimen (specimen 2).
3. Beam type specimens without slits (specimens 3 and 4).
4. Beam type specimens with slits (specimens 5 and 6).
5. Rectangular plate with slit (specimen 7).

All of the specimens, except specimen 7 which is made from 304 stainless steel, are made from ASTM A36 low carbon steel. The reason for choosing ASTM A36 low carbon steel for most of the specimens is because the material is very commonly used in welded structures.

2.2.1. Dimensions

Shown in Figures 2.1 to 2.7 are detailed dimensions of all the specimens.

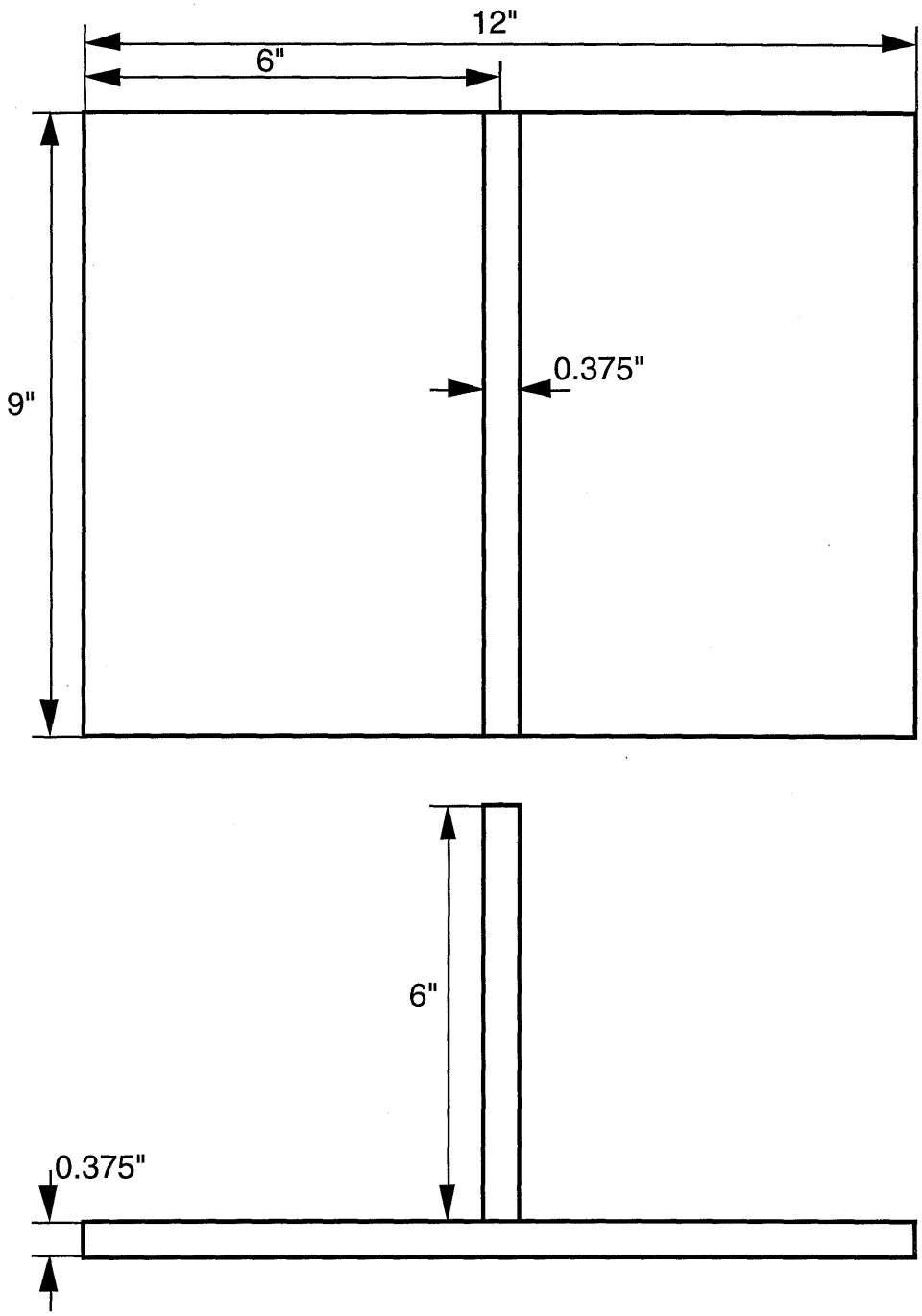

Figure 2.1. Dimensions of Specimen 1

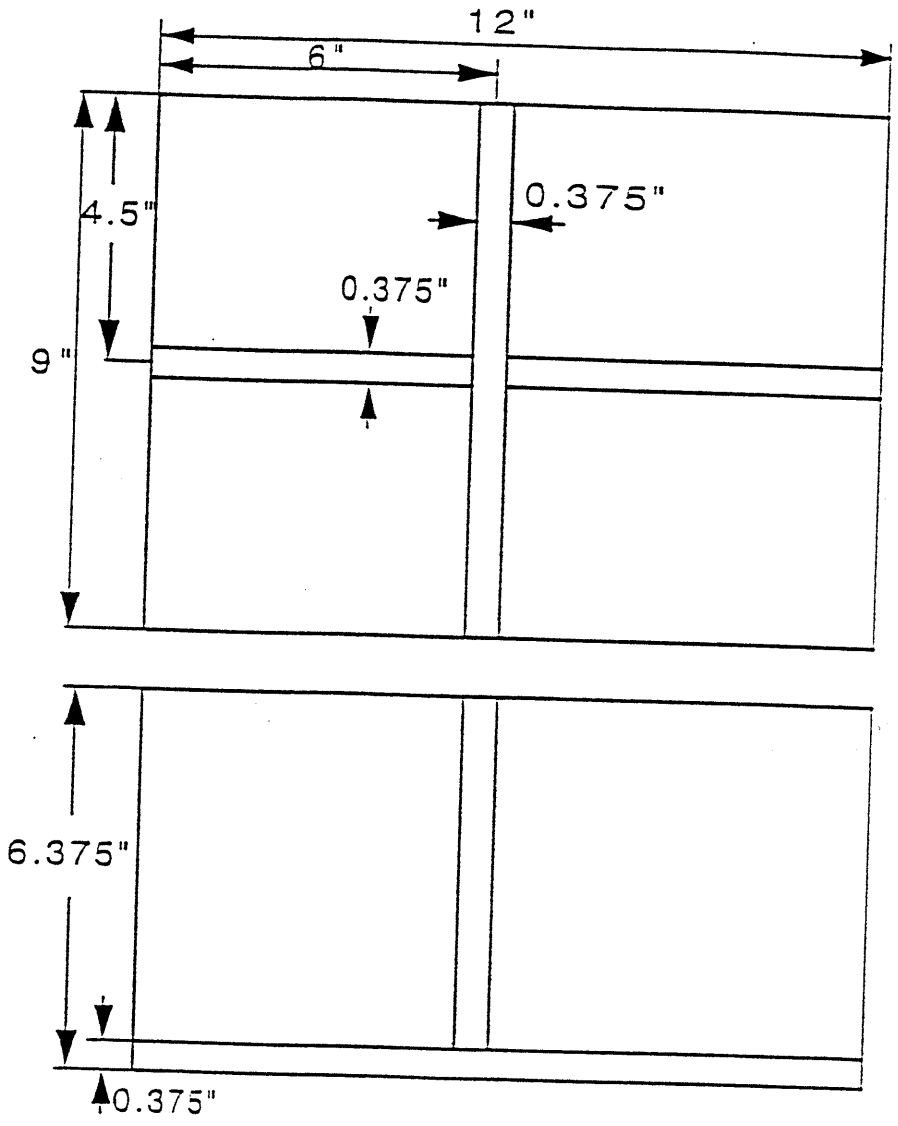

Figure 2.2. Dimensions of Specimen 2

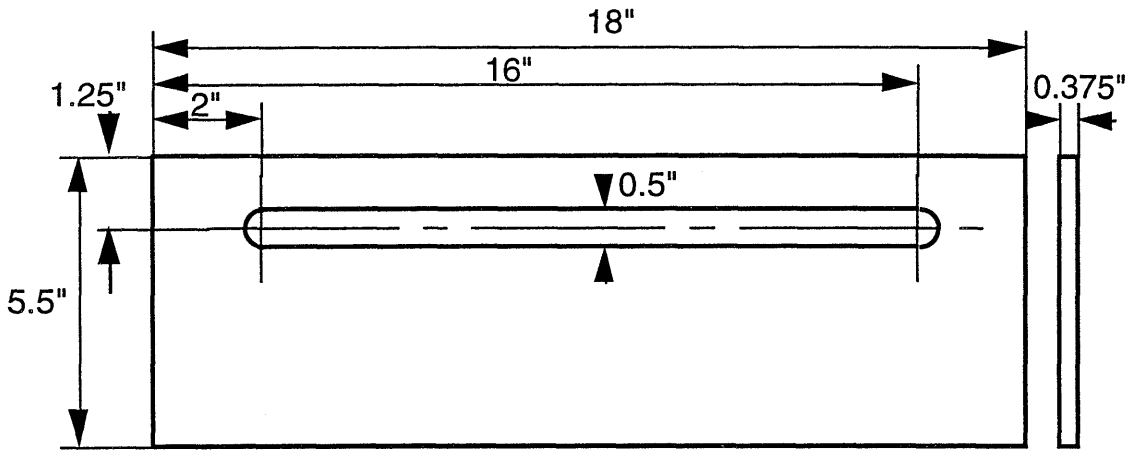

Figure 2.3. Dimensions of Specimen 3

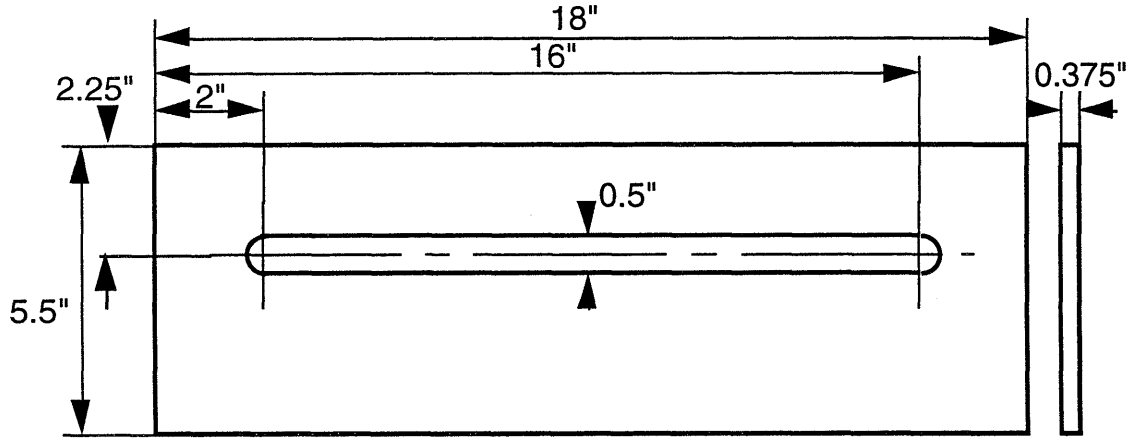

Figure 2.4. Dimensions of Specimen 4

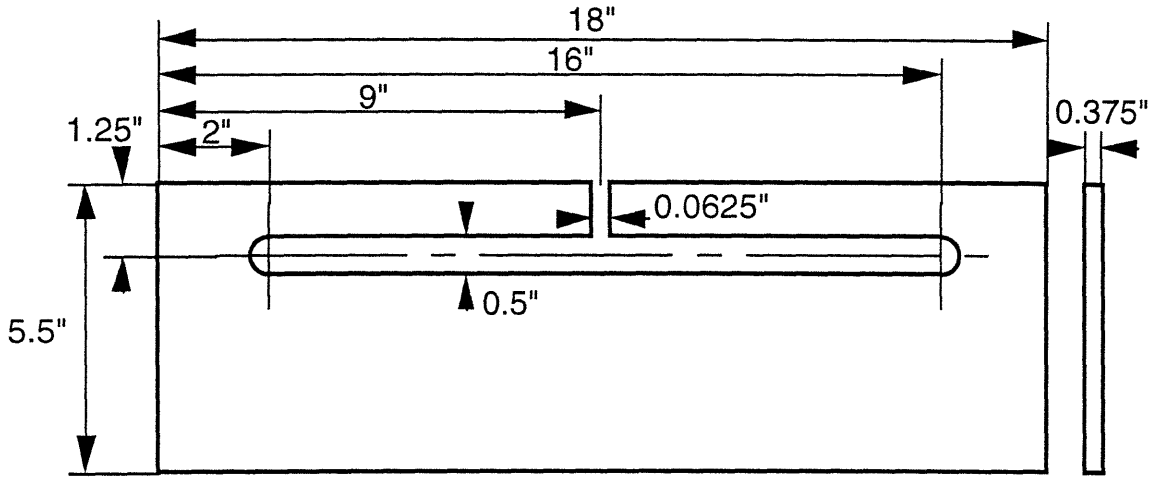

Figure 2.5. Dimensions of Specimen 5

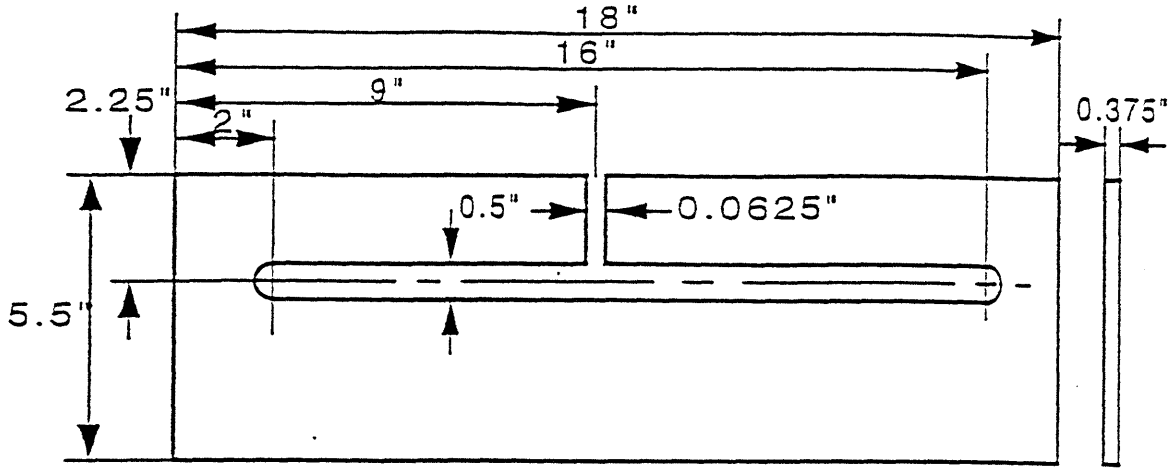

Figure 2.6. Dimensions of Specimen 6

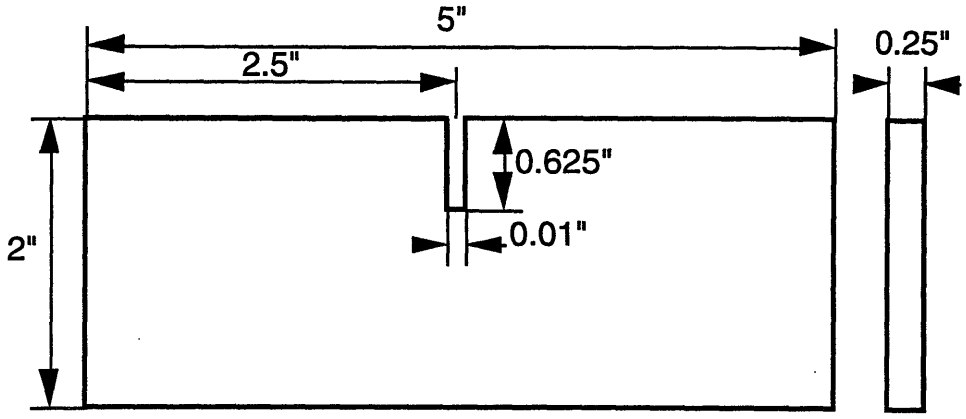

Figure 2.7. Dimensions of Specimen 7

2.3. Locations of Measurement Points

Ideally, the transient vertical movement at every point on the surface of every specimen is measured. However, there are only six available laser sensors in the Welding Systems Laboratory of MIT. Therefore, the measurement points were selected very carefully so that the transient vertical movement of every point on the surface of every specimen could be determined from the experimental distortion measurement results.

Shown in Figures 2.8 through 2.11 are the locations of the measurement points on the surfaces of all the specimens, as measured by the laser sensors. Since the locations of the measurement points for Specimens 3 through 6 are the same, only the measurement points for Specimen 3 are shown.

2.3.1. Locations of Measurement Points for Specimen 1

Figure 2.8 shows the top view for Specimen 1. As shown in the figure, there were only four laser sensors used, i.e. S3, S4, S5 and S6. S4, S5 and S6 were mounted to measure the transient vertical movement (perpendicular to

the paper) at three points located along a line approximately 7 cm away from the weld line. S3 was mounted to measure the transient vertical movement at a point located on the weld line.

During measurement, two fillet welding passes were applied to the specimen. The average velocity, current and voltage of the welding arc during the first pass were 0.1524 cm/s, 199 Amperes, and 13.6 Volts respectively. For the second pass, the average velocity, current and voltage of the welding arc were 0.1063 cm/s, 199 Amperes, and 13.6 Volts respectively.

Also during the measurement, the specimen was simply supported along two lines which were parallel to the welding directions and located at the two edges of the specimen.

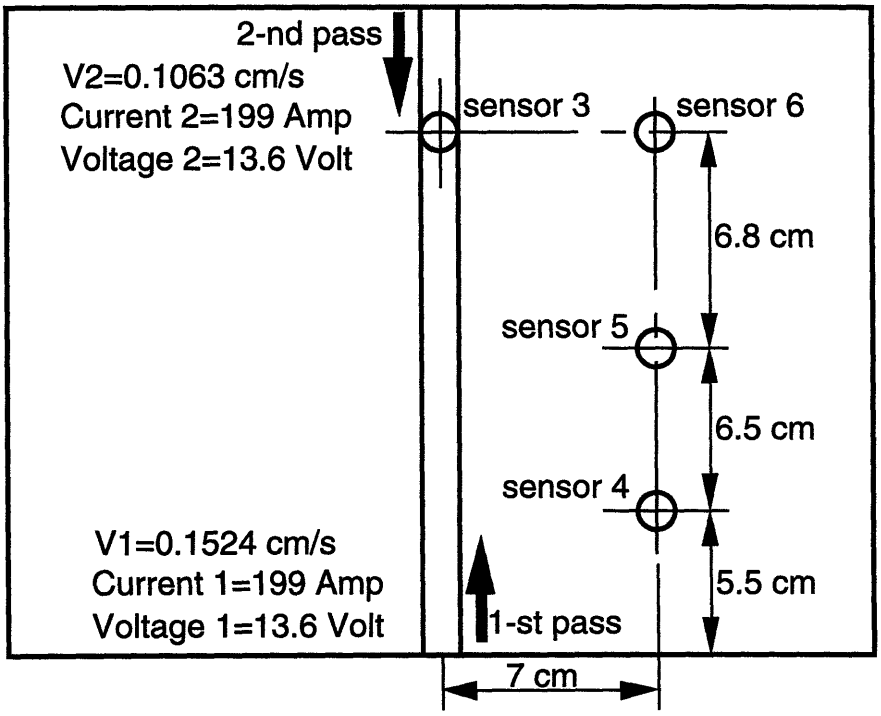

Figure 2.8. Locations of the measurement points on Specimen 1

2.3.2. Locations of Measurement Points for Specimen 2

Figure 2.9 shows the top view of Specimen 2. As shown in the figure, there were five laser sensors used, i.e. Sensor 2, Sensor 3, Sensor 4, Sensor 5 and Sensor 6. Sensor 2, Sensor 4 and Sensor 5 were mounted to measure the transient vertical movement (perpendicular to the paper) of three points located on weld line. Sensor 3 and Sensor 6 were mounted to measure the transient vertical movement of two other different points.

During the measurement, two fillet welding passes were applied to the specimen. During the first pass, the average velocity, current and voltage of the welding torch were 0.127 cm/s, 185 Amperes, and 13 Volts respectively. During the second pass, the average velocity, current and voltage of the welding torch were 0.127 cm/s, 185 Amperes, and 12.5 Volts respectively.

Also during measurement, the specimen was simply supported along two lines which were parallel to the weld direction and located at the two edges of the specimen.

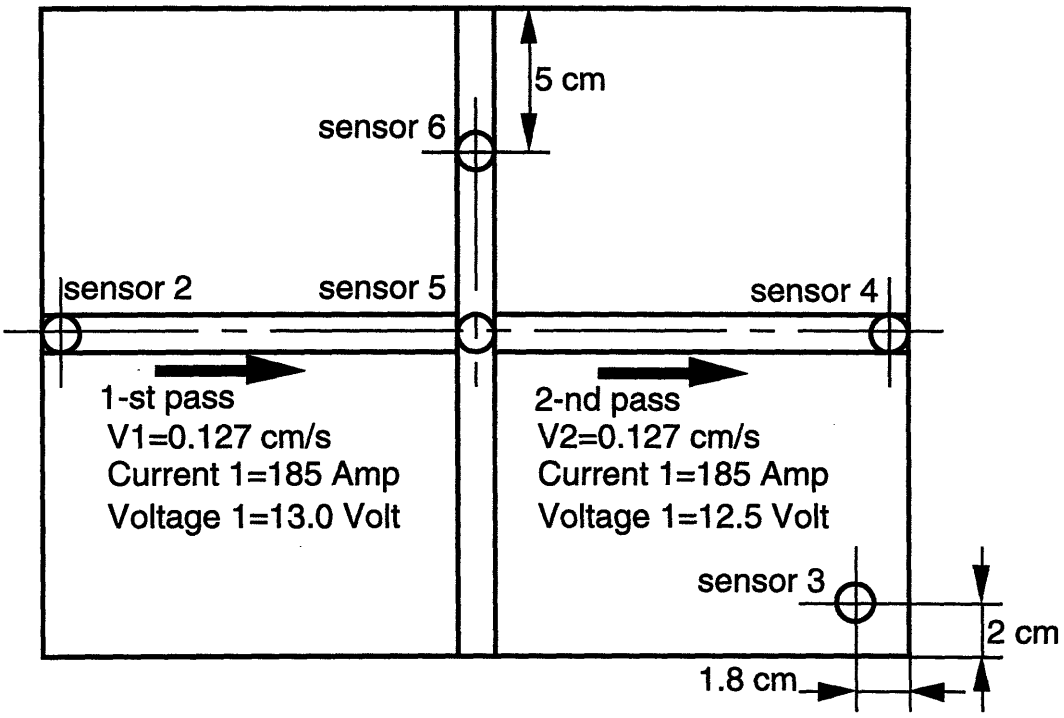

Figure 2.9. Locations of the measurement points on Specimen 2

2.3.3. Locations of Measurement Points for Specimens 3, 4, 5, and 6

As mentioned before, the locations of the measurement points for Specimens 3 through 6 were exactly the same. That is why only the locations of the measurement points for Specimen 3 are shown (Figure 2.10).

Shown in Figure 2.10 is front view of Specimen 3. As shown in the figure, there were five measurement points, i.e. S1, S2, S3, S4 and S5. The transient vertical movement (parallel to the paper) of the measurement points was measured.

During the measurement, the GTA welding was applied at a point located in center of the top edge of the specimen. The welding duration, current and voltage were 7 seconds, 151 Amperes, and 13 Volts respectively.

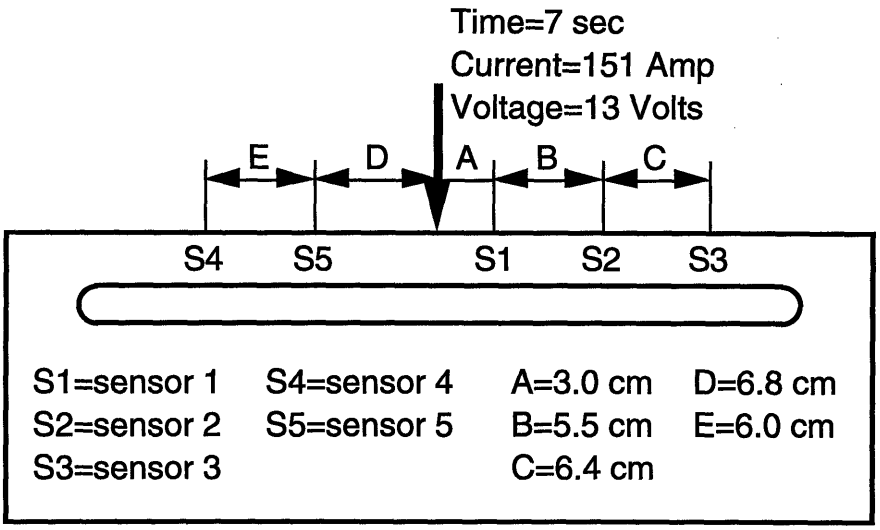

Figure 2.10. Locations of the measurement points on Specimen 3

2.3.4. Locations of Measurement Points for Specimen 7

The experimental investigation for Specimen 7 was done by Goktug [11]. He measured the transient vertical movement (parallel to the paper) of two measurement points. The first measurement point was located on top edge of the plate approximately 20 mm from one side edge, and the second measurement point was located on bottom edge of the plate approximately 7 mm from the same side edge.

During the measurement, the GTA welding was applied to a point located at the top tip of the slit. The duration, current and voltage of the GTA welding were approximately 5 seconds, 150 Amperes, and 13 Volts respectively.

Also during the measurement, the plate was fixed supported at a point located at center of the bottom edge of the plate.

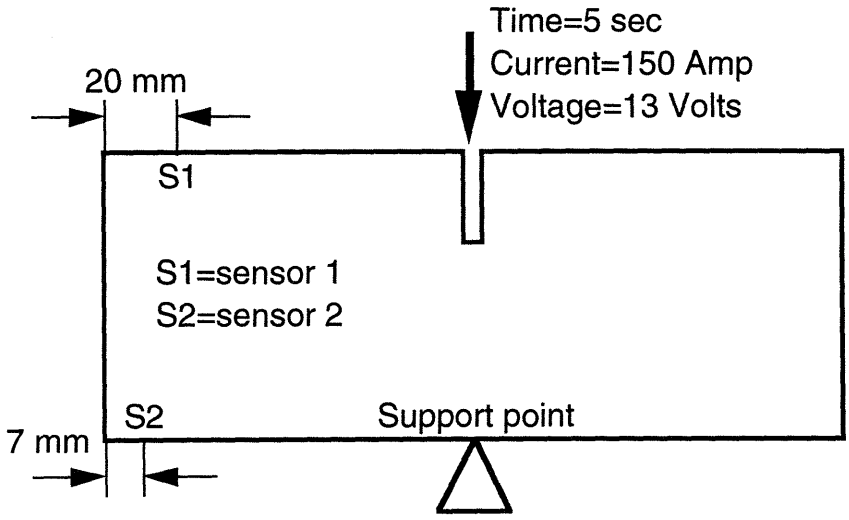

Figure 2.11. Locations of the measurement points on Specimen 7

2.4. Experimental Results

By using the experimental equipment described above, results of the experimental investigation were obtained.

2.4.1. Experimental Results of Specimen 1

Figures 2.12 through 2.20 show the results of the experimental investigation on transient movement at the measurement points on Specimen 1.

Starting from very beginning of first fillet welding pass, the measurement points had moved upward. The process are clearly shown in Figures 2.12 through 2.14. The largest upward movement was experienced at the point measured by Sensor 3. The upward movement of the measurement points measured by Sensors 4 and 5 are so small that they are barely seen as shown in Figures 2.15 and 2.16. The upward movement phenomena agrees with the previous explanation that the expansion of the upper part of the plate is more than that of the lower part of the plate due to the higher temperature in the upper part.

Then, after the measurement points reached their corresponding top positions, they moved downward until they reached their new corresponding final downward positions. The largest downward movement was experienced by the measurement point measured by Sensor 2 as shown in Figure 2.14. The downward movement phenomena also agrees with the previous explanation that the upper part of the plate shrinks as its temperature cools down.

Second fillet welding pass was conducted shortly after the first fillet welding pass without setting to zero the values in the laser sensors. That is why the initial positions for the measurement points at the second fillet welding pass are not zero.

During the second fillet welding pass, the measurement points showed similar movement behaviors to the ones during the first fillet welding pass. In other words, initially the measurement points moved upward, and then, they moved downward until they reached their corresponding final downward positions. The measurement point measured by Sensor 3 had the largest upward movement as well as the largest final downward movement.

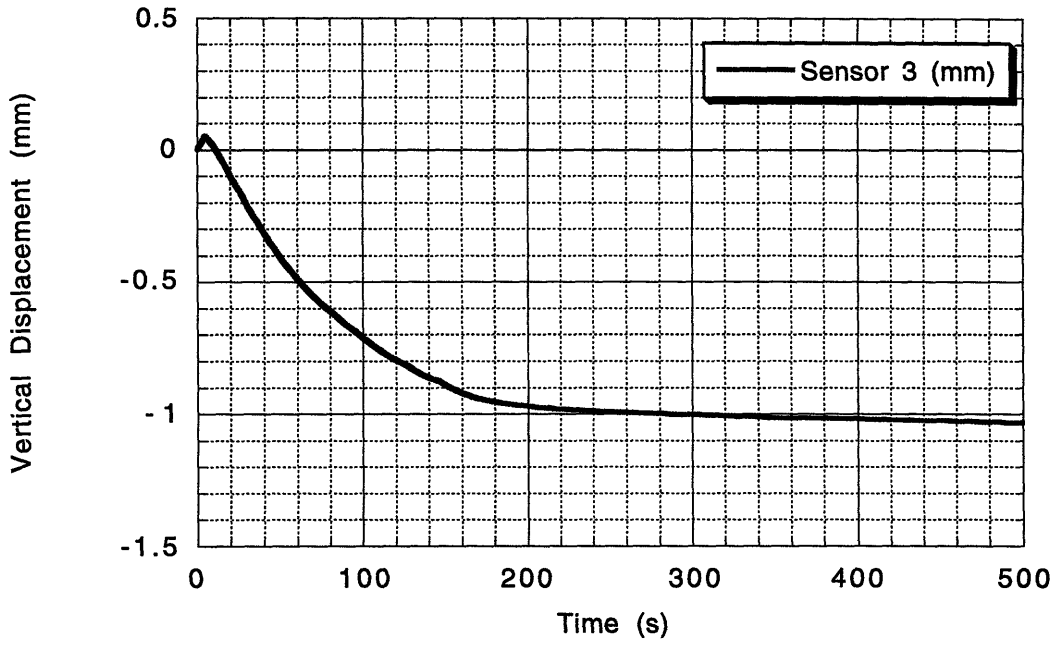

Figure 2.12. Vertical movement during the 1st pass measured by Sensor 3

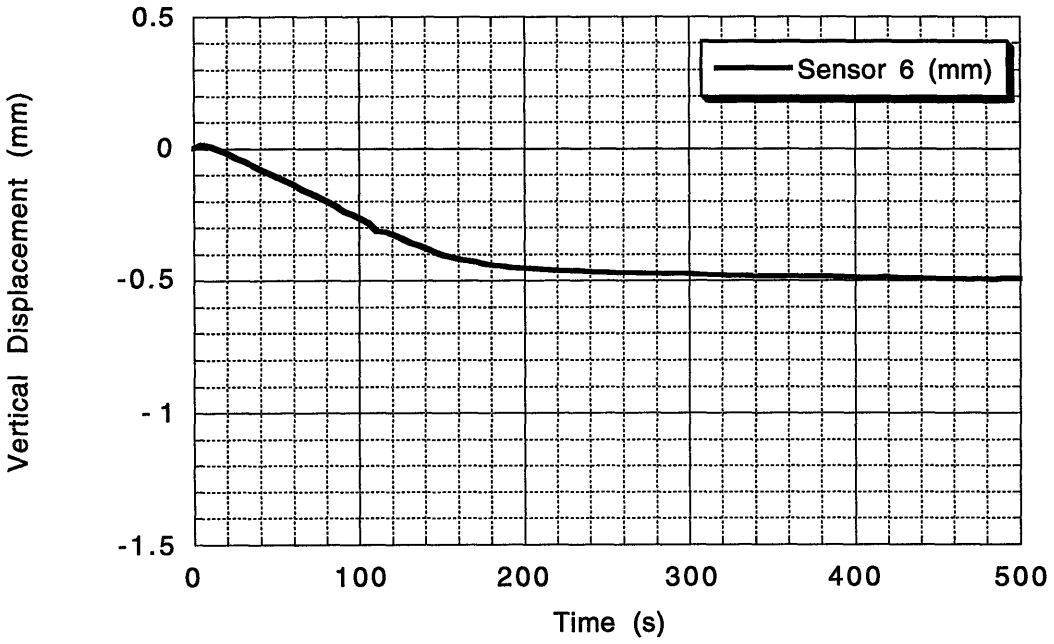

Figure 2.13. Vertical movement during the 1st pass measured by Sensor 6

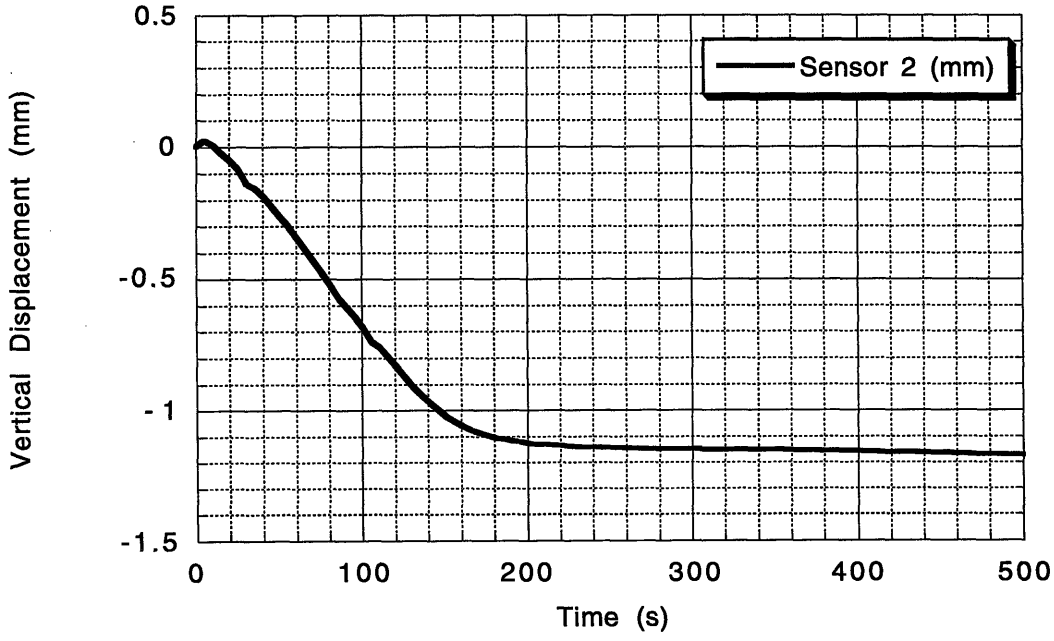

Figure 2.14. Vertical movement during the 1st pass measured by Sensor 2

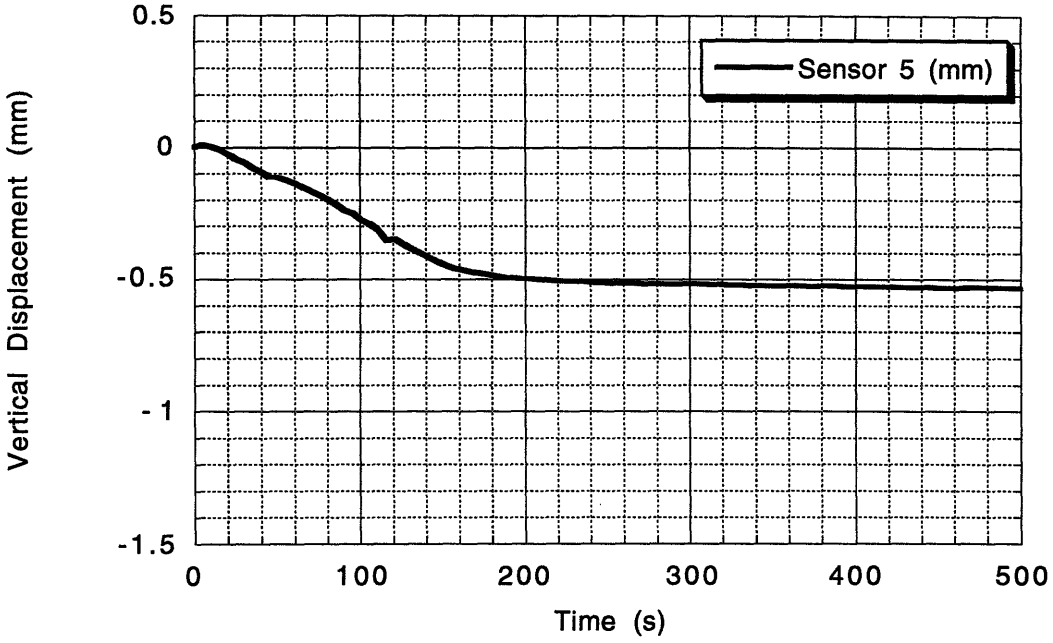

Figure 2.15. Vertical movement during the 1st pass measured by Sensor 5

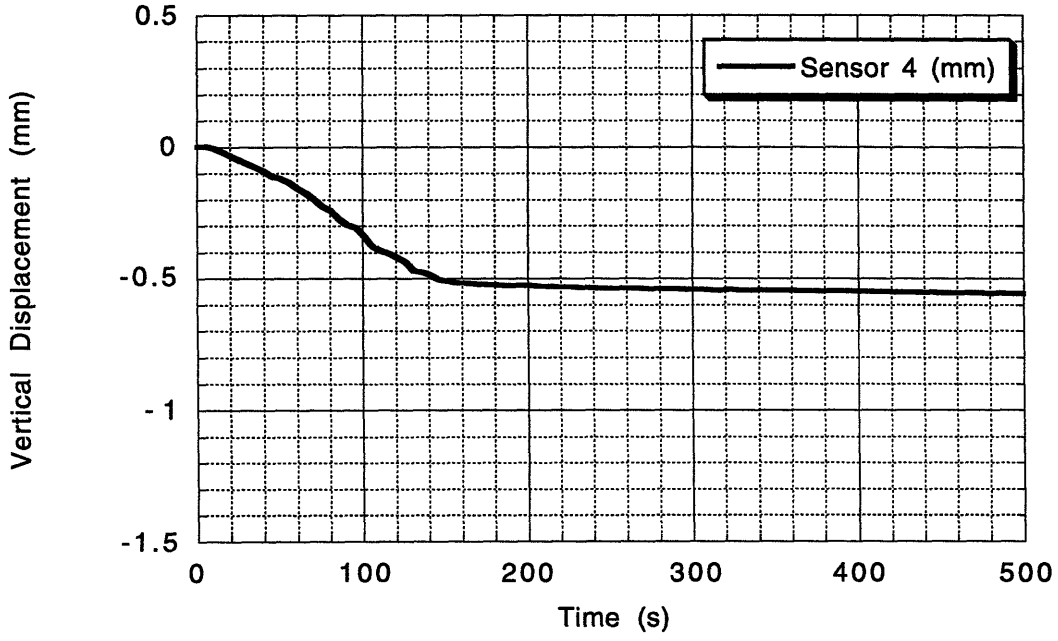

Figure 2.16. Vertical movement during the 1st pass measured by Sensor 4

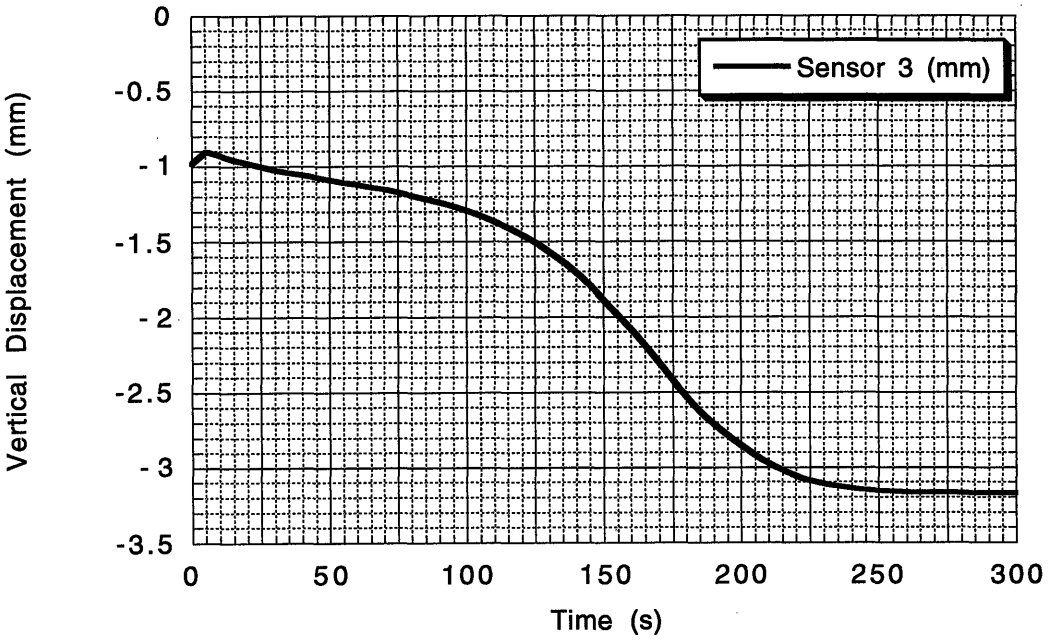

Figure 2.17. Vertical movement during the 2nd pass measured by Sensor 3

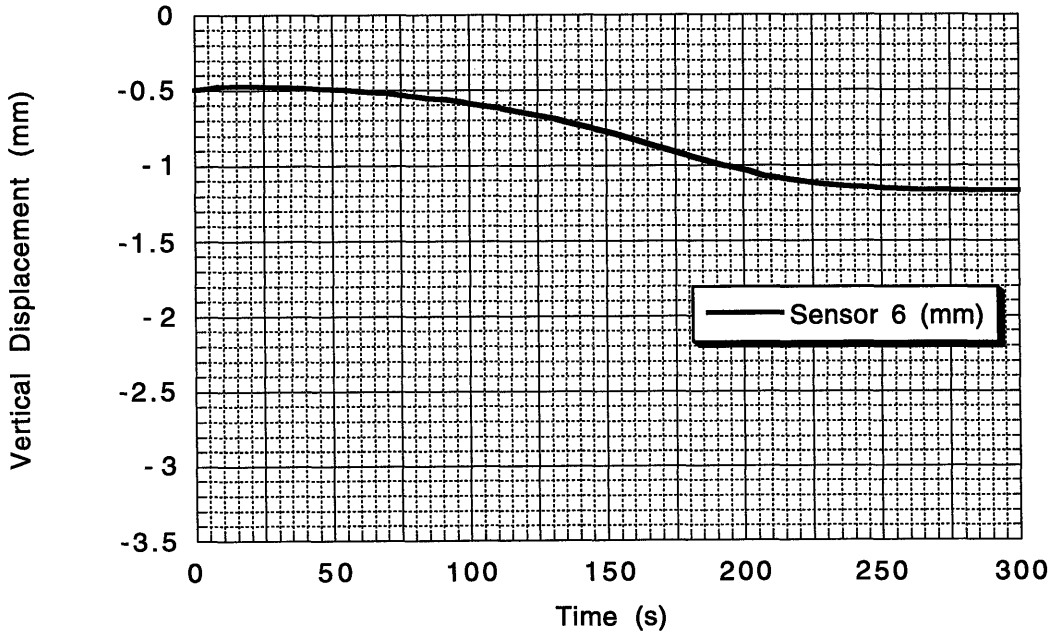

Figure 2.18. Vertical movement during the 2nd pass measured by Sensor 6

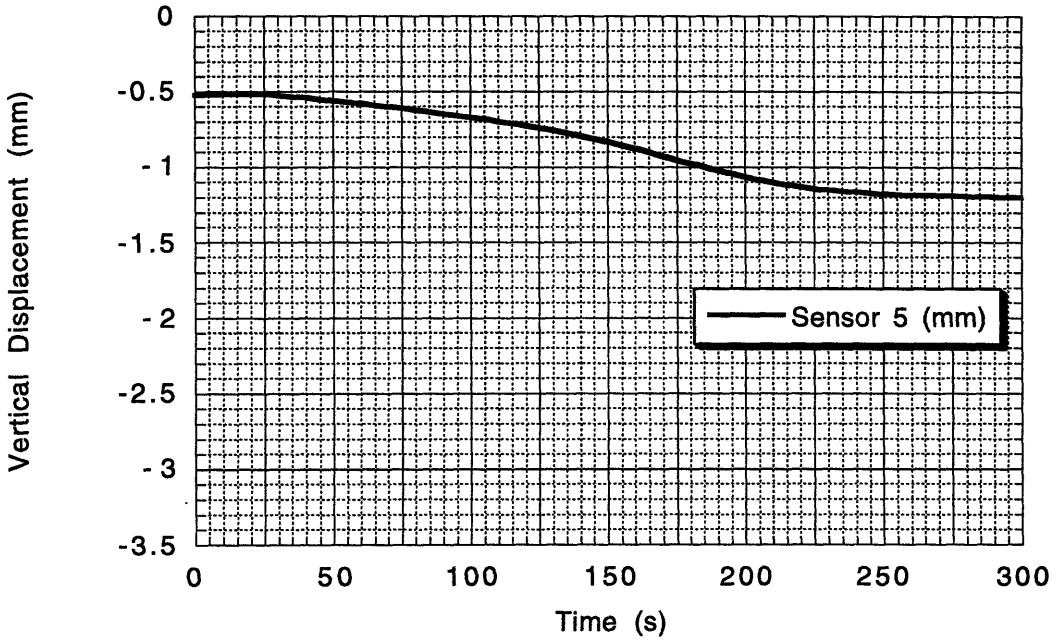

Figure 2.19. Vertical movement during the 2nd pass measured by Sensor 5

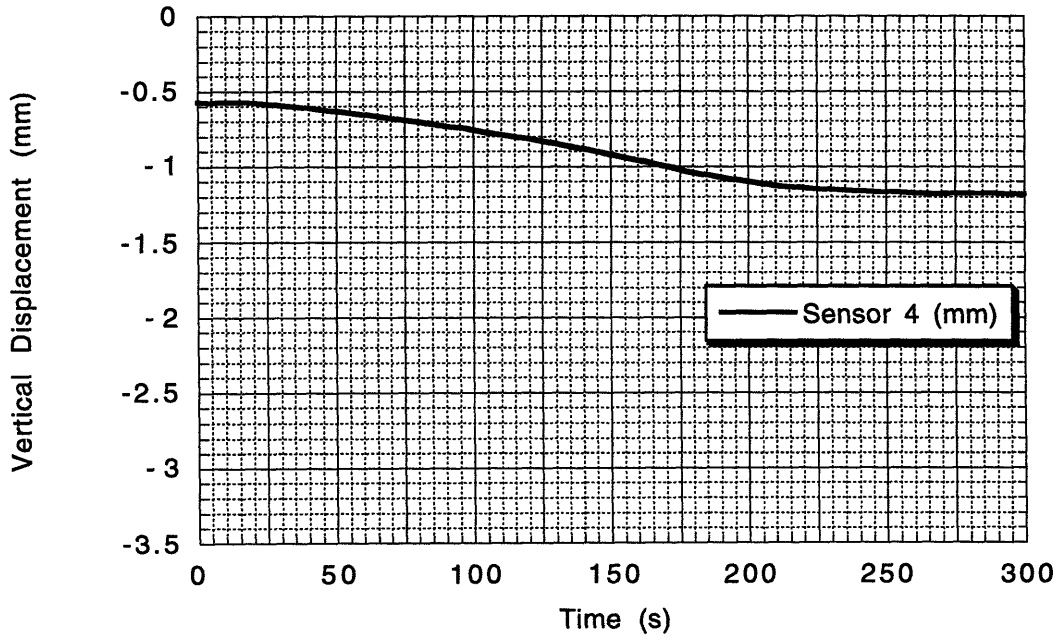

Figure 2.20. Vertical movement during the 2nd pass measured by Sensor 4

2.4.2. Experimental Results of Specimen 2

Figures 2.21 through 2.26 show the results of the experimental investigation on transient movement at the measurement points on Specimen 2.

At the beginning of the first fillet welding pass, the measurement points moved upward. The process is clearly shown in Figures 2.21 through 2.23. As before, the upward movement can be explained as in Specimen 1.

Then, after they reached their corresponding top positions, they moved downward until they reached their final corresponding downward positions. The largest downward movement was experienced by the measurement point measured by Sensor 2. Here, existence of the phenomena also has the same explanation as in Specimen 1.

As in Specimen 1, second fillet welding pass was conducted shortly after the first fillet welding pass without setting to zero initial values in the laser sensors.

During the second fillet welding pass, the measurement point measured by Sensor 2 did not move at all as shown in Figure 2.24. Meanwhile, the measurement points measured by Sensors 4 and 5 moved upward and then downward until they reached their corresponding final downward positions. The measurement point measured by Sensor 4 experienced the largest downward movement.

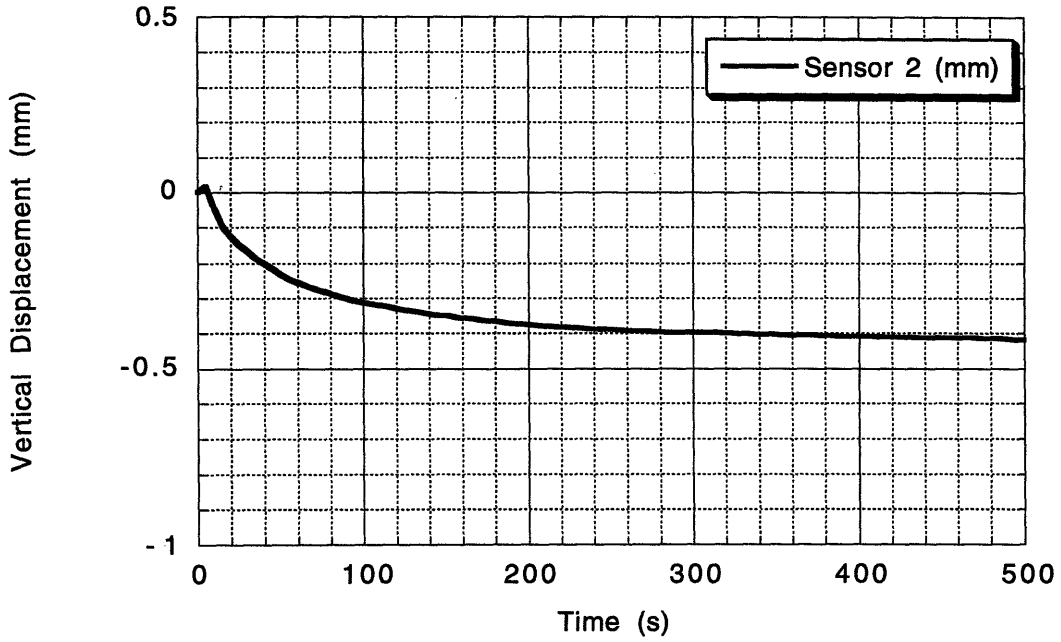

Figure 2.21. Vertical movement during the 1st pass measured by Sensor 2

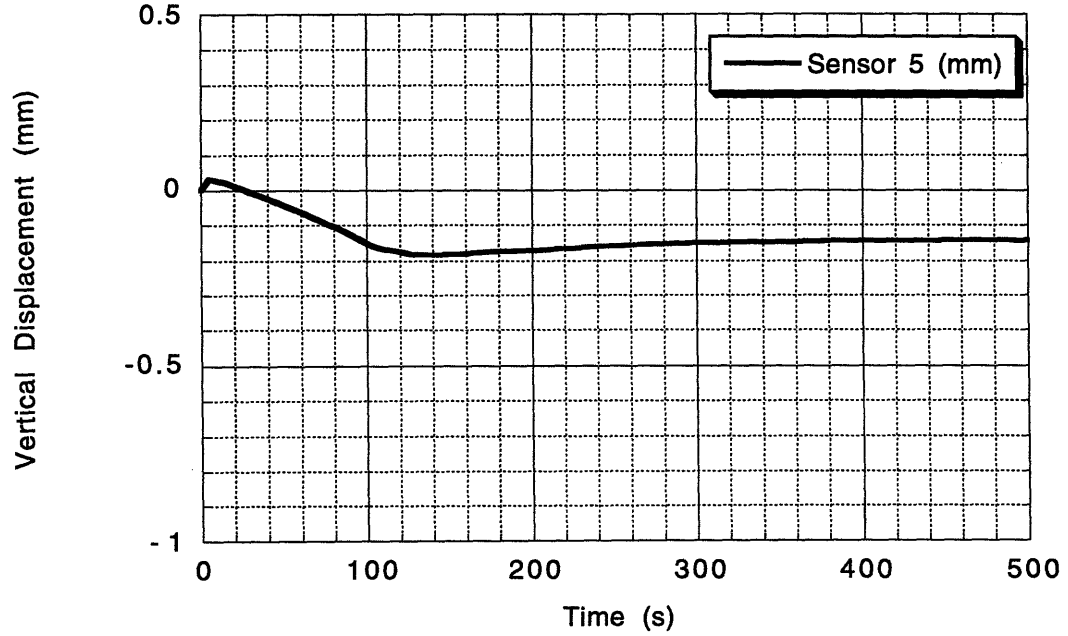

Figure 2.22. Vertical movement during the 1st pass measured by Sensor 5

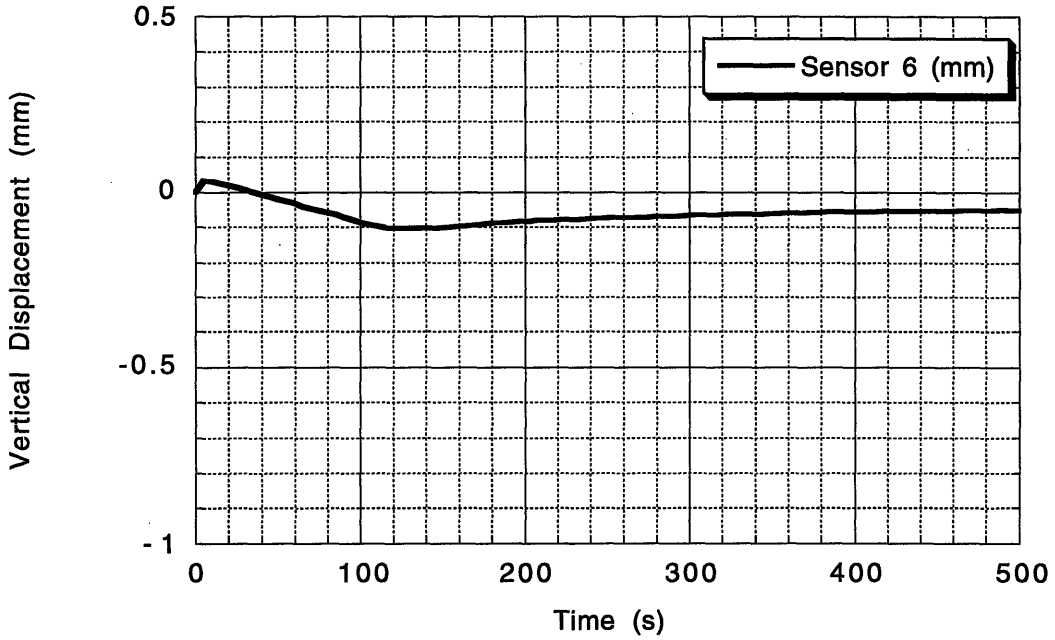

Figure 2.23. Vertical movement during the 1st pass measured by Sensor 6

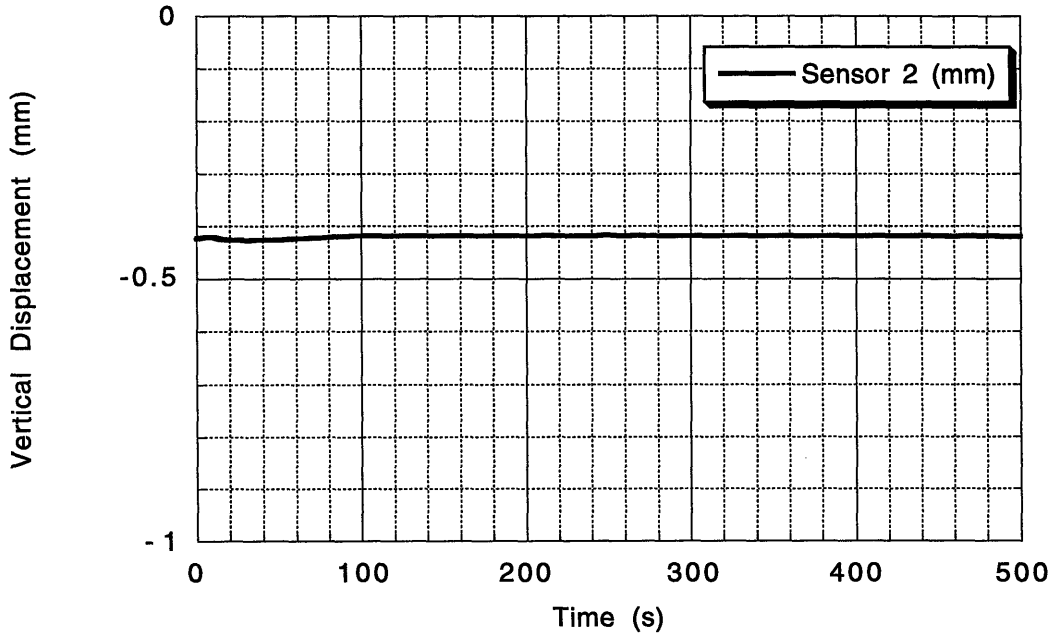

Figure 2.24. Vertical movement during the 2nd pass measured by Sensor 2

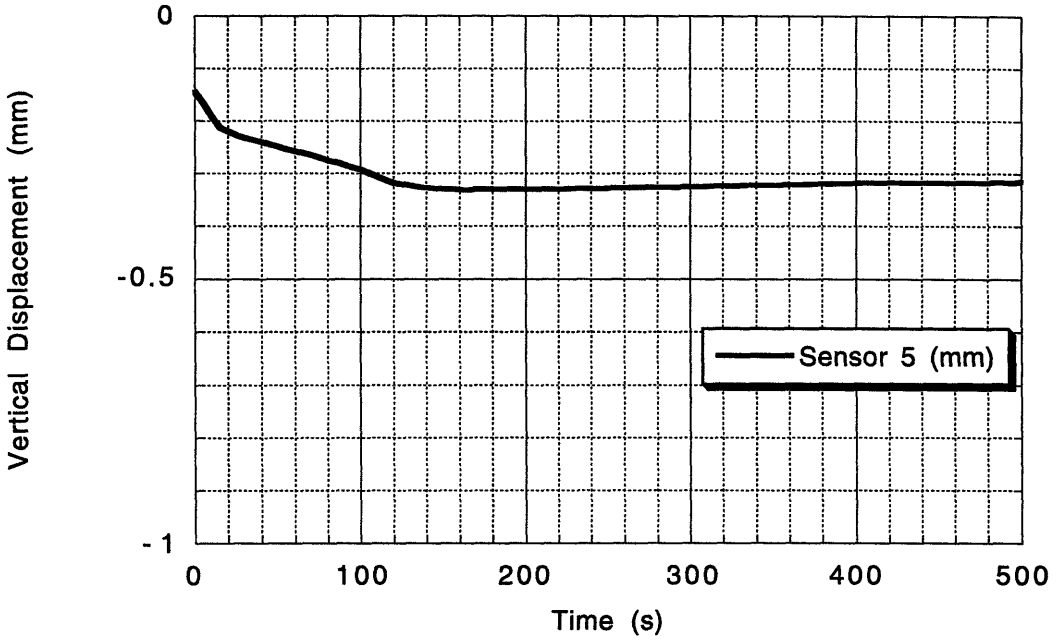

Figure 2.25. Vertical movement during the 2nd pass measured by Sensor 5

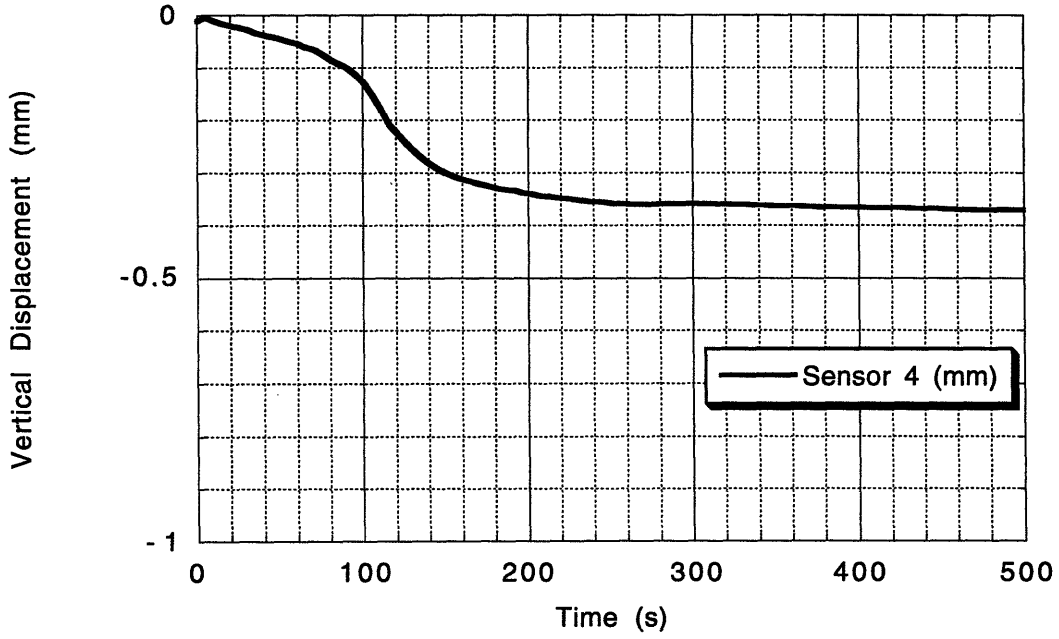

Figure 2.26. Vertical movement during the 2nd pass measured by Sensor 4

2.4.3. Experimental Results of Specimens 3 through 6

Figures 2.27 and 2.28 show the results of the experimental investigation on transient movement at the measurement points on Specimens 3 through 6.

During welding, the measurement points on Specimens 3 and 4 moved upward until they reached their corresponding peak values. The peak values of the measurement points on Specimen 3 are larger than those of the measurement points on Specimen 4 because Specimen 3 is thinner than Specimen 4.

Then, right after the welding, the measurement points on Specimens 3 and 4 moved downward until they reached their final corresponding positions. The final positions of the measurement points on Specimen 3 are larger than those of the measurement points on Specimen 4. This phenomena can be explained as in the previous paragraph.

Movement of the measurement points on Specimens 5 and 6 is very different from that of the measurement points on Specimens 3 and 4. During welding, the measurement points on Specimens 5 and 6 did not move in the vertical direction. The reason is because the specimens expanded to the spaces in the welding points that were provided by the slits. The expansion of the specimens will be shown clearly in the analytical section of this thesis.

Then, during cooling, the measurement points moved downward until they reached their final corresponding downward positions. The final downward positions of the measurement points on Specimen 5 are larger in magnitudes than those of the measurement points on Specimen 6 because Specimen 5 is thinner than Specimen 6.

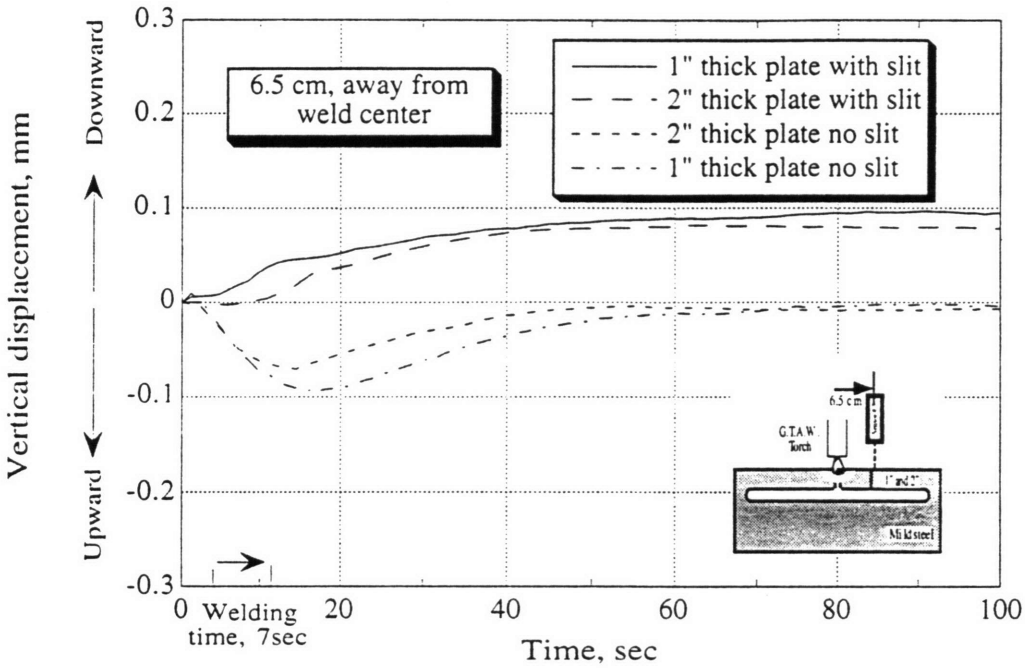

Figure 2.27. Vertical movement at 6.5 cm from the weld point on Specimens 3 through 6

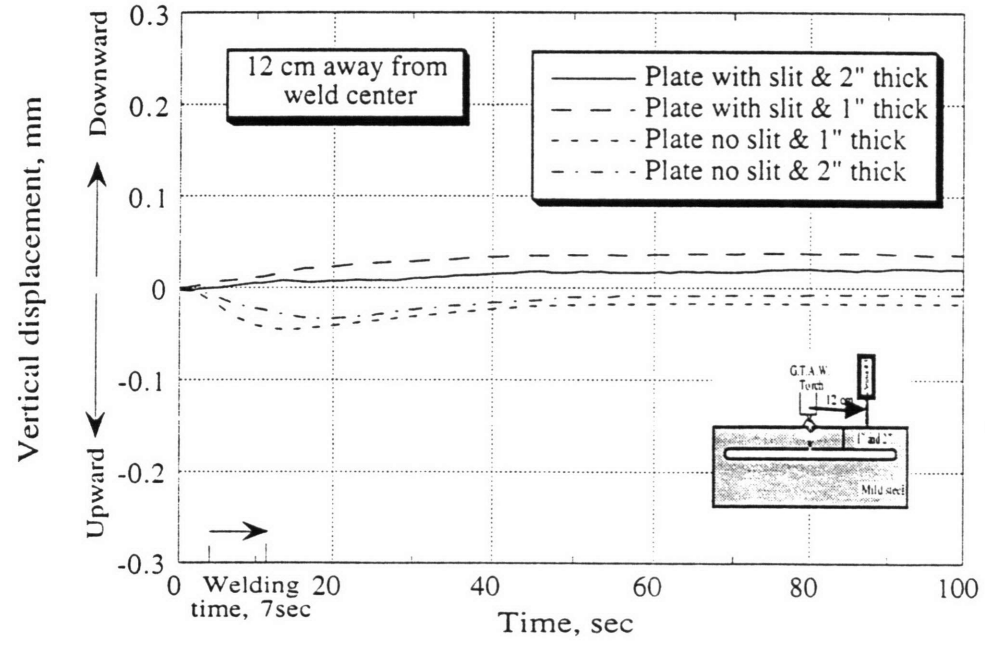

Figure 2.28. Vertical movement at 12 cm from the weld point on Specimens 3 through 6

2.4.4. Experimental Results of Specimen 7

The transient movement of Specimen 7 was investigated to see the effect of introducing a slit in a non-constraint plate in bead-on-point welding. The experimental investigation on the transient movement of Specimen 7 was done by Goktug [11] and the results of the experimental investigation are shown in Figures 2.29 and 2.30.

During welding, both the measurement points moved downward. The downward movement continued until approximately after the welding was finish. The measurement point located on the bottom edge had larger downward movement compared to the one located on the top edge of the plate.

Then, after they came to a full stop, they started to move upward until they reached their final upward positions. Looking at the figures, it looks like they had the same final upward positions. These results, as reported by Goktug, showed that the effect of introducing a slit is to reduce both the upward and downward movement.

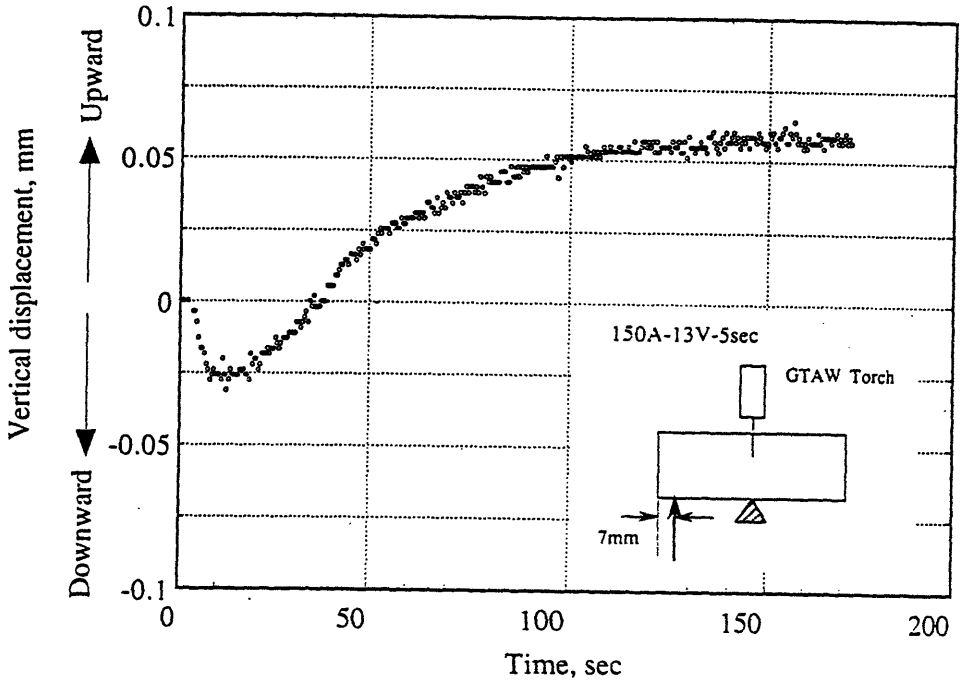

Figure 2.29. Vertical movement measured by Sensor 2

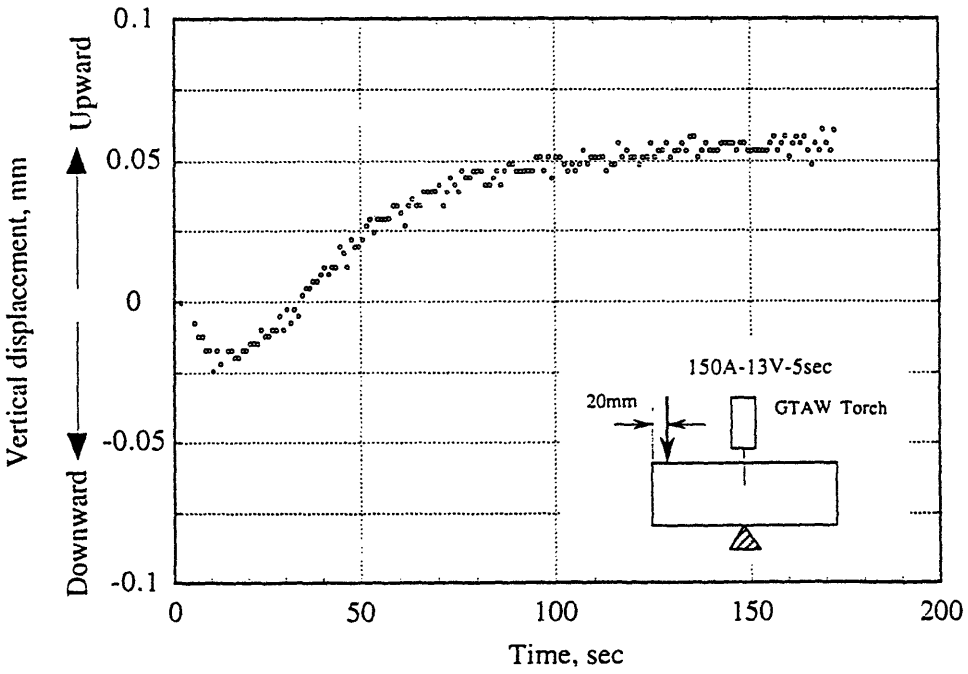

Figure 2.30. Vertical movement measured by Sensor 1

Chapter 3

Analytical Approach

The objective of the analytical approach was to simulate the creation of thermal stress and distortion due to the GTA welding in all specimens. The accuracy of the analytical approach was checked by comparing the analytical results with the experimental results.

To achieve this objective, finite element programs developed by ADINA, Inc. were used. In particular, the programs were ADINA-T, ADINA, and ADINA-PLOT.

In general, there were two steps in the analytical approach. In the first step, temperature change behaviors of all the points on the surfaces of the specimens were simulated by using the ADINA-T program. Then, in the second step, by using results obtained from the ADINA-T program as inputs, the creation of the thermal stress and distortion were simulated using the ADINA program.

3.1. ADINA-T Analysis

Due to the local heat of the welding arc, each point on the specimens experienced its own non uniform temperature change as time elapsed. In other words, as time elapsed, the temperature at each point on the specimens changed independently. In ADINA-T, the temperature at each point on the specimens was calculated at each time step.

Several important things that need to be considered carefully in modeling using ADINA-T.

3.1.1. Mesh Design

Several important things need to be considered in the mesh design of the specimens.

First, Specimens 3 through 7 were assumed to experience on-plane movement. Using ADINA-T, on-plane movement means movement parallel to X = 0 plane. Therefore, all quantities related to out of plane movement were assumed to be zero. In other words, plane stress or plane strain models were assumed. Details of the plane stress and plane strain models will be explained later. In general, two dimensional models were assumed for the specimens above.

Second, since transient movement of the specimens simulated in ADINA would be compared with the experimental one, the mesh of the specimens was designed in such ways that plots of the specimens' movements processed in ADINA-PLOT could be obtained at the same points as the experimental measurement points.

Third, to model the heat input from the welding arc, Rykalin [17,18] has suggested that Gaussian's normal distribution is an excellent model. Detail of Gaussian's normal distribution will be explained in the heat input section of this thesis. The problem with using the Gaussian's normal distribution model in ADINA-T is that while the model assumes continuous heat input distribution, ADINA-T can only assume discrete heat input distribution. To solve the problem, i.e. to approximate Gaussian's normal distribution, very dense mesh was created in the vicinity of welded point. For other locations, the mesh densities were less.

Figures 3.1 through 3.5 show the mesh designs for Specimens 3 through 7.

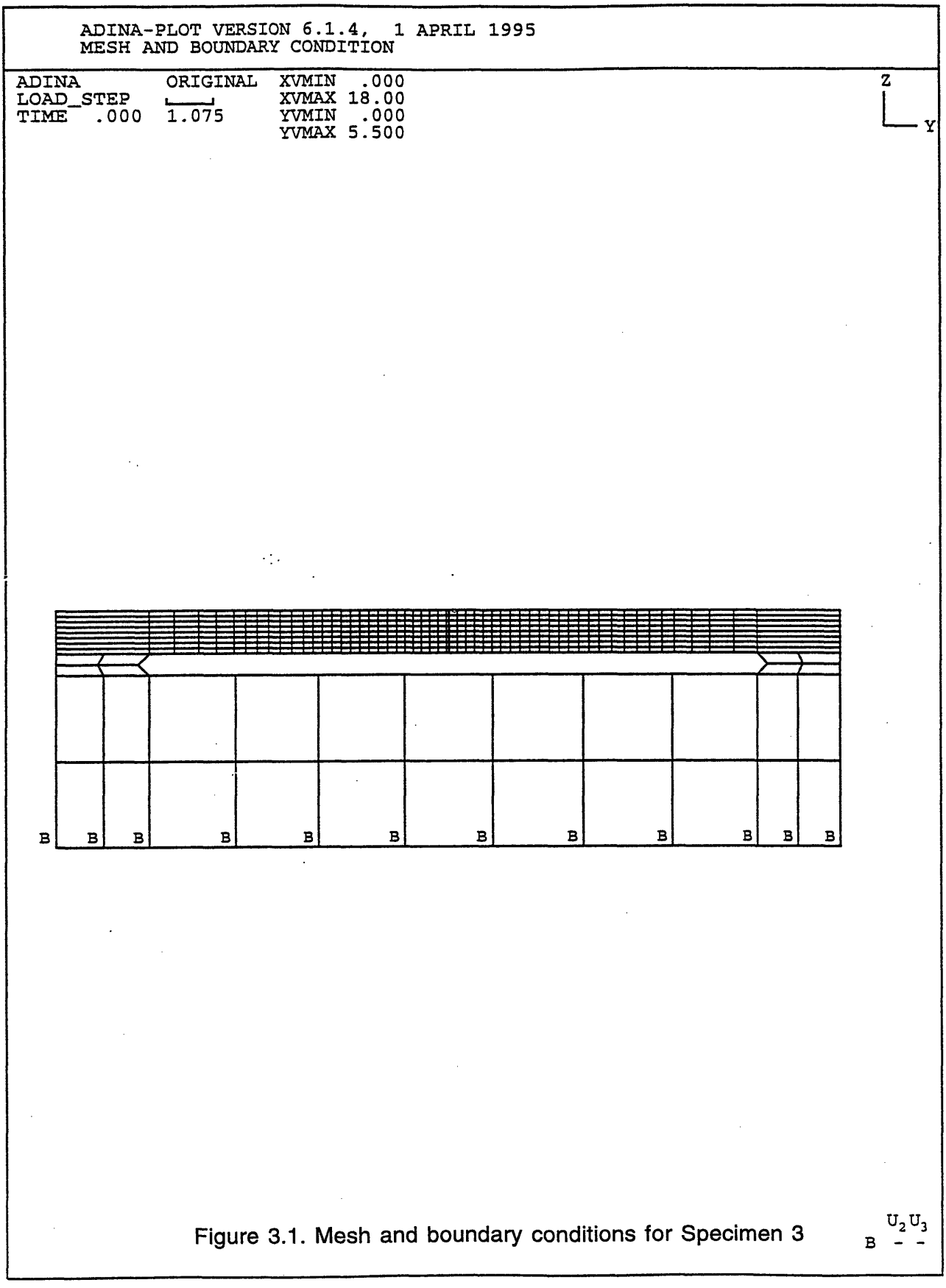

Figure 3.1. Mesh and boundary conditions for Specimen 3

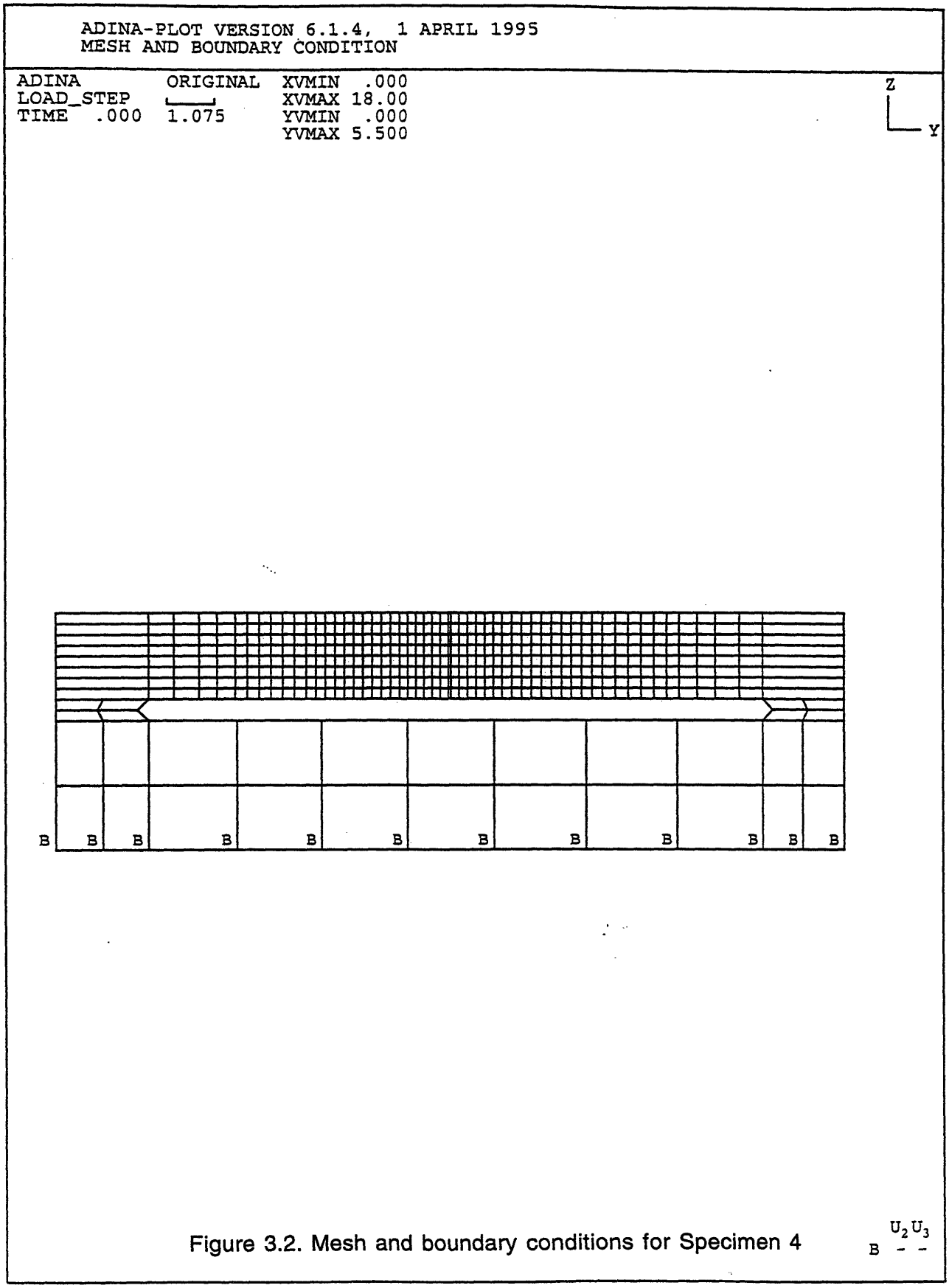

Figure 3.2. Mesh and boundary conditions for Specimen 4

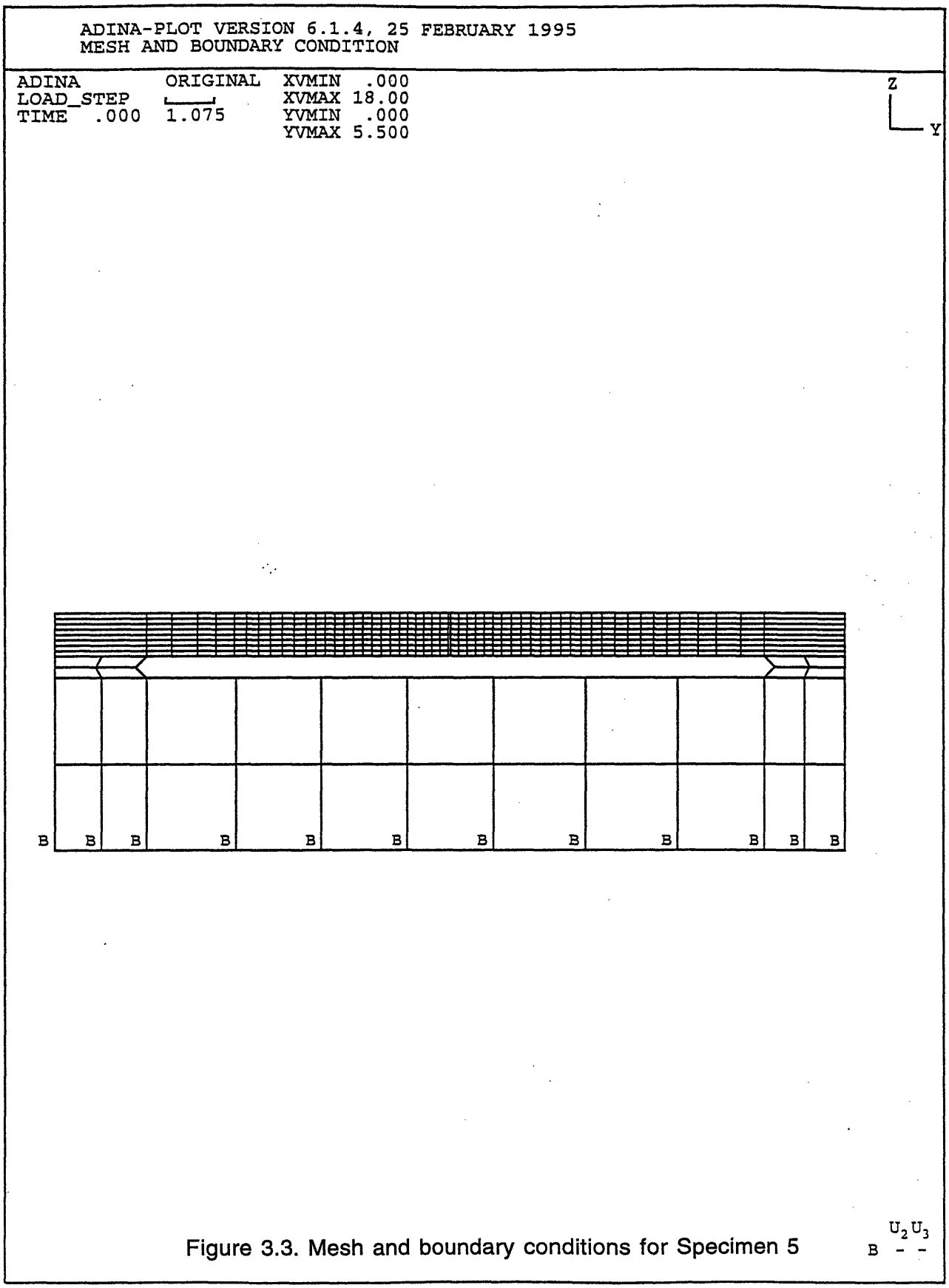

Figure 3.3. Mesh and boundary conditions for Specimen 5

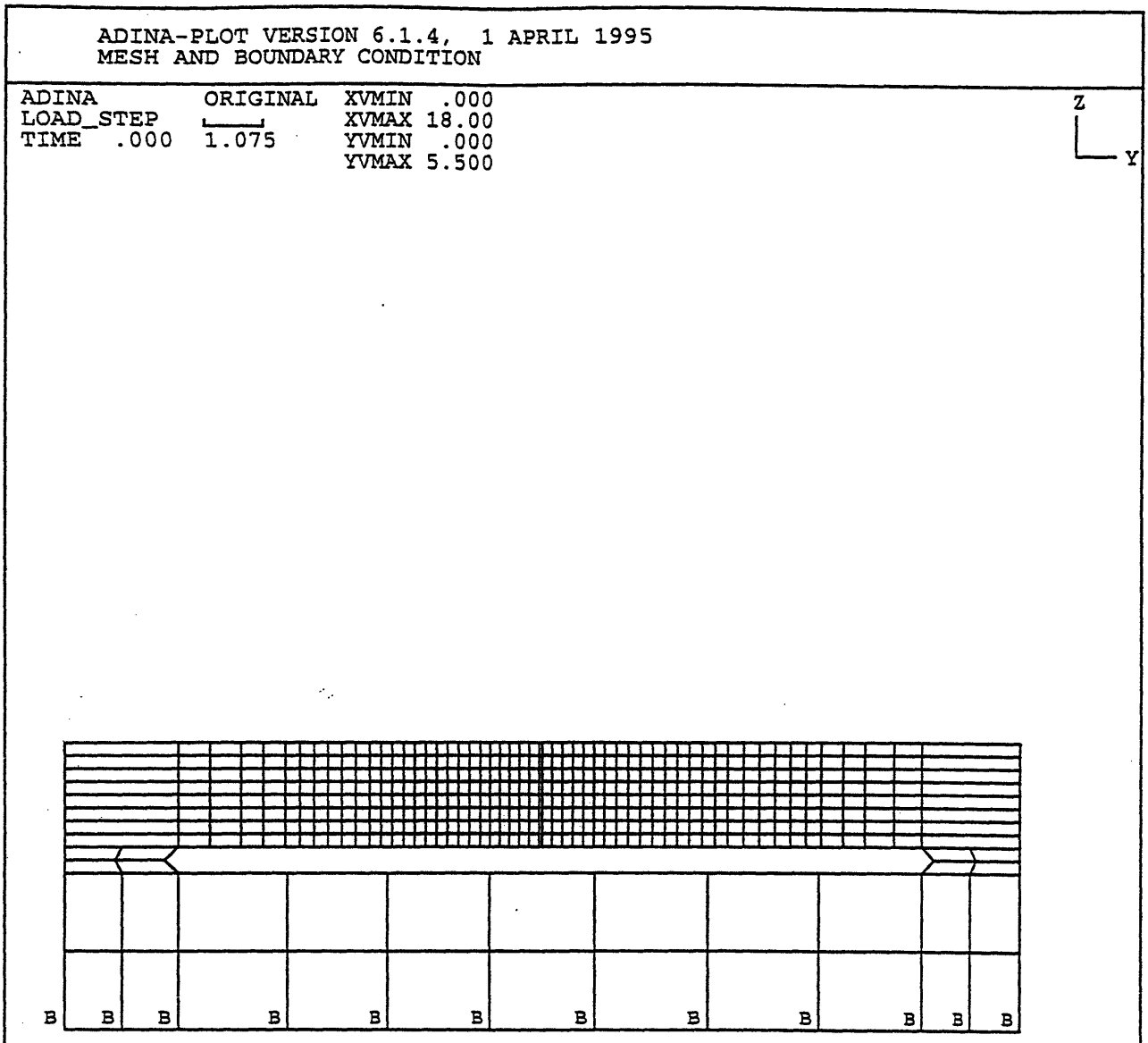

Figure 3.4. Mesh and boundary conditions for Specimen 6

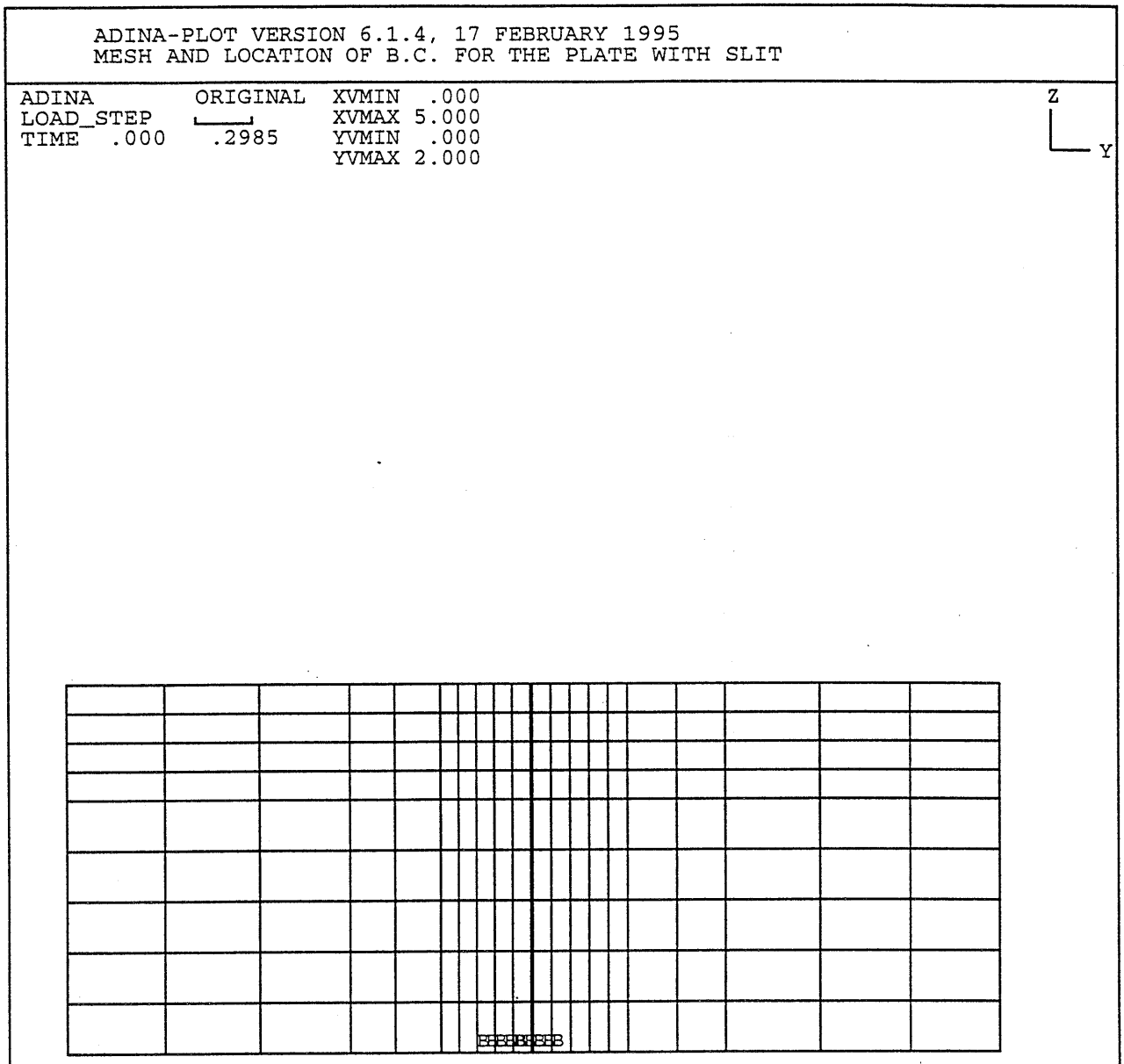

Figure 3.5. Mesh and boundary conditions for Specimen 7

3.1.2. Specimens with Slits Vs Specimens without Slits

The specimens can be classified into two groups: the specimens with slits and those without slits.

For the specimens with slits, before and during the welding, there were no connections in the slits. During some period of the welding, the materials in the vicinity of the welding region melted and became molten pools. Then, after the welding, the molten pools solidified causing the slits to be connected.

The whole process during and after the welding is shown in Figures 3.6 and 3.7.

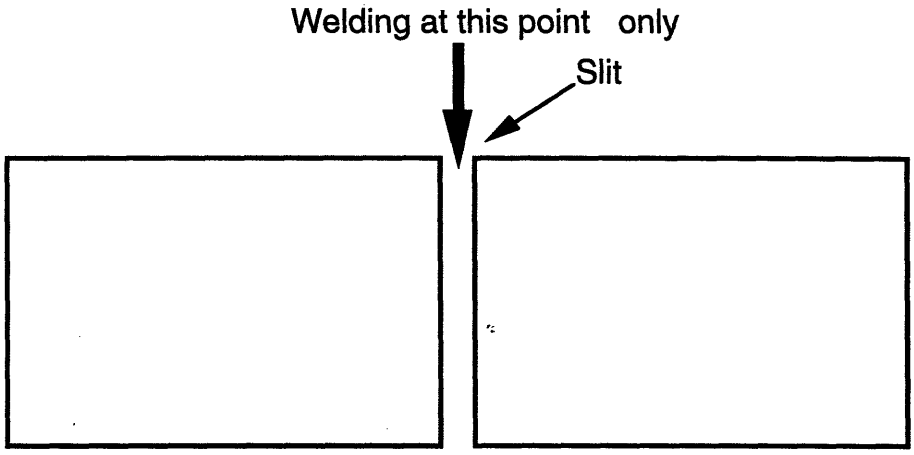

Figure 3.6. A specimen with a slit, before and during welding

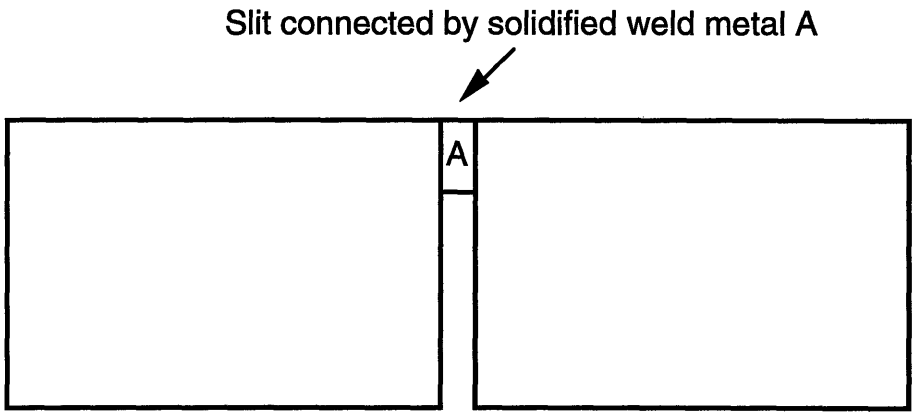

Figure 3.7. The same specimen after the weld metal solidifies

These unconnected conditions before and during the welding, of course, do not occur in the specimens without slits.

The conditions explained in the previous paragraphs were taken into account in both ADINA-T and ADINA programs by using available element birth option. Using this option, the elements in the slits which simulate the solidified weld metals did not exist during the welding. They only started to exist immediately after the welding. These were done by specifying the element birth of these weld metals to be after the welding was completed. Of course, the element birth options were used only in the specimens with slits. For the specimens without slits, all the elements started to exist at time equaled to zero.

3.1.3. Welding Arc Heat Input Distribution

As mentioned before, the welding arc heat input distribution was modelled using Gaussian's normal distribution. Figure 3.8 shows Gaussian's normal distribution.

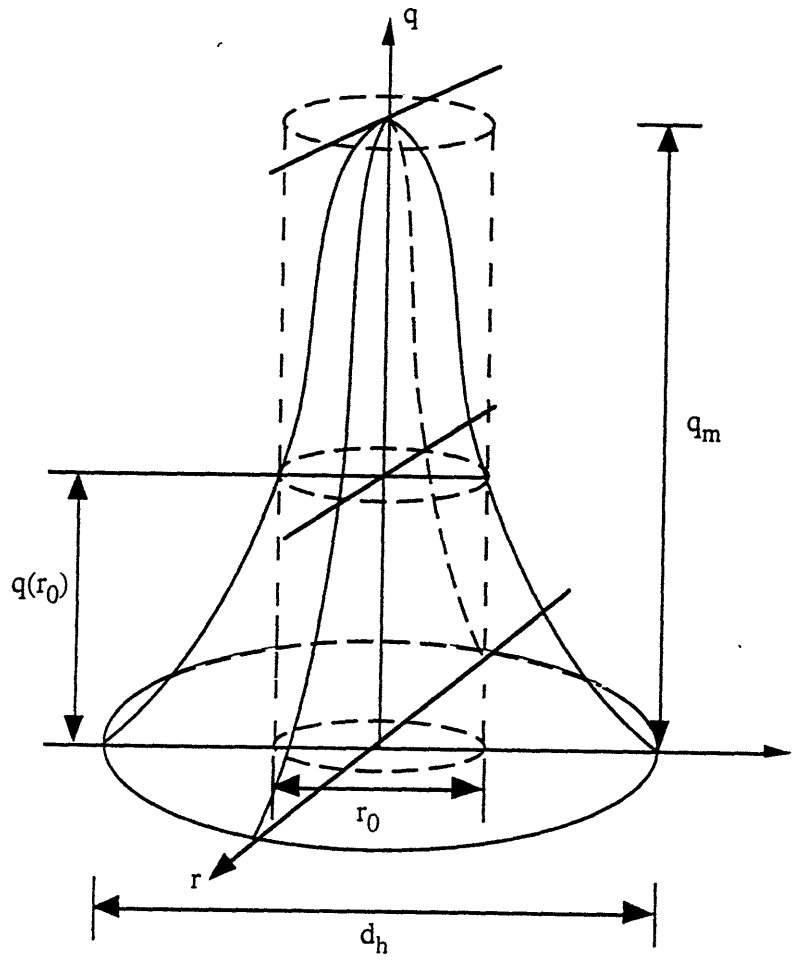

Figure 3.8. Gaussian's normal distribution

Heat flux at any point inside the Gaussian's surface is calculated by using the following formula:

$$q(r) = q_{\max} e^{-kr^2} \quad \text{.....(3.1)}$$

where :

$q(r)$:	heat flux at any point inside the Gaussian's surface
$q_{\max}$:	heat flux at r = 0
k:	a coefficient
r:	radial distance

Below are the derivations to obtain formulas for $q_{\max}$ and k.

$$Q = \eta VI$$

where:

Q: total welding heat input

η: efficiency of welding process

V: voltage of welding process

I: current of welding process

$$Q = \int_0^{\infty} q(r) 2\pi r dr$$

$$Q = 2\pi q_{\max} \int_0^{\infty} r e^{-kr^2} dr$$

$$Q = \frac{\pi q_{\max}}{k}$$

$$q_{\max} = \frac{Qk}{\pi} \quad \text{.....(3.2)}$$

$r_h = 0.5 d_h$ is defined to be a location on which the value of $q(r)$ is $0.05 q_{\max}$. Therefore,

$$q(r_h) = 0.05 q_{\max} = q_{\max} e^{-kr_h^2}$$

$$e^{-kr_h^2} = 0.05$$

$$kr_h^2 = 3.0$$

$$k = \left[\frac{3.46}{d_h}\right]^2 \quad \text{.....(3.3)}$$

By substituting equations (3.2) and (3.3) into equation (3.1), heat flux at any point inside the Gaussian's surface can be expressed as the following:

$$q = q\left[\eta, V, I, d_h, r\right] \quad \text{.....(3.4)}$$

3.1.4. Initial Conditions

In ADINA-T, initial temperature for every point on the specimens needs to be specified. Otherwise, it will be set to a default value of zero. The initial temperature is the temperature at a time equal to zero.

For the specimens without slits, the initial temperature at every point on the specimens was specified to be the same as the surrounding temperature.

For the specimens with slits, there were two types of initial temperatures. At every point not located at the slits, the initial temperature was specified to be the same as the surrounding temperature. At every point located at the slits, the initial temperature was specified to be the same as the temperature at its closest neighbor point at the time when the slits started to connect.

3.1.5. General Heat Transfer Formulas

Bathe and co-workers [6,7,20] formulated the following heat transfer equations for the finite element method.

$$\frac{\partial}{\partial x}\left[\lambda_x \frac{\partial \theta}{\partial x}\right] + \frac{\partial}{\partial y}\left[\lambda_y \frac{\partial \theta}{\partial y}\right] + \frac{\partial}{\partial z}\left[\lambda_z \frac{\partial \theta}{\partial z}\right] = -q^B \quad \text{.....(3.5)}$$

$$\theta|_{S1} = \theta_e \quad \text{.....(3.6)}$$

$$\lambda_n \frac{\partial \theta}{\partial n}\bigg|_{S2} = q^S \quad \text{.....(3.7)}$$

where:

$\theta|_{Si}$: surface temperature of the body

θ_e: temperature of environment

λ_n: thermal conductivity of the body

η: normal direction

q^S: heat flow on the surface of the body

Equation 3.5 is a heat flow equilibrium equation that is valid inside the body, while equations 3.6 and 3.7 are valid on the surface of the body.

By using the variational principle, the heat conduction and its associated boundary conditions can be written as the following:

$$\Pi = \int_V \frac{1}{2}\left\{\left[\lambda_x \frac{\partial \theta_e}{\partial x}\right]^2 + \left[\lambda_y \frac{\partial \theta}{\partial y}\right]^2 + \left[\lambda_z \frac{\partial \theta}{\partial z}\right]^2\right\} dV$$

$$- \int_V \theta q^B dV - \int_{\Gamma_2} \theta^S q^S dS - \sum_i \theta^i Q^i \quad \text{.....(3.8)}$$

With the stationarity of Π, the heat flow equilibrium at time $t + \alpha\Delta t$ can be obtained as the following:

$$\int_V \delta\theta' T_{t+\alpha\Delta t} \lambda_{t+\alpha\Delta t} \theta' dV = {}_{t+\alpha\Delta t}Q + \int_{S_c} \delta\theta^S {}_{t+\alpha\Delta t} h \left[{}_{t+\alpha\Delta t}\theta_e - {}_{t+\alpha\Delta t}\theta^S \right] dS$$

$$- \int_{S_r} \delta\theta^S {}_{t+\alpha\Delta t} \chi \left[{}_{t+\alpha\Delta t}\theta_r - {}_{t+\alpha\Delta t}\theta^S \right] dS \quad \text{.....(3.9)}$$

where:

θ^S: surface temperature of the body

θ_e: temperature of the environment

θ_r: radiating surface temperature

δ: variation symbol

χ: radiation coefficient

S_c: convection surface area

S_r: radiation surface area

θ'^T: $\theta'^T = \left[\frac{\partial\theta}{\partial x} + \frac{\partial\theta}{\partial y} + \frac{\partial\theta}{\partial z}\right]$

λ: $\begin{bmatrix} \lambda_x & 0 & 0 \\ 0 & \lambda_y & 0 \\ 0 & 0 & \lambda_z \end{bmatrix}$

Then, by linearization of equation (3.9), the following heat flow equilibrium for a single element is obtained:

$$\left[{}^tK\lambda + {}^tKc + {}^tKr\right]\Delta\theta^{(i)} = {}^{t+\alpha\Delta t}Q + {}^{t+\alpha\Delta t}Q^{c(i-1)}$$

$$+ {}^{t+\alpha\Delta t}Q^{r(i-1)} - {}^{t+\alpha\Delta t}Q^{\lambda(i-1)} \quad \text{.....(3.10)}$$

where:

$${}^{t+\alpha\Delta t}\theta^{(i)} = {}^{t+\alpha\Delta t}\theta^{(i-1)} + \Delta\theta^{(i)} \quad \text{.....(3.11)}$$

3.1.6. Heat Conduction

As described before, heat travels by conduction inside the body. To simulate heat conduction, ADINA-T requires input of the physical properties of the specimens, i.e. thermal conductivity, specific heat and density of both low carbon and stainless steels. The physical properties of both materials are temperature dependent. Table 3.1 lists the values of thermal conductivity, specific heat and density of low carbon steel, and figures 3.9 and 3.10 show the values of thermal conductivity and specific heat of stainlees steel.

Temperature, Θ (°F)	Conductivity, κ (Btu/hr.ft.°F)	Specific Heat, c (Btu/lbm.°F)	Density, ρ (lbm/in^3)
70	20.02	0.102	0.284
200	20.88	0.110	0.283
400	21.29	0.120	0.282
600	21.01	0.132	0.280
800	20.68	0.148	0.279
1000	19.49	0.166	0.277
1200	20.06	0.178	0.276
1400	14.91	0.190	0.275
1600	15.29	0.173	0.275
1800	15.68	0.156	0.275
2000	15.25	0.156	0.275
2200	16.38	0.156	0.275
2400	16.69	0.156	0.275
2600	16.99	0.156	0.275

Table 3.1. Thermal conductivity, specific heat and density of low carbon steel

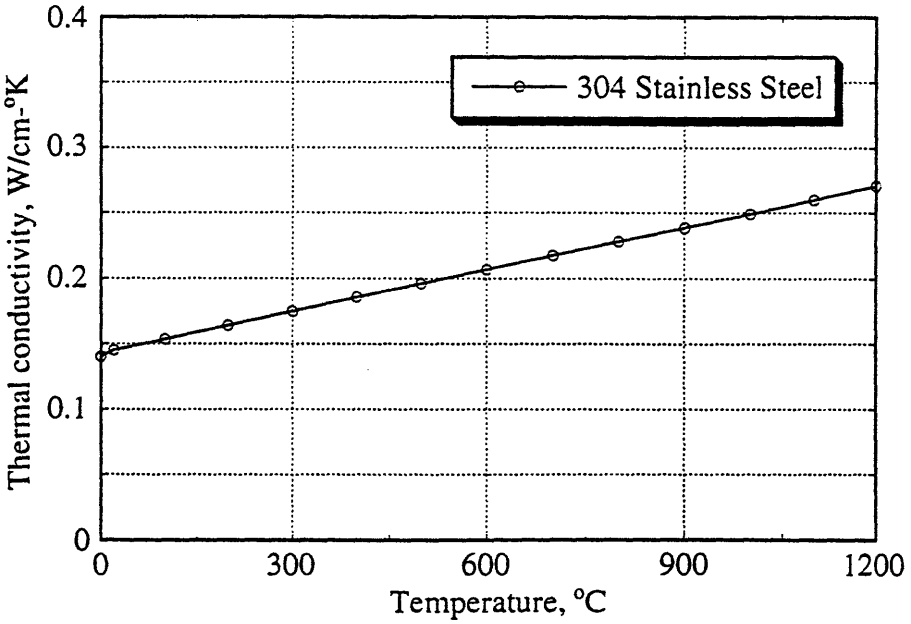

Figure 3.9. Thermal conductivity of stainless steel

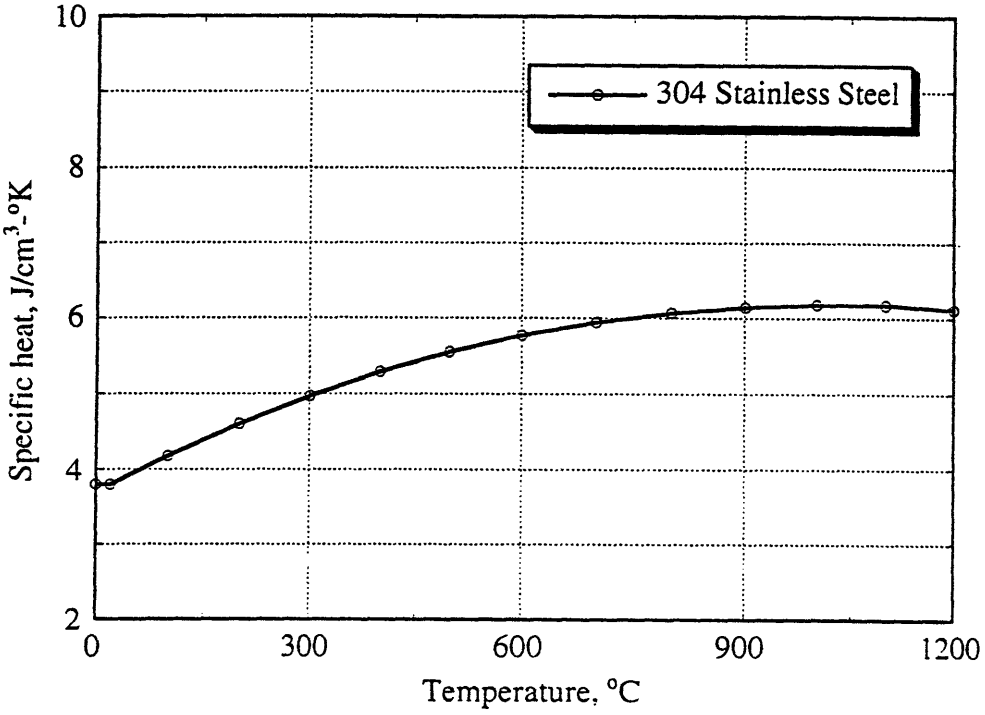

Figure 3.10. Specific heat of stainless steel

3.1.7. Boundary Conditions

The specimens had two types of boundary conditions, i.e. convection and radiation boundary conditions.

In ADINA-T, the convection boundary condition is modelled as the following:

$$q^S = h\left[\theta_e - \theta^S\right] \quad \text{.....(3.12)}$$

where:

q^S: heat flow from the surface of the body to its surroundings

h: convection coefficient

θ_e: temperature of the surroundings

θ^S: surface temperature of the body

The values of the specimens' convection coefficient, as shown in figure 3.11, were assumed to obey the semi empirical correlation that was proposed by Lienhard [13].

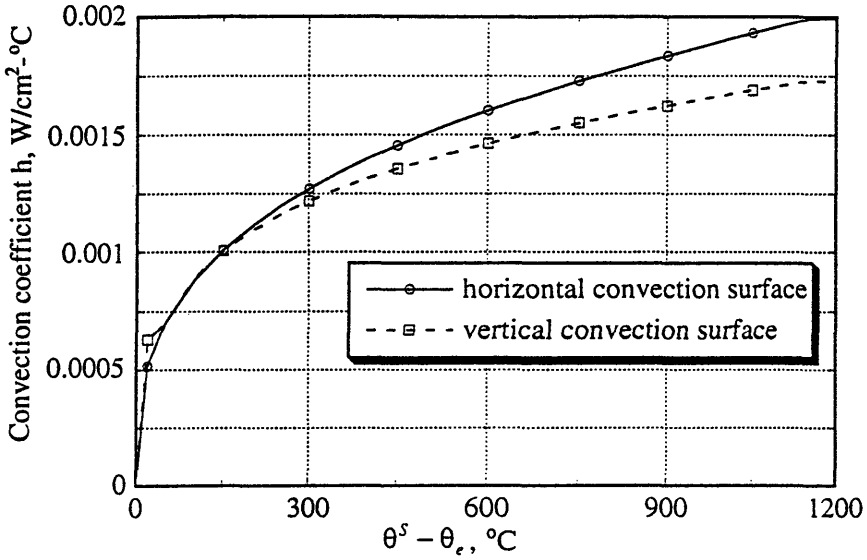

Figure 3.11. Convection coefficient of the specimens

In ADINA-T, radiation boundary condition is modelled as the following:

$$q^S = \sigma f e\left[\theta_r{}^4 - \left(\theta^S\right)^4\right] \quad \text{.....(3.13)}$$

where:

q^S: heat flow from the surface of the body to its surrounding

σ: Steffan Boltzman's coefficient

f: shape factor

e: emissivity

θ_r: temperature of the surrounding

θ^S: surface temperature of the body

The values of σ, f, and e of the specimens were 5.67×10^{-12} W/cm^{2}K^4, 1.0, and 0.8 respectively.

3.2. ADINA-T Results

Figures 3.12 through 3.14 show the temperature distributions on the surface of Specimen 5 at several different times. Shown in Figures 3.15 to 3.17 are the temperature distributions on the surface of Specimen 6 at several different times. The behaviors of the temperature distributions as time elapses on the surfaces of Specimens 5 and 6 are believed to be the same as the ones on the surfaces of Specimens 3 and 4 respectively. The reason is because Specimens 3 and 5 are almost exactly the same in terms of material type and dimension. The same reason is true for Specimens 4 and 6. In other words, the behaviors of the temperature distributions as time elapses on the surfaces of Specimens 5 and 6 can be used well enough to represent the behaviors of

the temperature distributions as time elapses on the surfaces of Specimens 3 and 4 respectively.

As shown in the figures, the temperature distributions in the specimens are radially symmetrical with the welded points as the centers. As the radial distance from the welded points increases, the temperature decreases. It is also clearly shown that the maximum temperature occurred at the welding points during the welding. Only small parts of the specimens in the vicinity of the welding zone experienced high temperature processes.

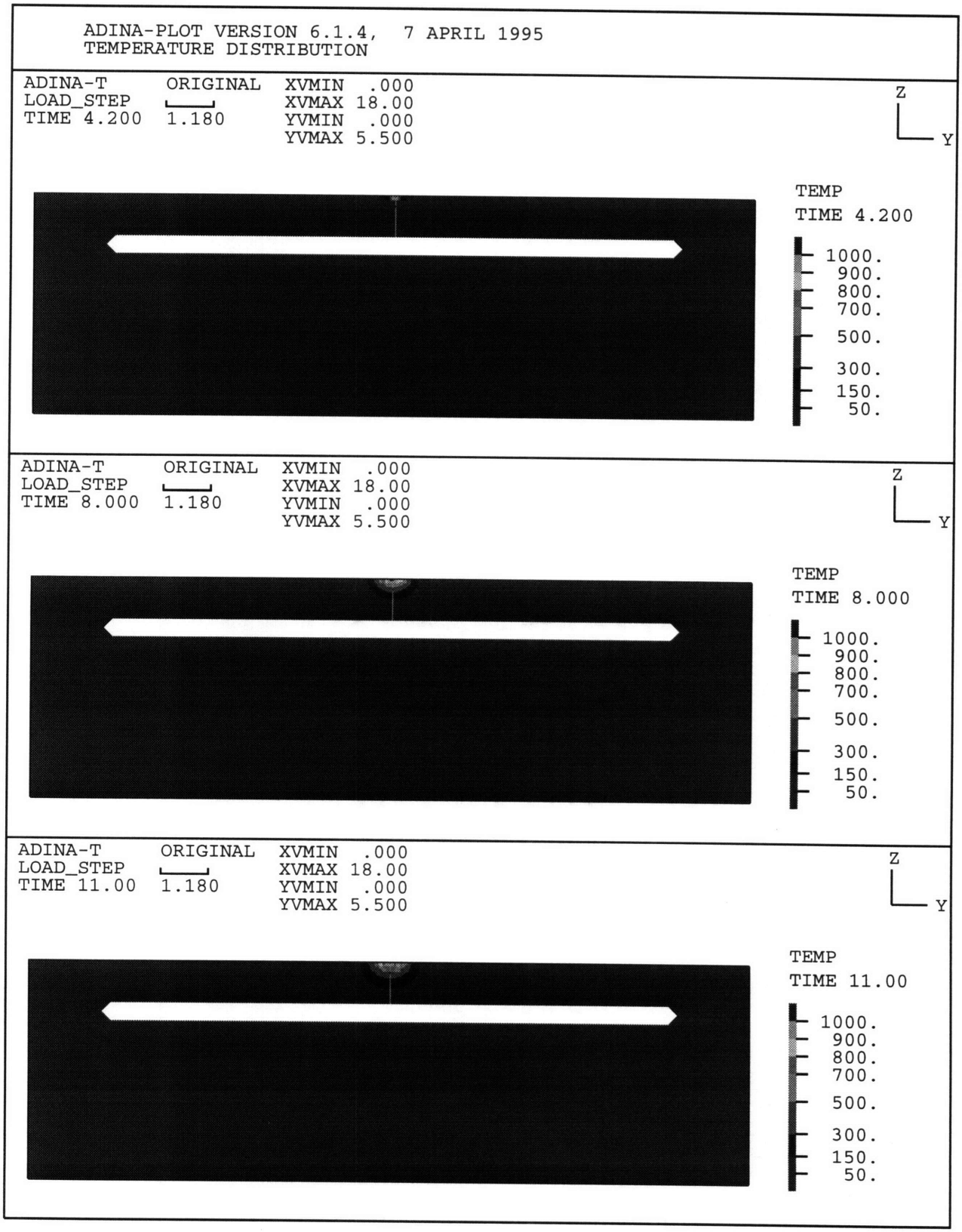

Figure 3.12. Temperature distributions on the surface of Specimen 5 at 4.2, 8.0, and 11.0 seconds

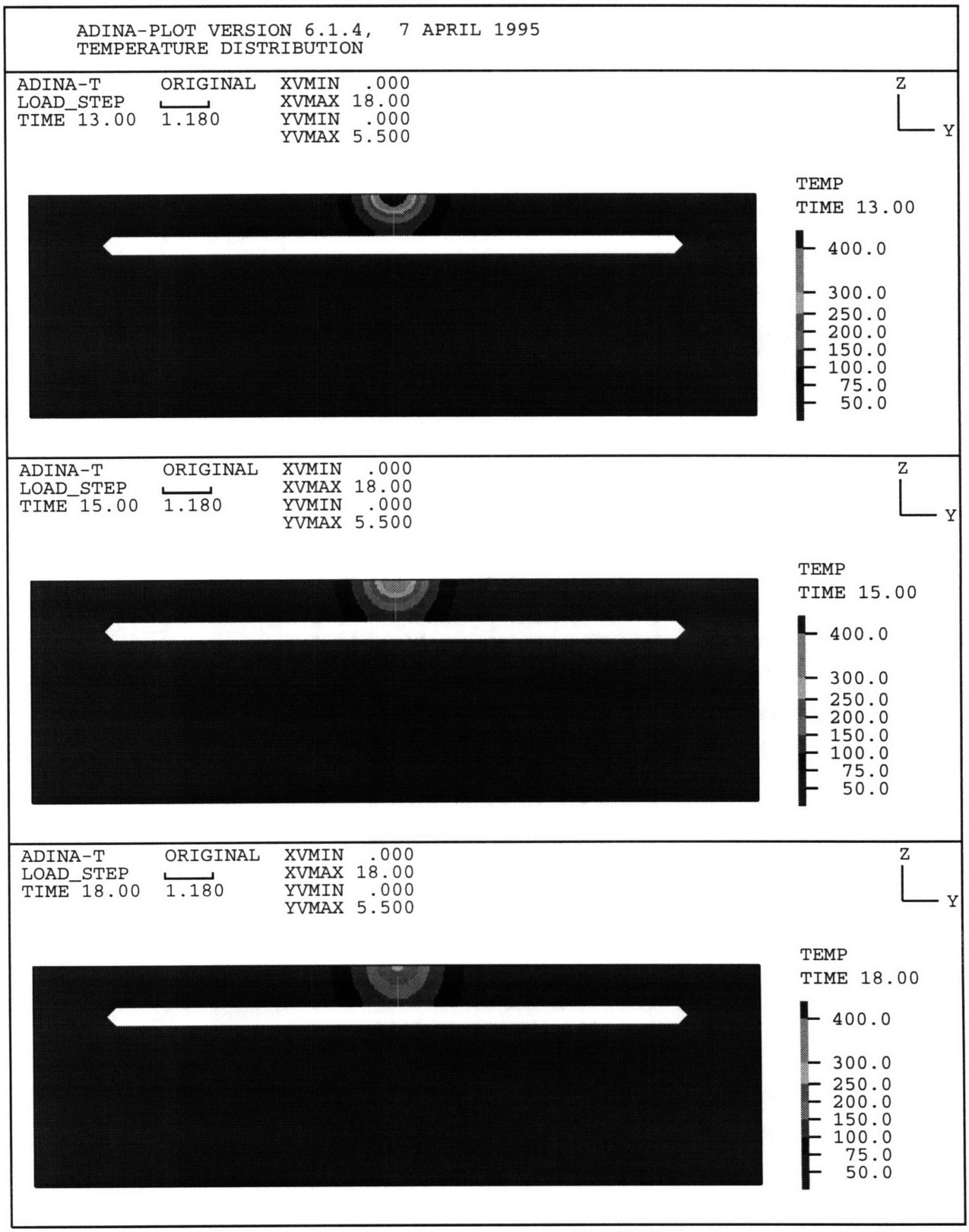

Figure 3.13. Temperature distributions on the surface of Specimen 5 at 13.0, 15.0, and 18.0 seconds

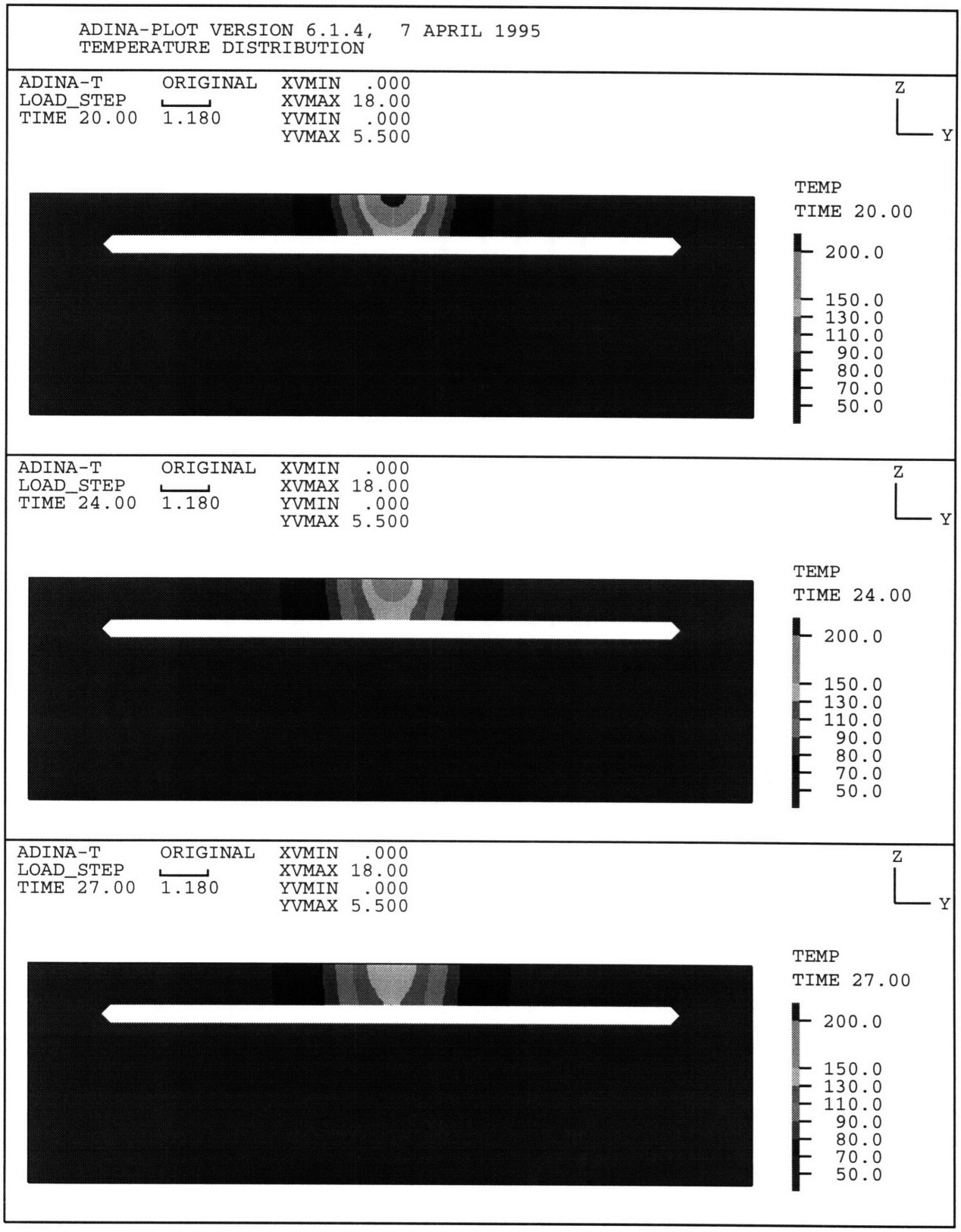

Figure 3.14. Temperature distributions on the surface of Specimen 5 at 20.0, 24.0, and 27.0 seconds

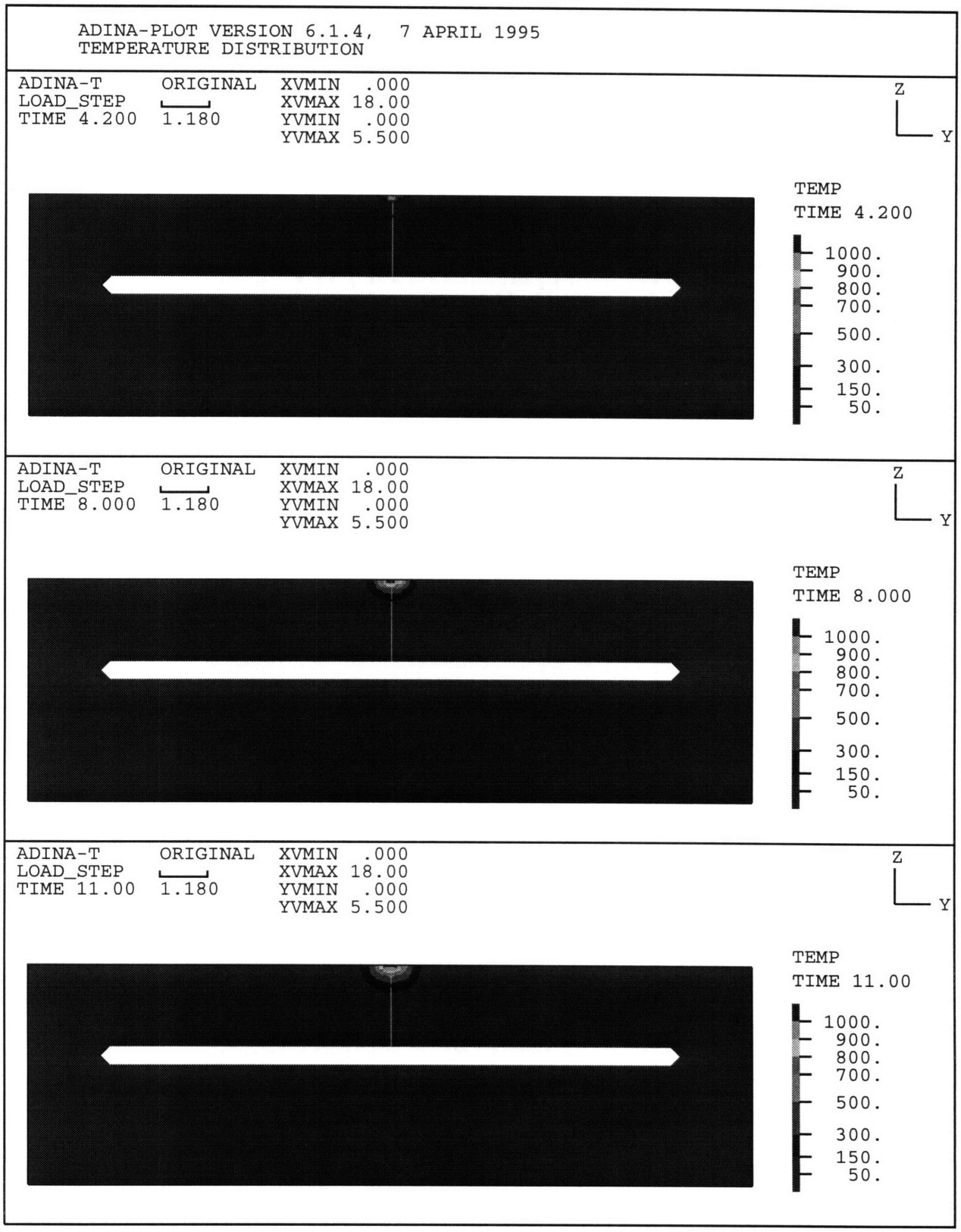

Figure 3.15. Temperature distributions on the surface of Specimen 6 at 4.2, 8.0, and 11.0 seconds

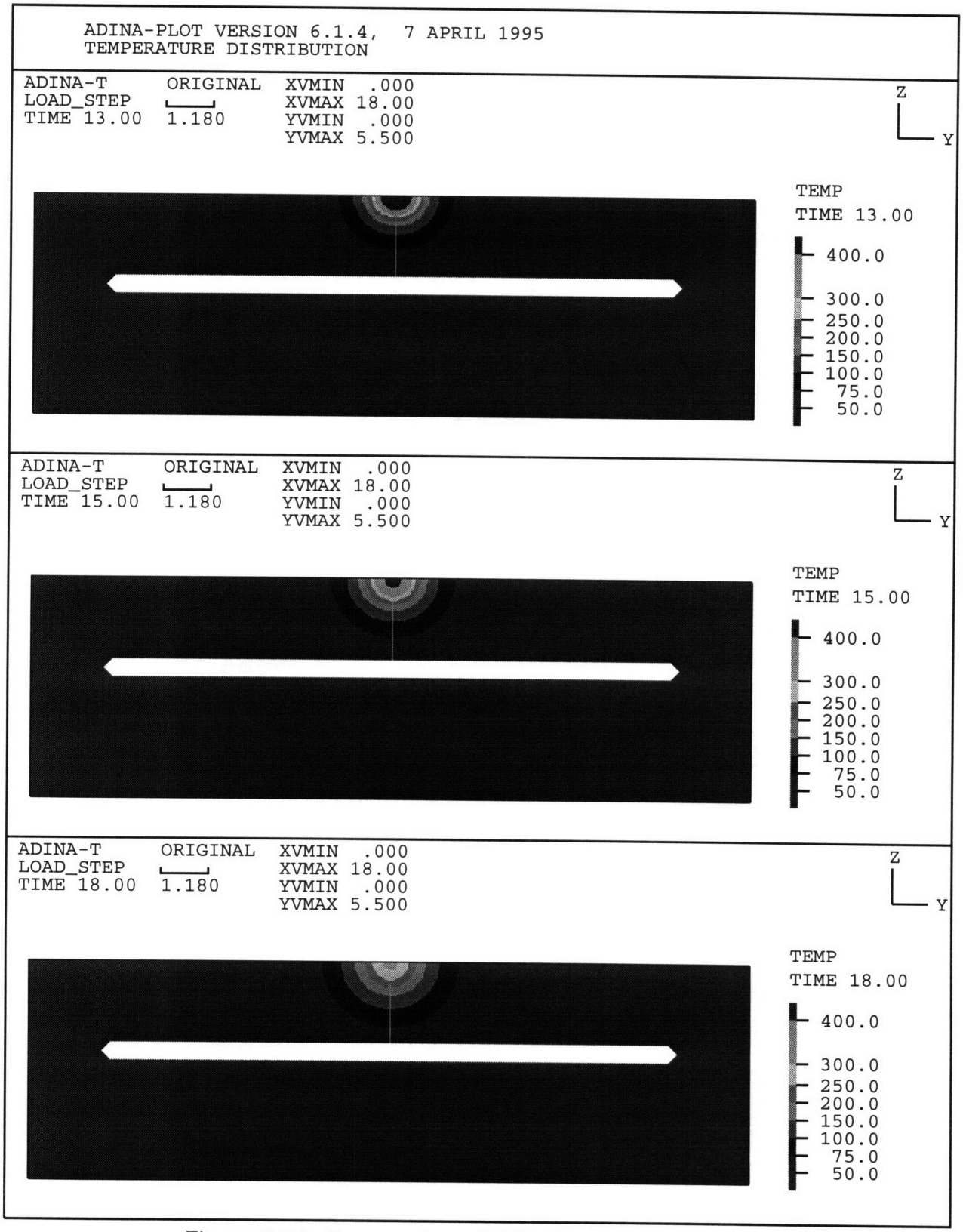

Figure 3.16. Temperature distributions on the surface of Specimen 6 at 13.0, 15.0, and 18.0 seconds

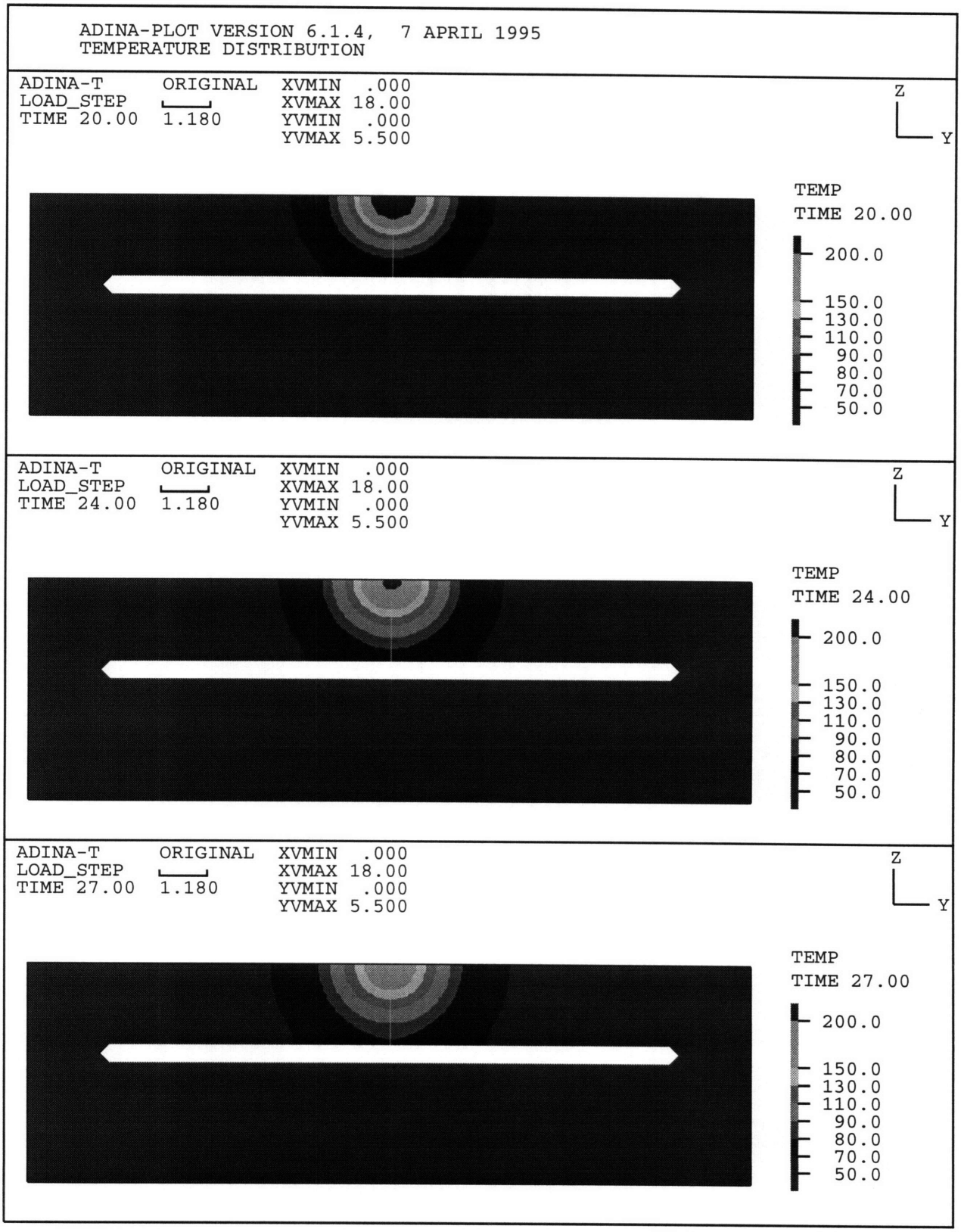

Figure 3.17. Temperature distributions on the surface of Specimen 6 at 20.0, 24.0, and 27.0 seconds

Shown in Figures 3.18 through 3.20 are the heat flux distributions on Specimen 7 at several different times. Heat flux always travels from a higher temperature point to a lower temperature point. It is shown clearly that the heat fluxes travelled from the welded spot to the bottom left and right corners of the plate. This means that the highest temperature region is the welding spot and the lowest temperature region is furthest from the welding spot.

Shown in Figures 3.21 through 3.23 are the temperature distribution on Specimen 7 at several different times. As in Specimens 3 through 6, the temperature distribution is radially symmetrical with the welding spot as the center. As the radial distance from the welded spot increases, the temperature decreases. In Specimens 3 through 6, only a small part of the plate experienced high temperature process.

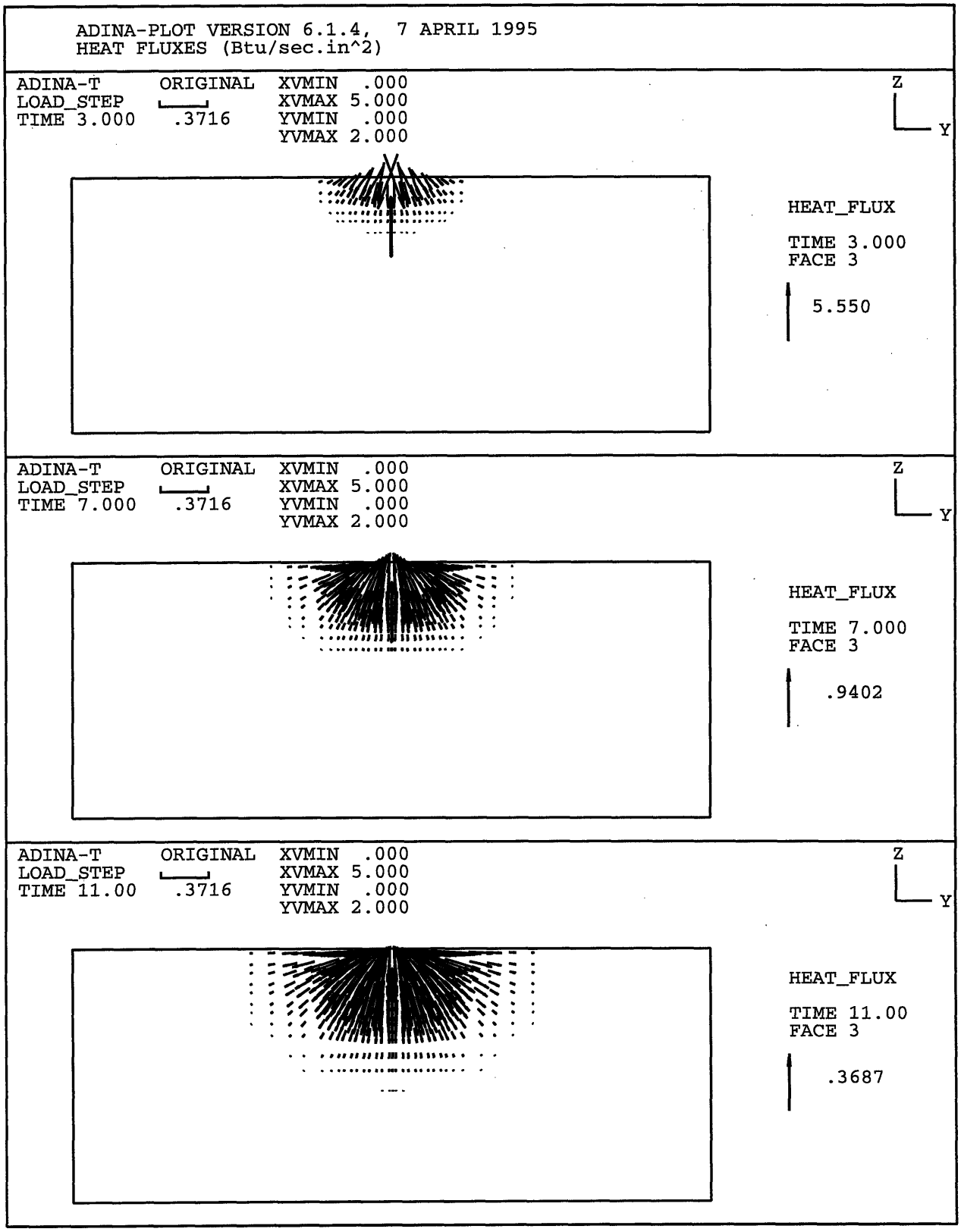

Figure 3.18. Heat fluxes on the surface of Specimen 7 at 3.0, 7.0, and 11.0 seconds

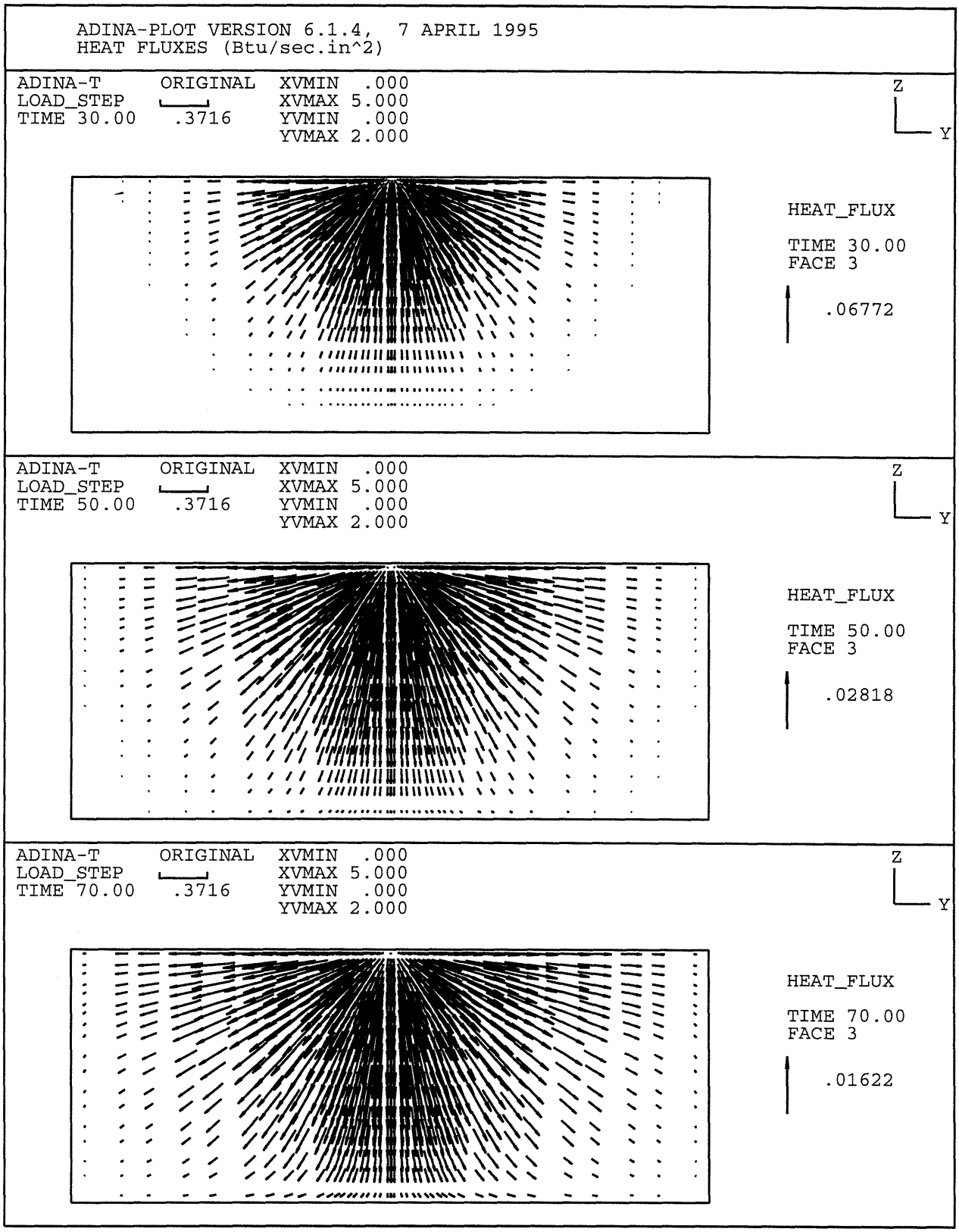

Figure 3.19. Heat fluxes on the surface of Specimen 7 at 30.0, 50.0, and 70.0 seconds

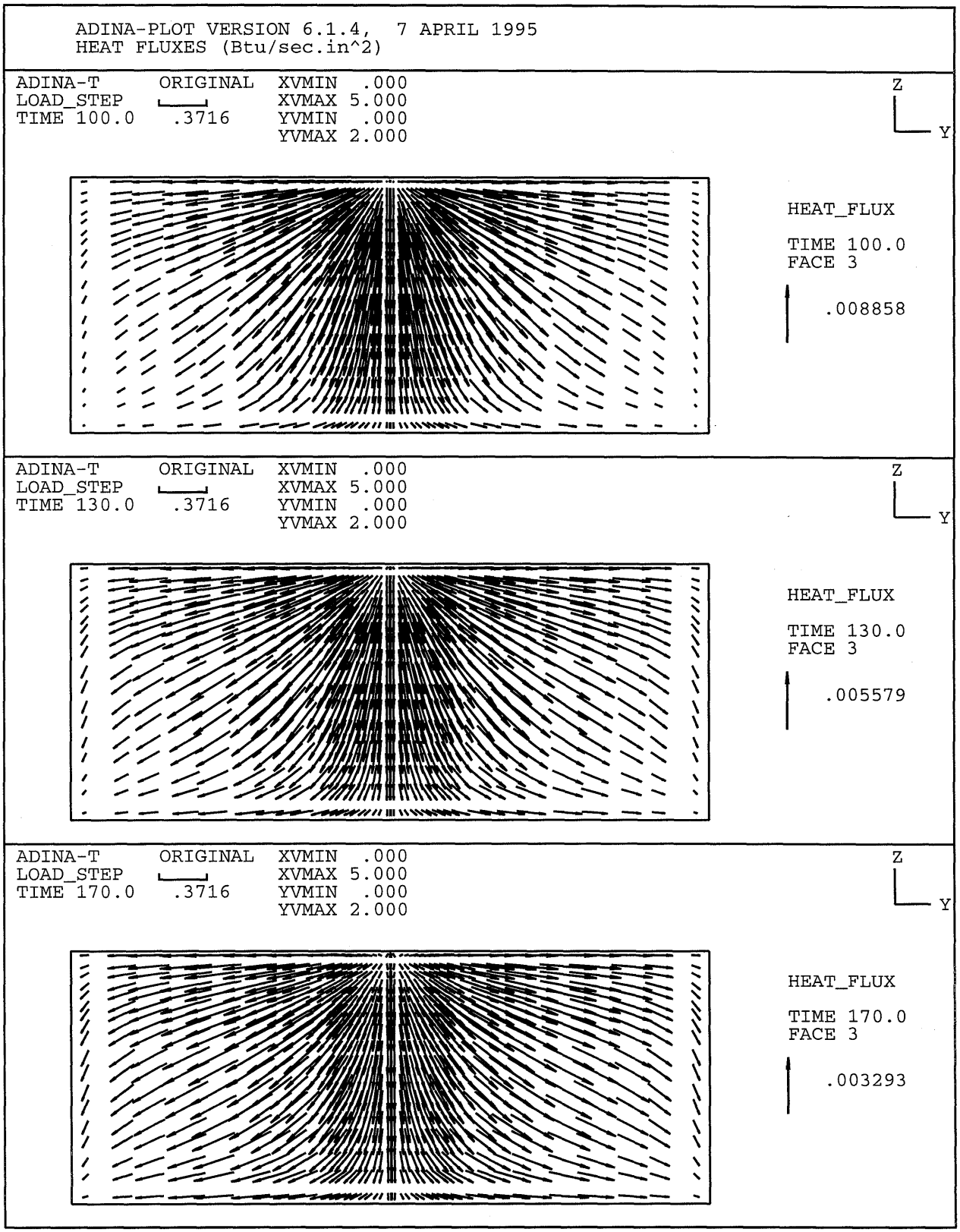

Figure 3.20. Heat fluxes on the surface of Specimen 7 at 100.0, 130.0, and 170.0 seconds

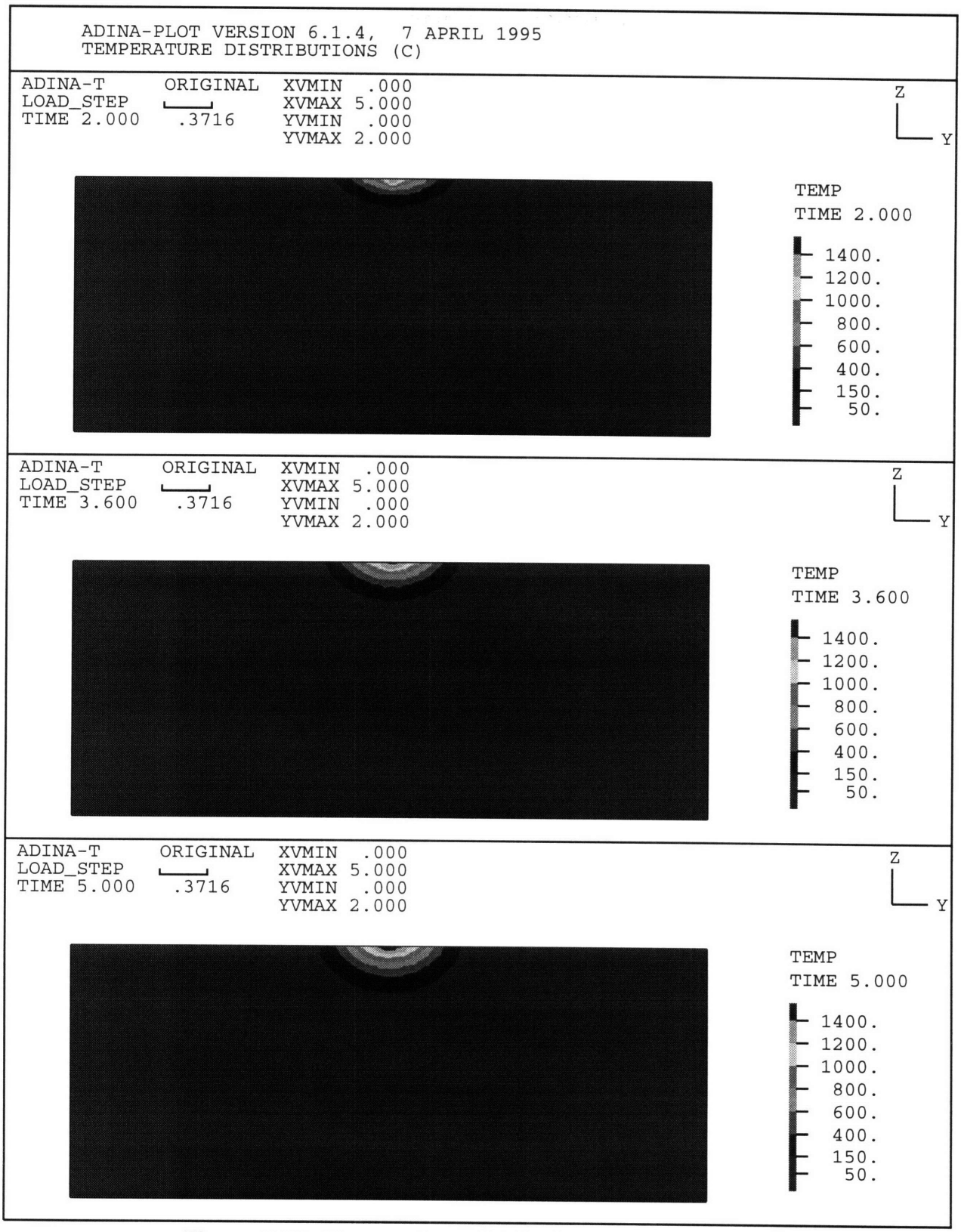

Figure 3.21. Temperature distributions on the surface of Specimen 7 at 2.0, 3.6, and 5.0 seconds

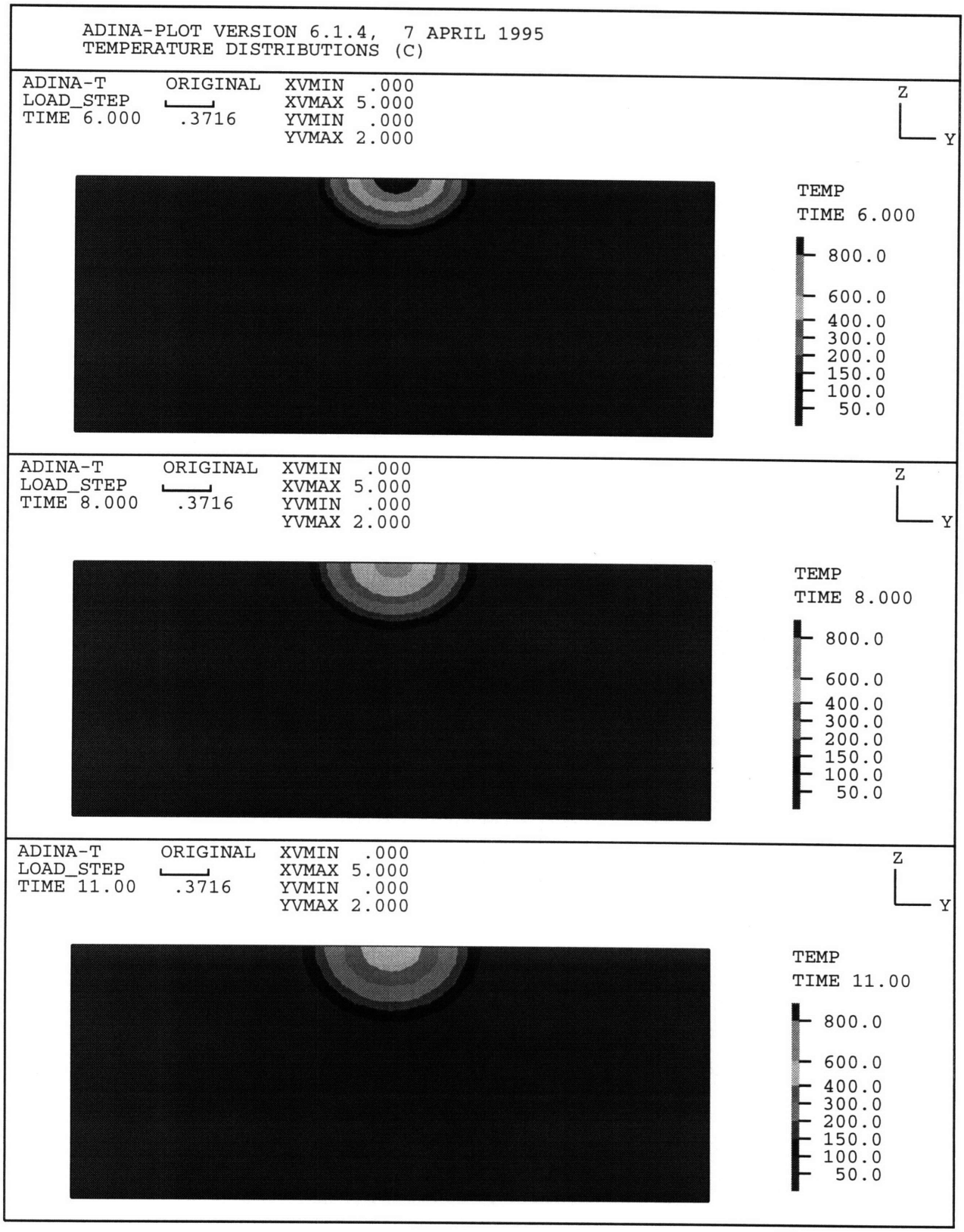

Figure 3.22. Temperature distributions on the surface of Specimen 7 at 6.0, 8.0, and 11.0 seconds

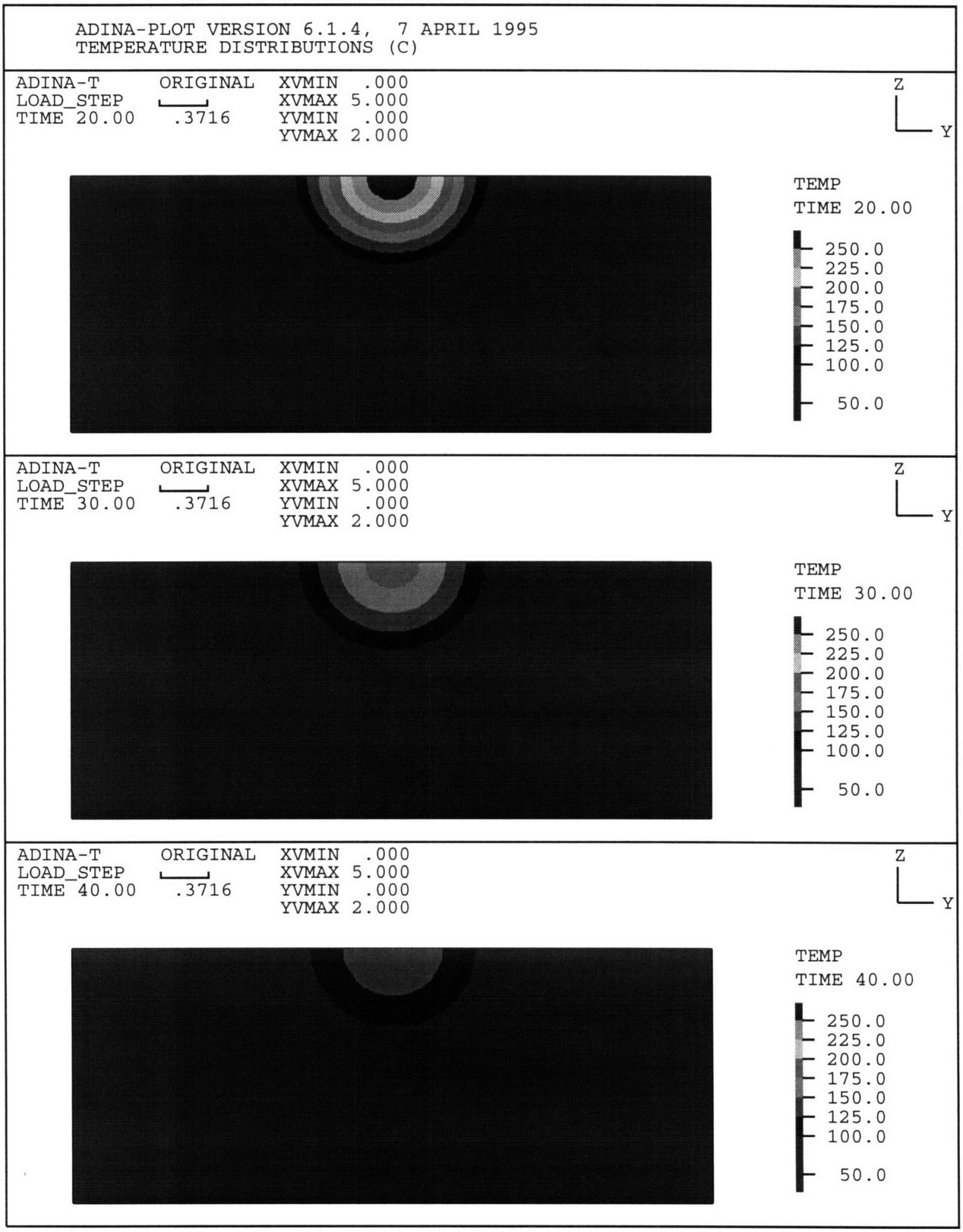

Figure 3.23. Temperature distributions on the surface of Specimen 7 at 20.0, 30.0, and 40.0 seconds

3.3. ADINA Analysis

3.3.1. Mesh

For every specimen, the mesh design in ADINA program was exactly the same as its mesh design in ADINA-T program. Otherwise, the ADINA program cannot be run. In particular, related to the ADINA program, plane stress models were assumed for Specimens 3 through 7. By using the plane stress models in the ADINA program, Goktug [11] investigated a specimen similar to Specimen 7. He reported that the ADINA results agreed with his experimental data. For this reason, the plane stress models were assumed for Specimens 3 through 7.

Using the plane stress model, σ_{xx}, τ_{xy}, and τ_{xz} were zero. Figure 3.24 shows how the plane stress model looks.

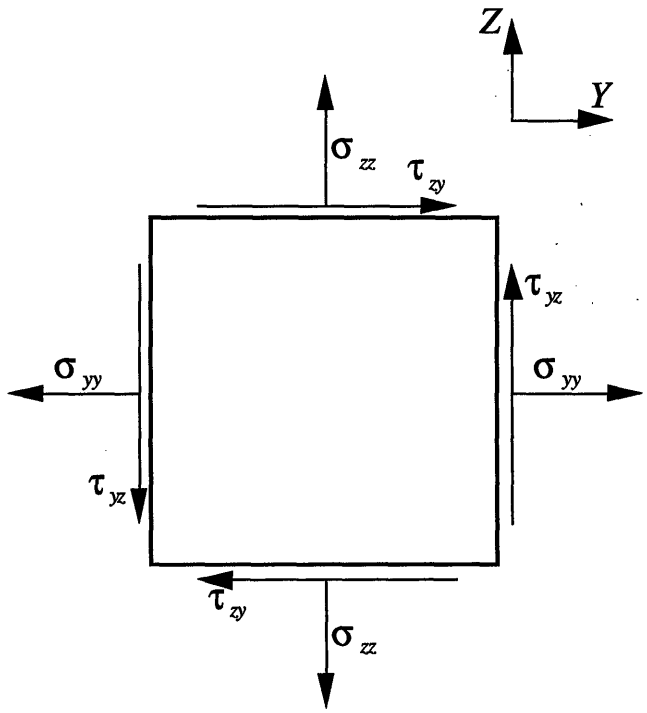

Figure 3.24. Plane stress state

3.3.2. Initial Conditions

For the specimens without slits, initial values of strain and stress on every point were assumed to be zero. The initial values of strain and stress were the values of strain and stress at the initial temperature, i.e. the surrounding temperature. By assuming this condition, the specimens have been assumed to be the ideal specimens. In reality, the specimens should have some values of initial strain and stress from previous works applied onto them.

For the specimens with slits, the initial values of strain and stress on every point not located in the slits were also zero. However, since the initial temperature for every point located in the slits was higher than the surrounding temperature, the initial values of strain and stress there were not zero.

3.3.3. Boundary Conditions

Boundary condition is one of the most important inputs in ADINA program because it describes how a specimen is supported. In particular, the boundary condition command in the ADINA program specifies directions in which a point is fixed.

For Specimens 3 through 6, their boundary conditions are shown in Figures 3.1 through 3.4. All the points located at the bottom edges of Specimens 3 through 6 were fixed in the Y and Z directions. These boundary conditions describe that the bottom edges of the specimens were not affected by the heat from the welding arcs. It is possible to assume this because the specimens were relatively large.

For Specimen 7, the boundary condition is shown in Figure 3.5. Only a few points located at the center of the bottom edge were fixed in the Y and Z directions. This boundary condition simulates the tack welding applied to the center of the bottom edge of the plate as shown in Figure 2.11.

3.3.4. Load

Non-uniform temperature distribution is created in a specimen when welding is applied to the specimen. This is because the welding is applied only to a small region of the specimen. As a consequence, different points on the specimen expand at different rates. In other words, incompatible strain distribution is created in the specimen. This incompatible strain distribution, in turn, creates stress and distortion in the specimen. From this process, it can be concluded that the heat from the welding is the initial source of the stress and distortion in the specimen.

In this investigation, the temperature distributions in the specimens at all stages were calculated in ADINA-T. These temperature distributions were used as load inputs in the ADINA program.

3.3.5. Material Properties

In ADINA, mechanical properties of the specimens are required as inputs. Listed in Table 3.2 are the mechanical properties of low carbon steel.

Θ: temperature (^{0}F)

E: Young's modulus (ksi)

v: Poisson's ratio

σ: yield stress (ksi)

E_t: tangent modulus (ksi)

α: linear expansion coeff. (in/in.^{0}F)

Θ	σ	E	E_t	v	α
70	36.0	30.0E+3	1.6E+3	0.3	6.55E-6
200	32.0	29.6E+3	1.58E+3	0.308	6.55E-6
400	29.0	28.8E+3	1.54E+3	0.324	6.97E-6
600	25.0	27.7E+3	1.48E+3	0.338	7.35E-6
800	22.0	26.0E+3	1.39E+3	0.349	7.75E-6
1000	17.0	22.7E+3	1.21E+3	0.369	8.06E-6
1200	14.2	14.0E+3	0.75E+3	0.376	8.5E-6
1400	6.0	5.0E+3	0.27E+3	0.384	8.15E-6
1600	3.0	4.2E+3	0.23E+3	0.391	6.95E-6
1800	1.0	3.0E+3	0.16E+3	0.415	7.0E-6
2000	0.8	2.1E+3	0.11E+3	0.423	7.23E-6
2200	0.7	1.2E+3	0.06E+3	0.447	7.3E-6
2400	0.1	0.3E+3	0.01E+3	0.465	7.5E-6
2600	0.0	0.0	0.0	0.464	7.5E-6

Table 3.2. Mechanical properties of low carbon steel

Listed in Table 3.3 are mechanical properties of a stainless steel.

Θ:	temperature (^{0}C)	σ:	yield stress (N/cm^2)
E:	Young's modulus (N/cm^2)	E_t:	tangent modulus (N/cm^2)
v:	Poisson's ratio	α:	linear expansion coeff. (μcm/cm.^{0}C)

Θ	σ	E	E_t	v	α
20	25.4E+6	21.0E+6	0.53E+6	0.288	17.02
38	24.4E+6	20.0E+6	0.5E+6	0.297	17.06
93	21.1E+6	19.2E+6	0.48E+6	0.302	17.22
149	19.1E+6	18.8E+6	0.47E+6	0.307	17.37
204	17.6E+6	18.4E+6	0.46E+6	0.310	17.53
260	16.6E+6	17.9E+6	0.45E+6	0.313	17.69
316	15.5E+6	17.7E+6	0.44E+6	0.315	17.85
371	15.0E+6	17.0E+6	0.43E+6	0.317	18.01
427	14.3E+6	16.6E+6	0.42E+6	0.319	18.17
538	13.2E+6	15.5E+6	0.39E+6	0.322	18.48
593	12.5E+6	15.0E+6	0.38E+6	0.323	18.64
649	11.9E+6	14.6E+6	0.36E+6	0.325	18.80
704	11.2E+6	14.1E+6	0.35E+6	0.327	18.96
760	9.9E+6	13.4E+6	0.33E+6	0.327	19.12
816	7.9E+6	12.5E+6	0.31E+6	0.329	19.28
1000	0.1E+6	5.3E+6	0.13E+6	0.330	20.0
1200	0.01E+6	1.3E+6	0.03E+6	0.330	20.0

Table 3.3. Mechanical properties of a stainless steel

3.4. ADINA Results

While Figure 3.25 shows the transient movement of the points on Specimen 3 as calculated in the ADINA program, Figure 3.26 shows the transient movement of the measurement points on Specimen 4 as calculated in the ADINA program.

From the figures, it can be seen that all the measurement points moved upward during the welding. During the welding, the measurement point located closest to the welded region had the largest peak value of distortion, while the measurement point located furthest from the welded region had the lowest peak value of distortion. In addition, by comparing Figure 3.25 with 3.26, it can be seen that the larger width decreases the peak value of the distortion.

After the welding was finished, i.e. during the cooling, all the measurement points moved downward until they reached their corresponding final positions. Generally, the width of the specimen did not significantly affect the final positions of most of the measurement points. This phenomena can be seen in both figures as they had the same final positions for most but not all of the measurement points. However, as the width gets larger, rate of the downward movement gets smaller. It can be seen in the figures that the slope of the downward movement in Figure 3.25 is larger in magnitude than the one in Figure 3.26.

To see the whole distortion pictures of Specimens 3 and 4, Figures 3.27 to 3.32 are presented. The figures show the distorted shapes of the specimens at several different times. During the welding, the specimens moved upward. The point that was located in the welding spot had the largest upward movement, while the point that was located far away from the welding spot had the smallest upward movement. In other words, as the distance from the welding spot decreases, the upward movement increases.

Then, after the welding was finished, the specimens began to move downward. The regions in the vicinity of the welding spots moved downward deeply, finally creating concave shapes in the welding spot regions.

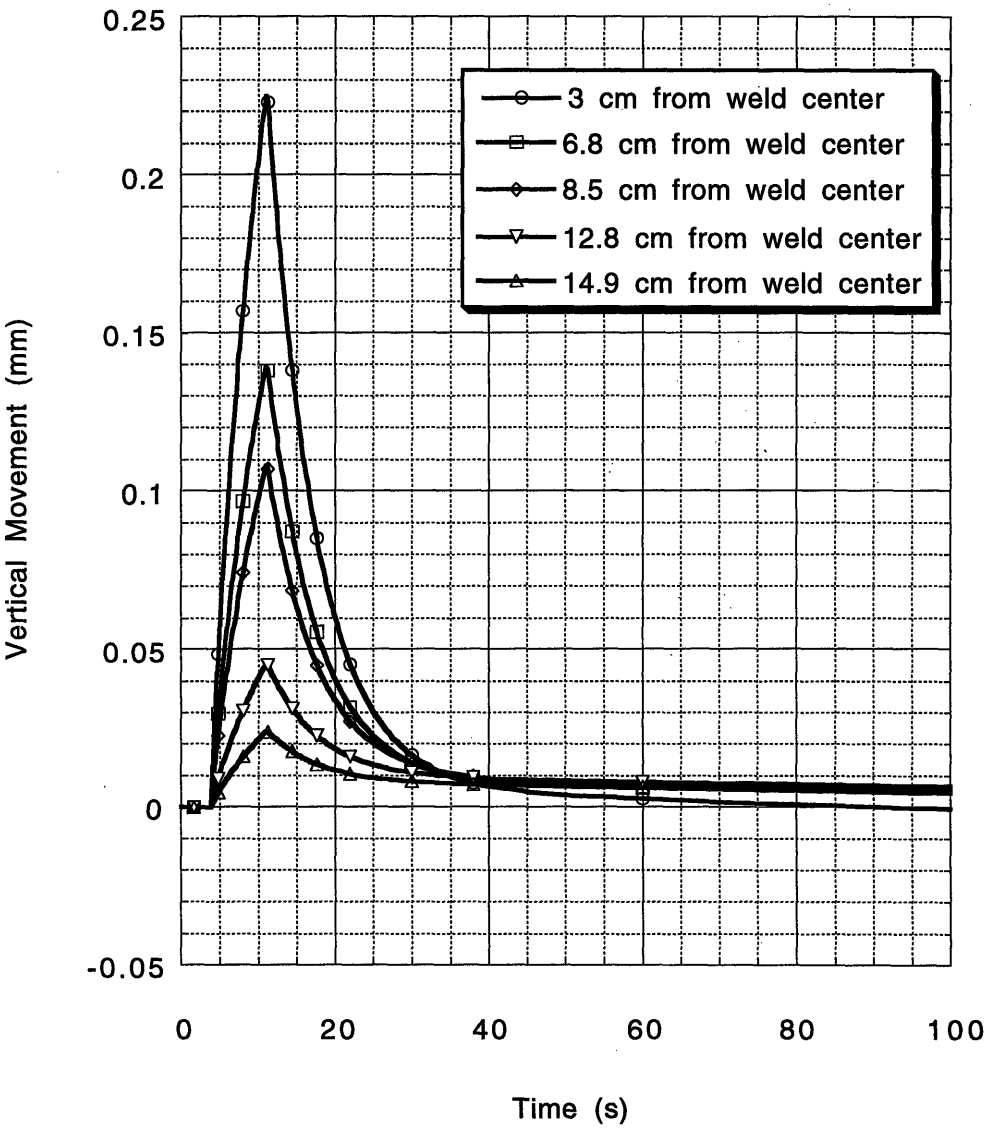

Figure 3.25. Vertical movements at the measurement points of Specimen 3 as calculated by ADINA

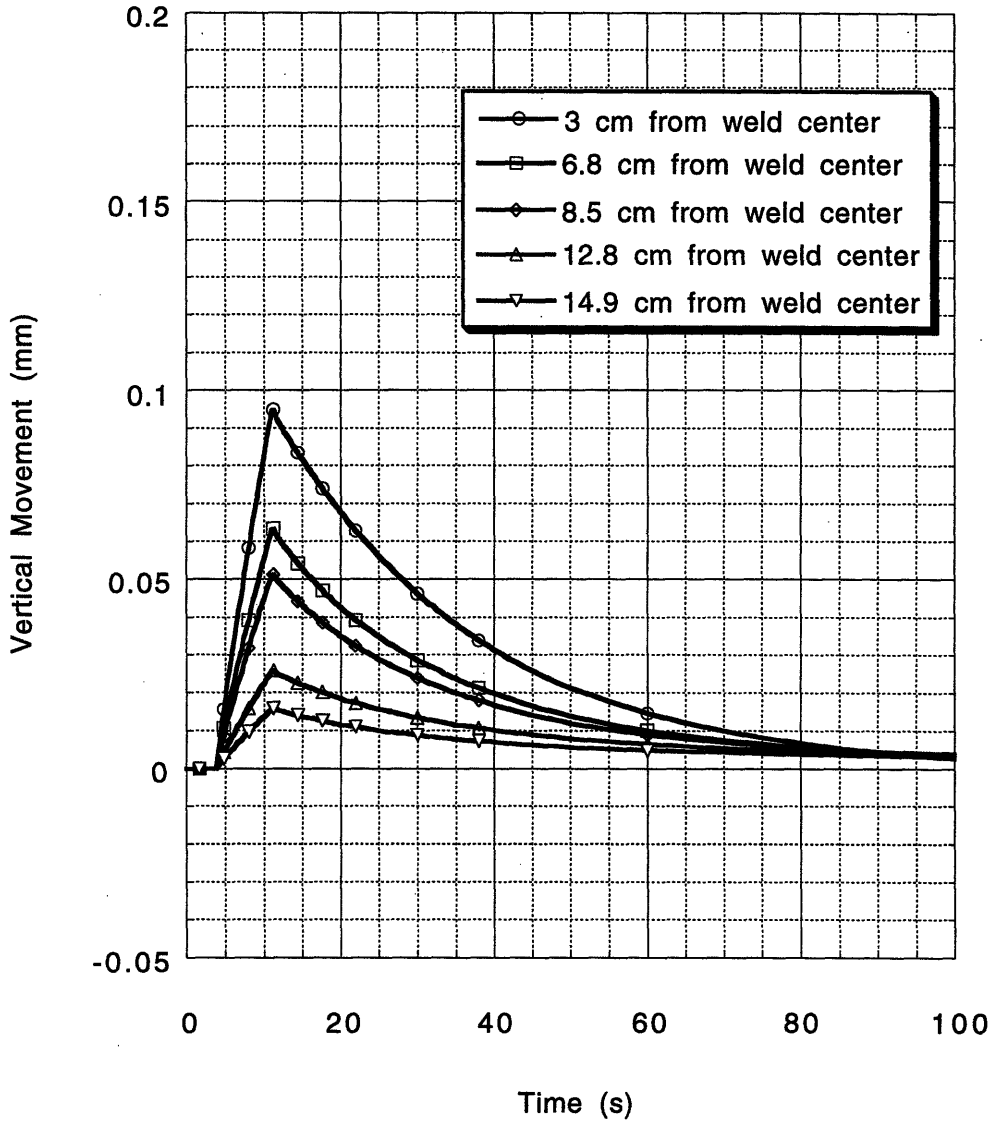

Figure 3.26. Vertical movements at the measurement points of Specimen 4 as calculated by ADINA

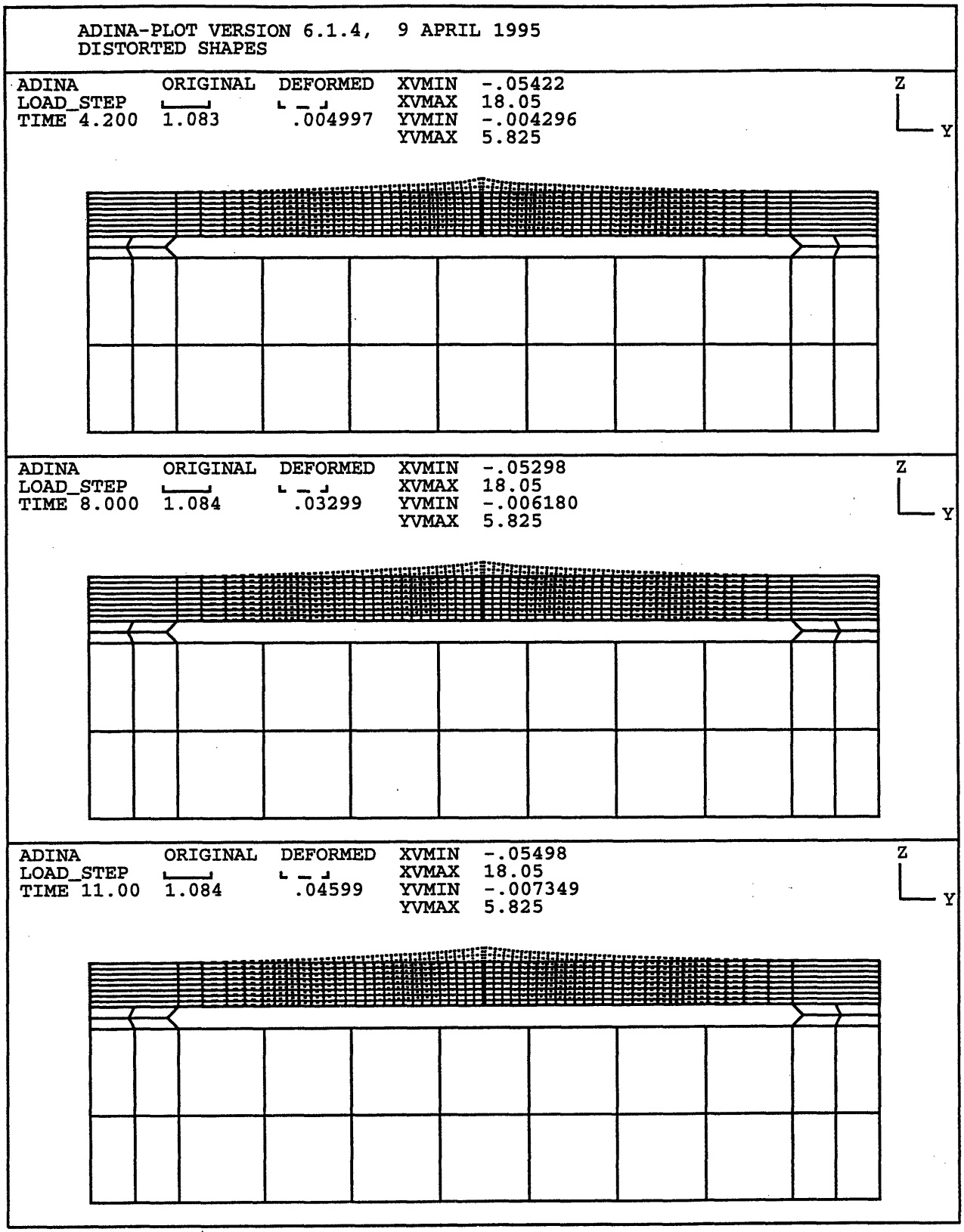

Figure 3.27. Distorted shapes of Specimen 3
at 4.2, 8.0, and 11.0 seconds

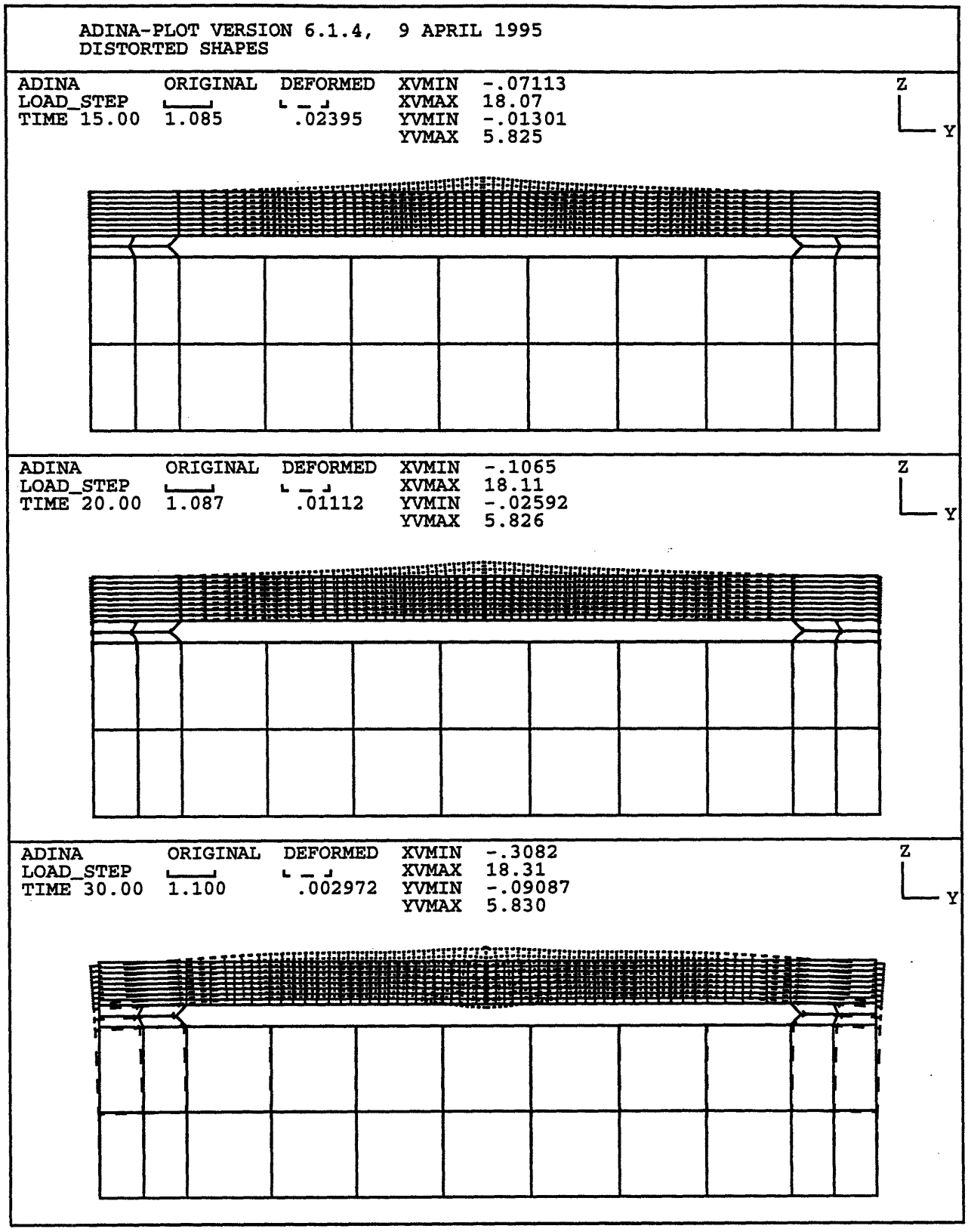

Figure 3.28. Distorted shapes of Specimen 3
at 15.0, 20.0, and 30.0 seconds

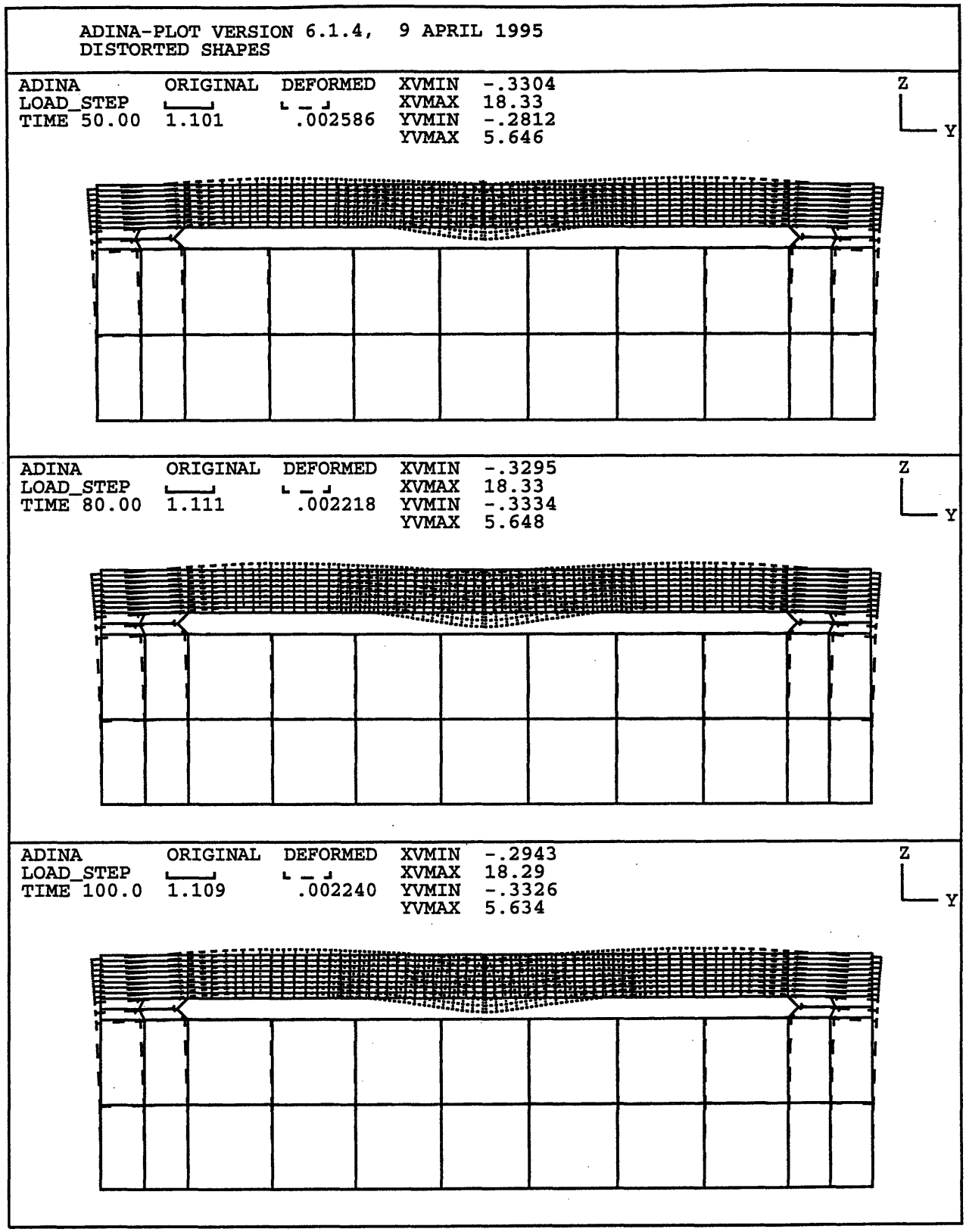

Figure 3.29. Distorted shapes of Specimen 3
at 50.0, 80.0, and 100.0 seconds

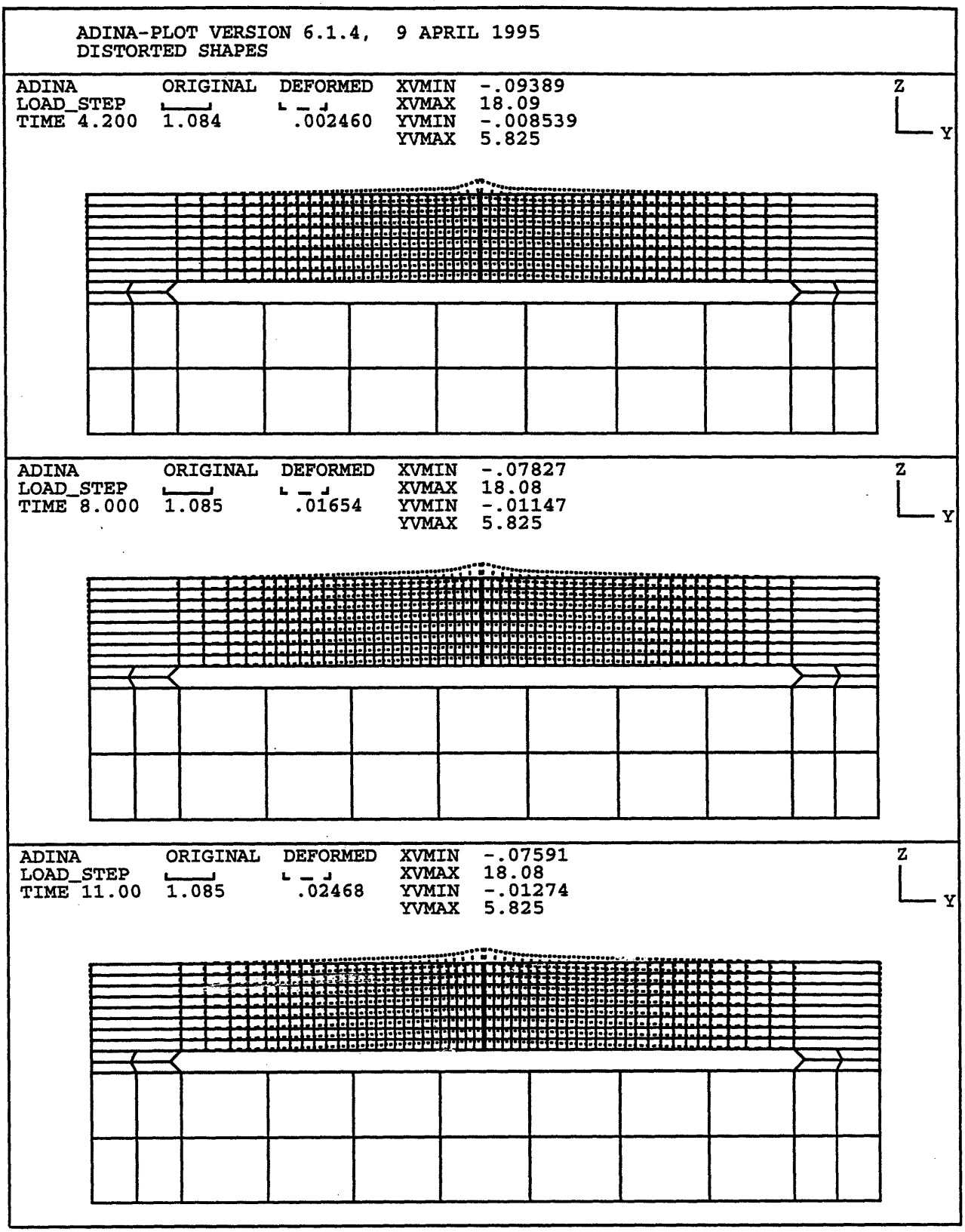

Figure 3.30. Distorted shapes of Specimen 4
at 4.2, 8.0, and 11.0 seconds

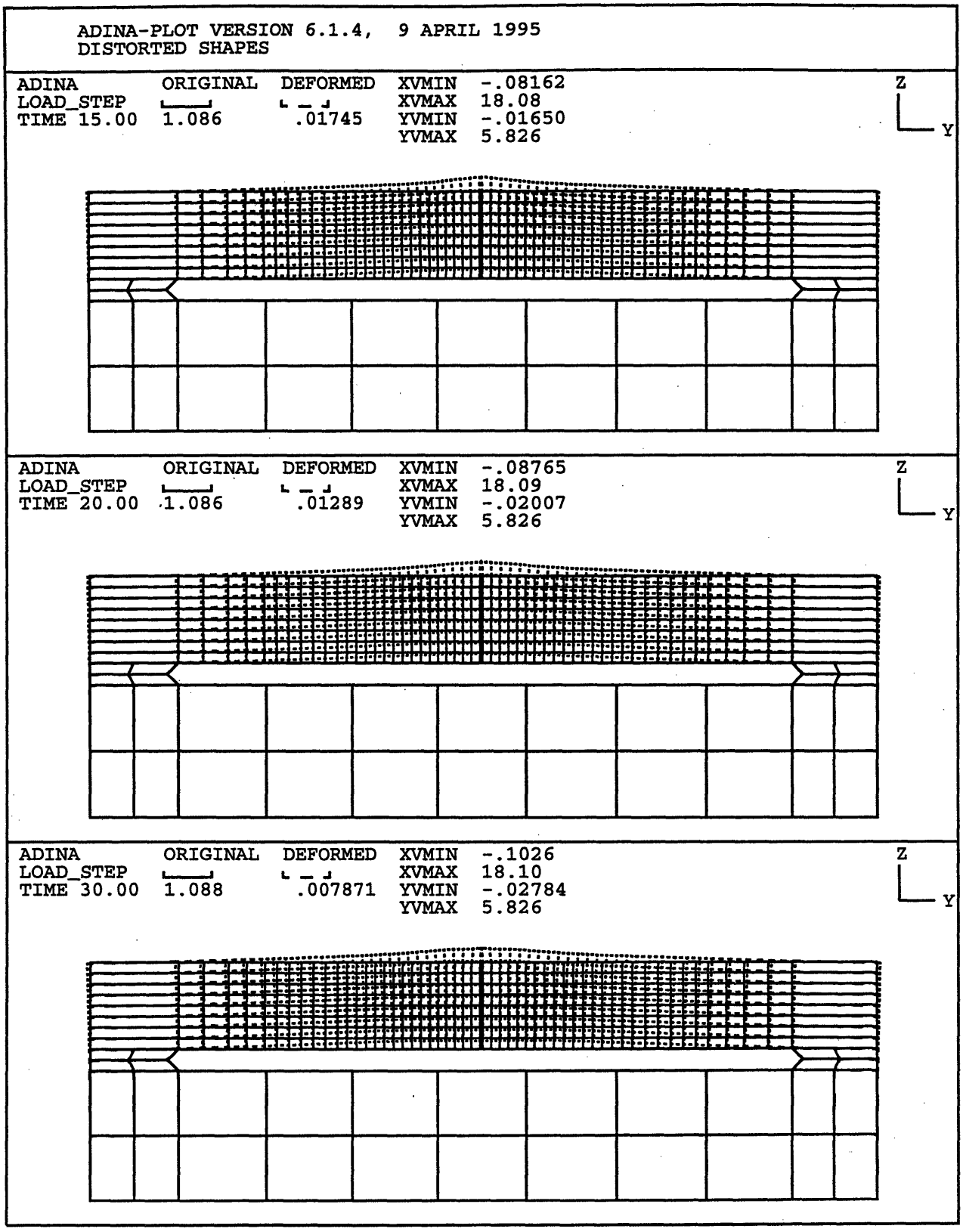

Figure 3.31. Distorted shapes of Specimen 4 at 15.0, 20.0, and 30.0 seconds

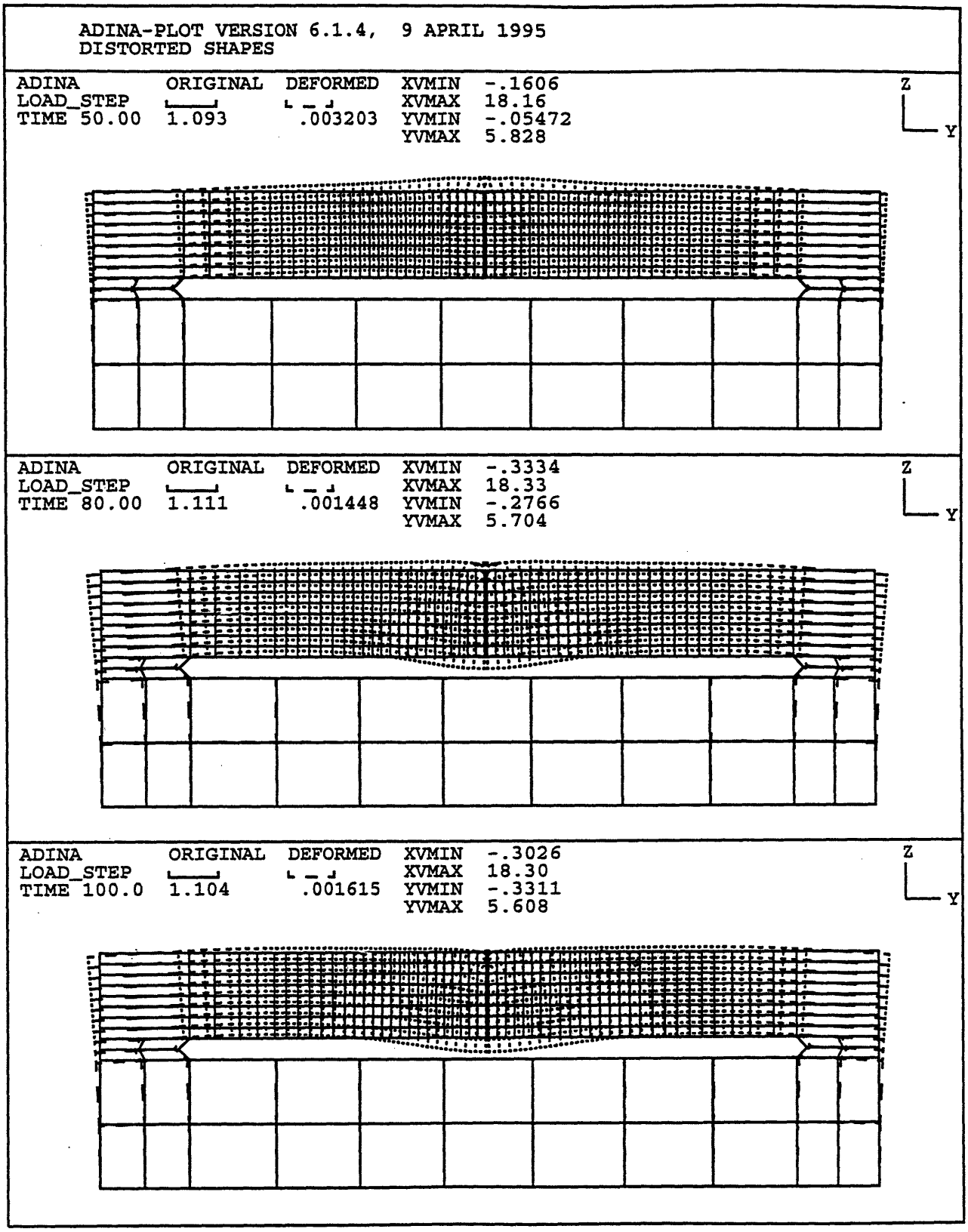

Figure 3.32. Distorted shapes of Specimen 4
at 50.0, 80.0, and 100.0 seconds

Shown in Figures 3.33 and 3.34 are the transient movement at the measurement points on Specimens 5 and 6 as calculated in the ADINA program.

As shown in the figures, the measurement points did not move upward during the welding. This phenomena are clearly shown by the horizontal curves in the figures during the welding. In addition, all the measurement points showed the same movement behavior during the welding. Also, it is shown that the width did not affect the movement behavior of the measurement points because the two graphs are approximately the same during the welding period.

Then, after the welding was finished, the measurement points moved downward. The measurement point located closest from the welding spot had deepest downward movement, while the measurement point located furthest from the welding spot had shallowest downward movement. In other words, as the distance from the welding spot decreases, the downward movement increases in magnitude. Also shown in the figures is the fact that as the width increases the downward movement decreases in magnitude. The final downward position in Figure 3.34 is less than the one in Figure 3.33.

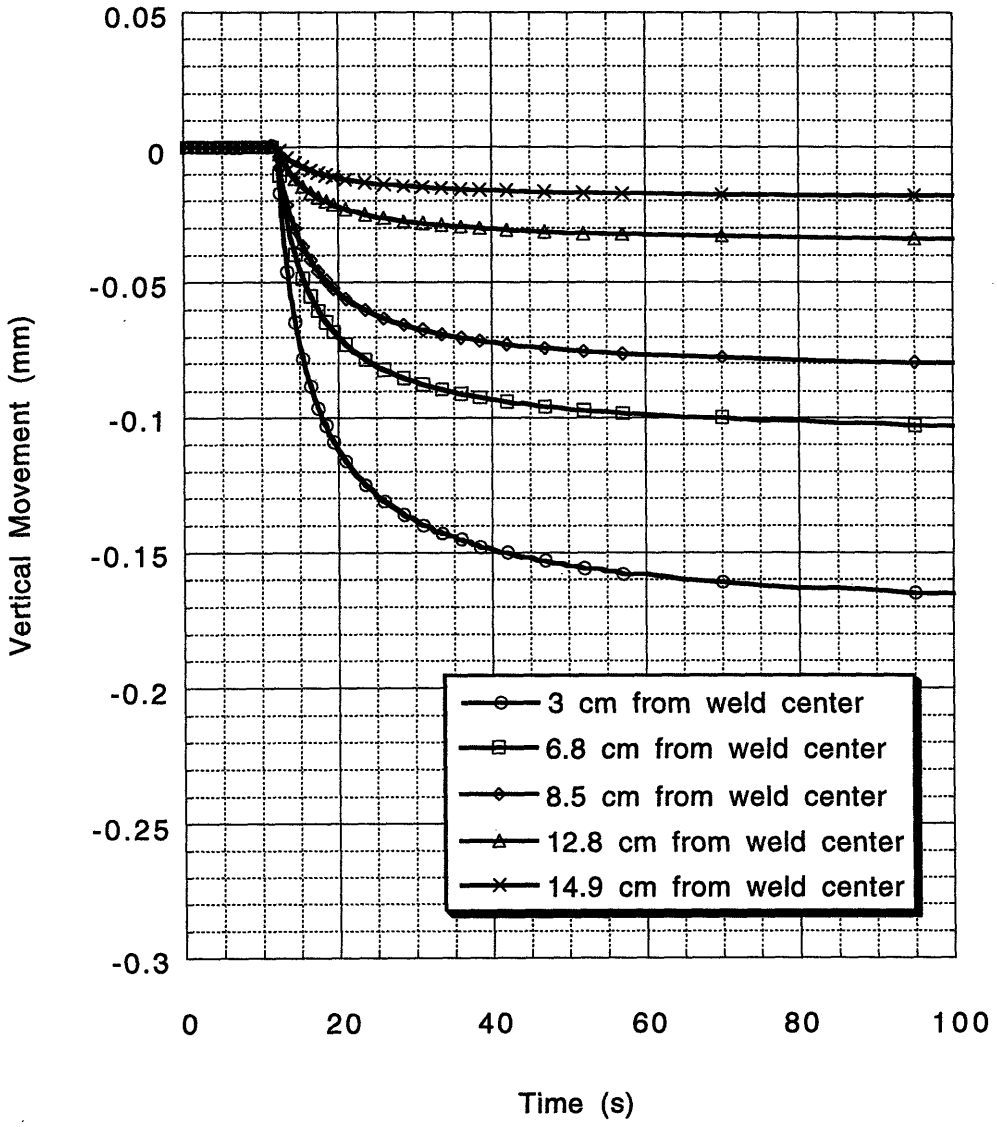

Figure 3.33. Vertical movements at the measurement points of Specimen 5 as calculated by ADINA

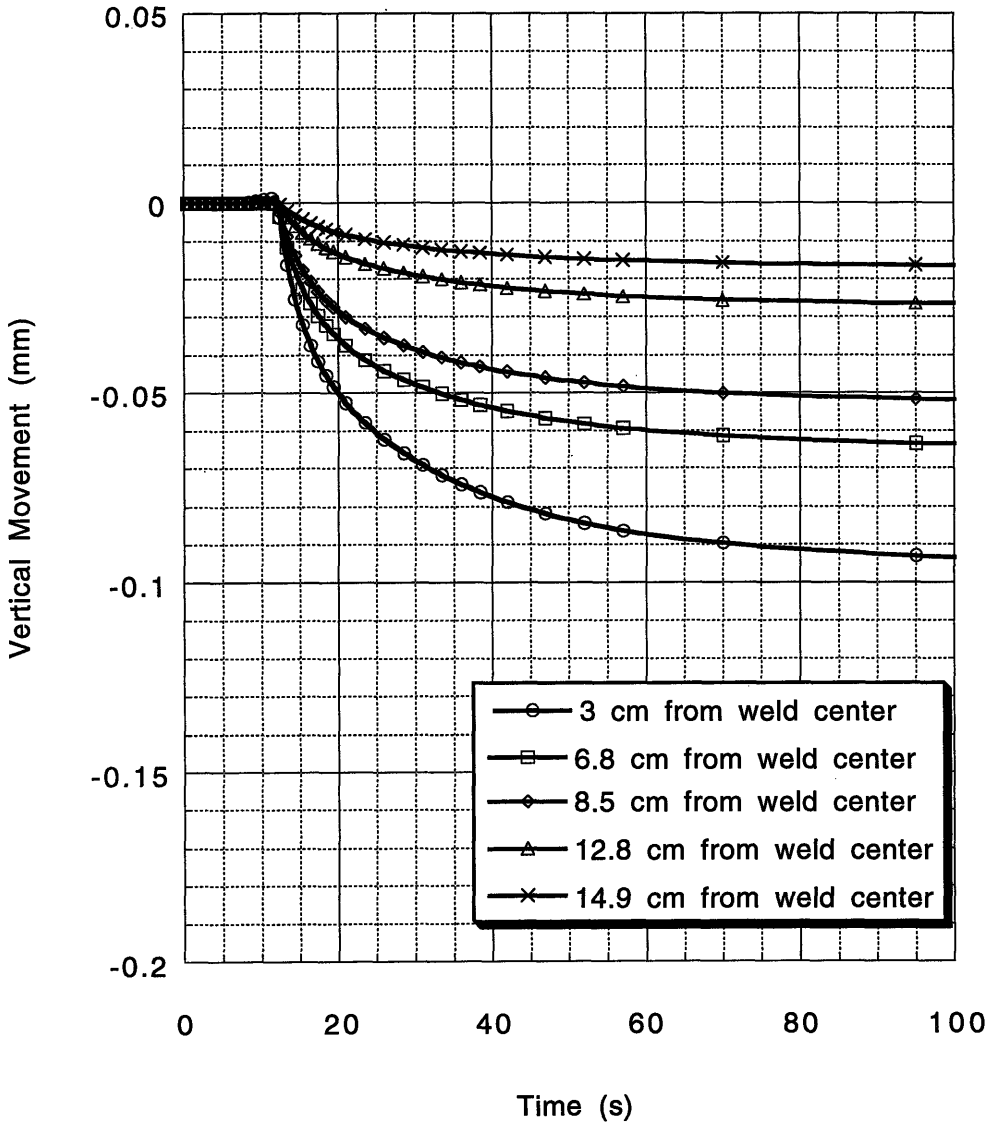

Figure 3.34. Vertical movements at the measurement points of Specimen 6 as calculated by ADINA

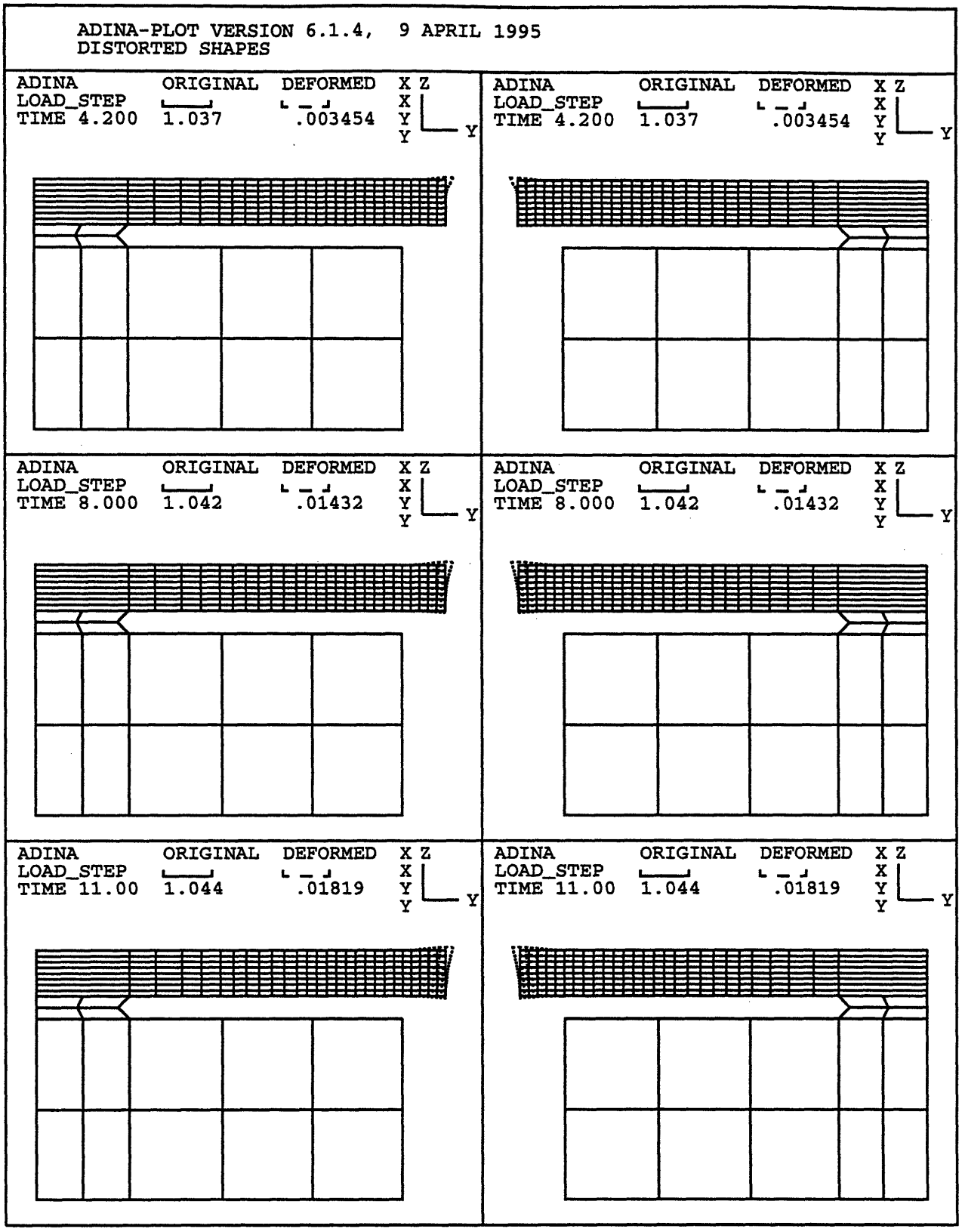

Figure 3.35. Distorted shapes of Specimen 5
at 4.2, 8.0, and 11.0 seconds

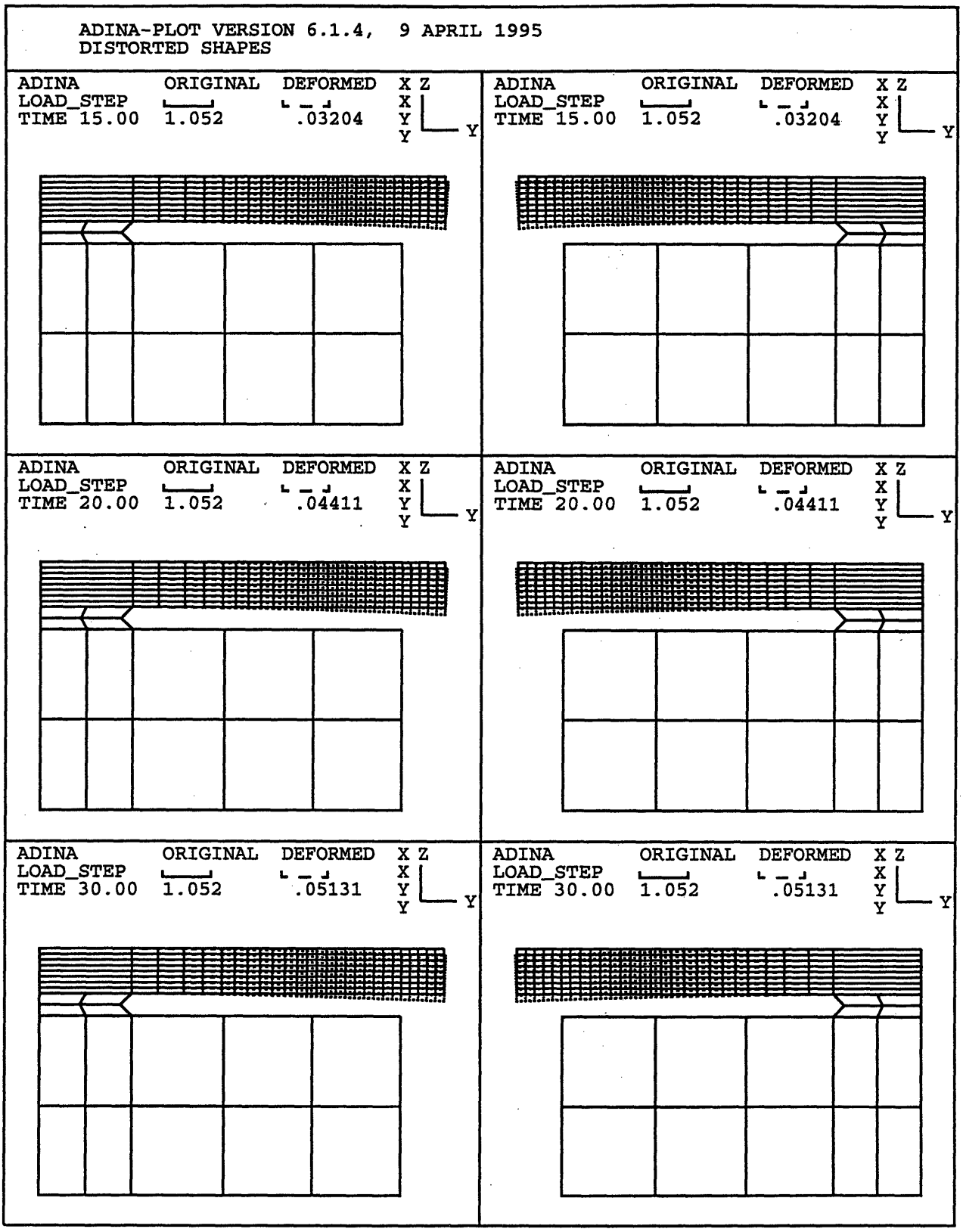

Figure 3.36. Distorted shapes of Specimen 5
at 15.0, 20.0, and 30.0 seconds

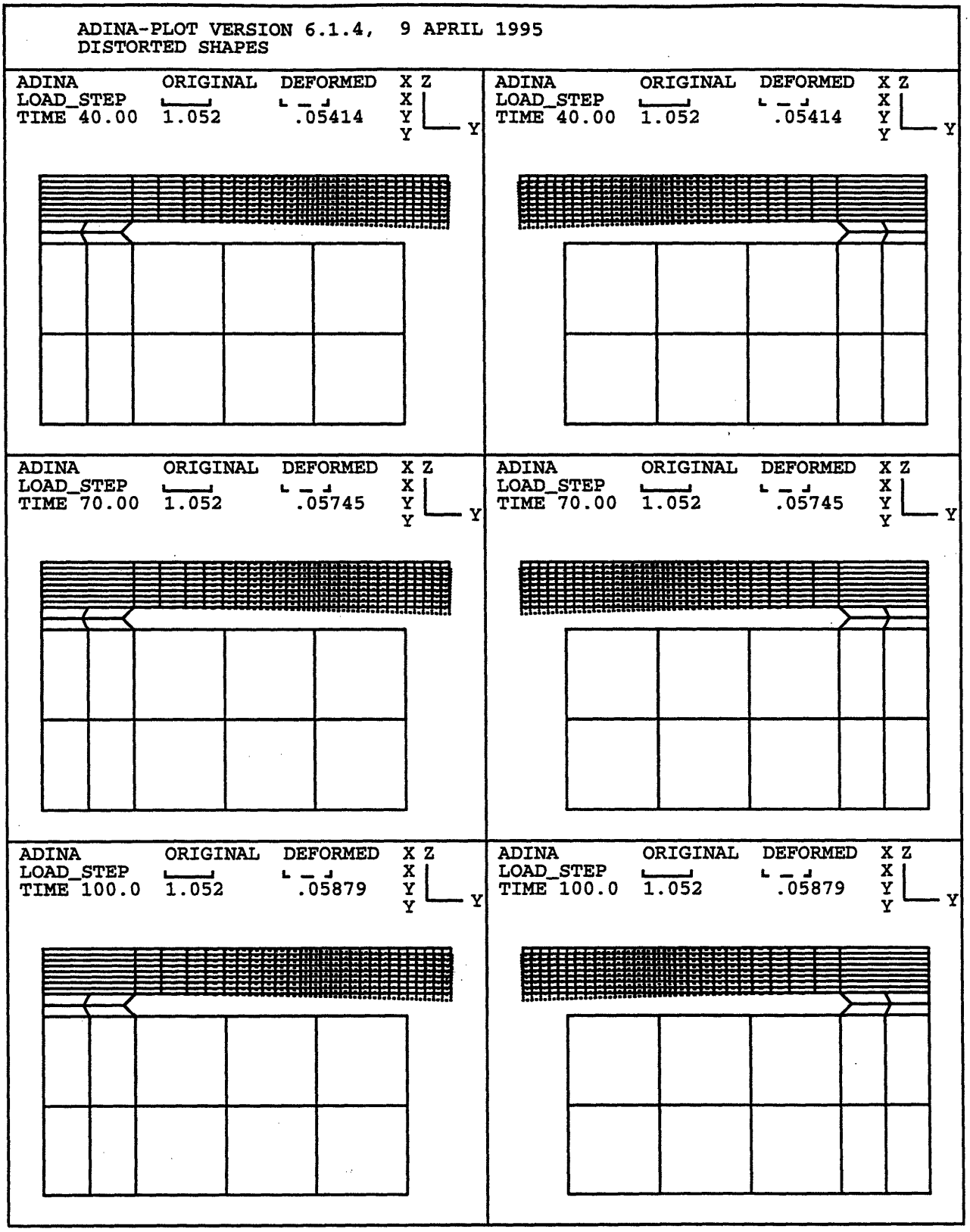

Figure 3.37. Distorted shapes of Specimen 5
at 40.0, 70.0, and 100.0 seconds

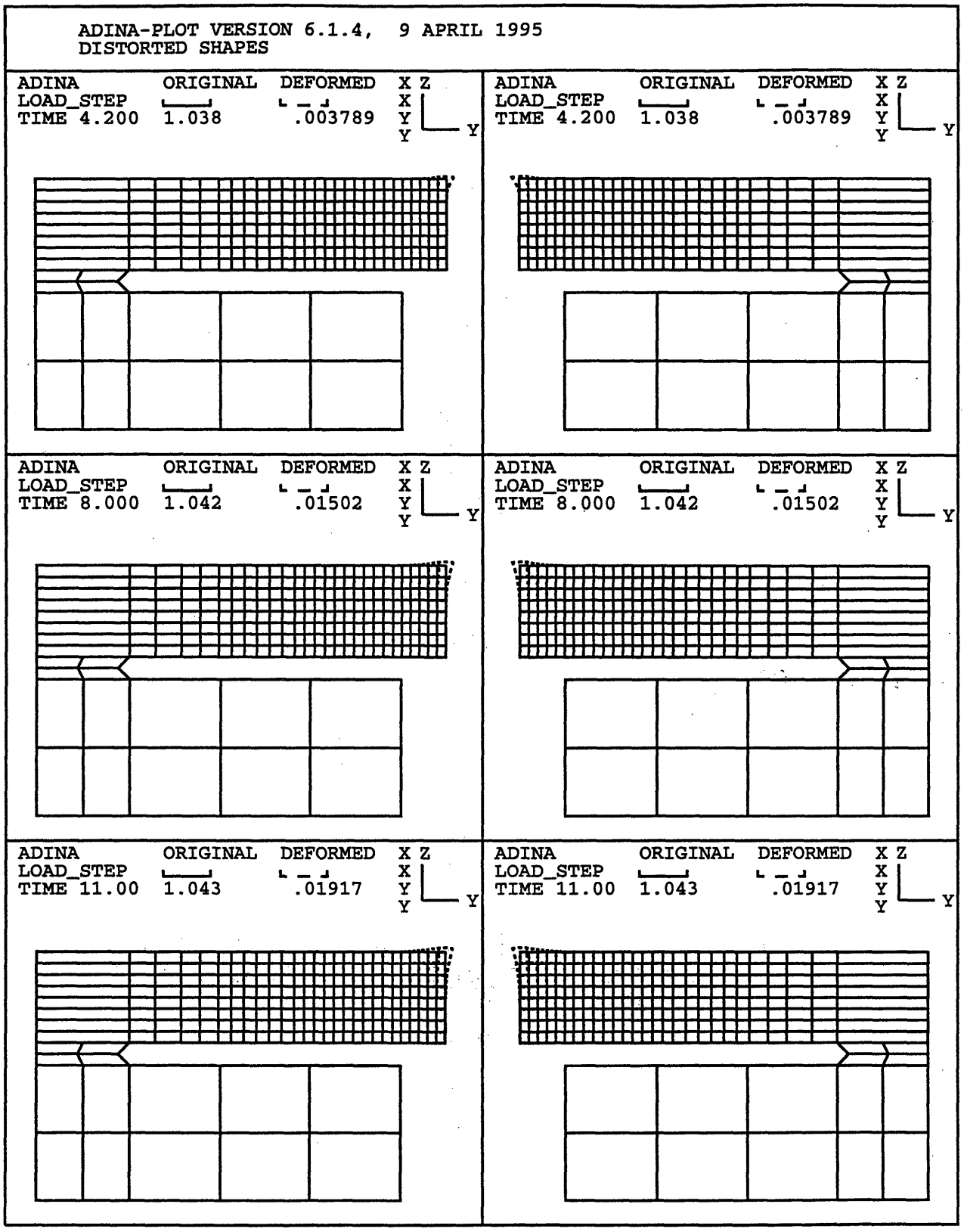

Figure 3.38. Distorted shapes of Specimen 6
at 4.2, 8.0, and 11.0 seconds

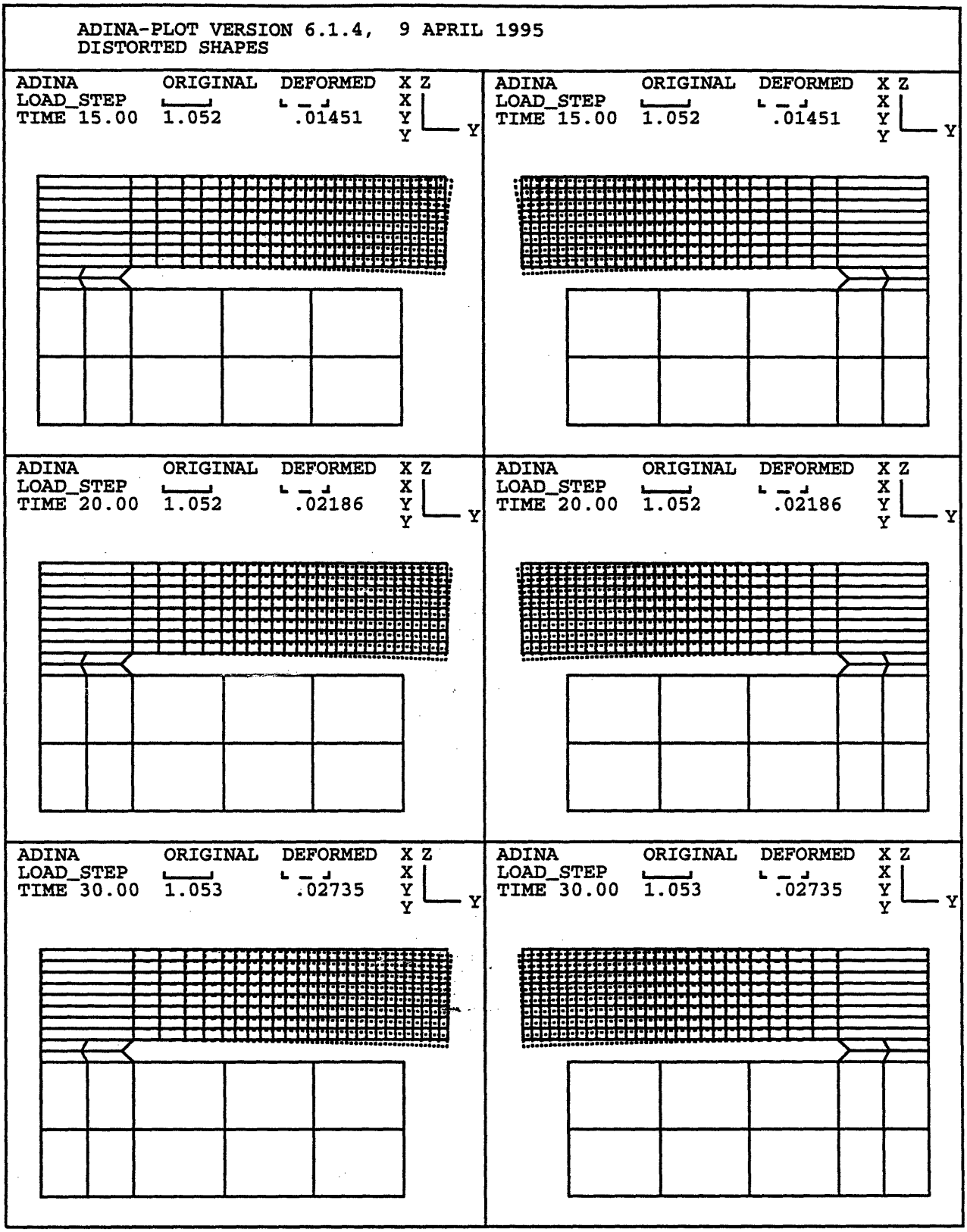

Figure 3.39. Distorted shapes of Specimen 6
at 15.0, 20.0, and 30.0 seconds

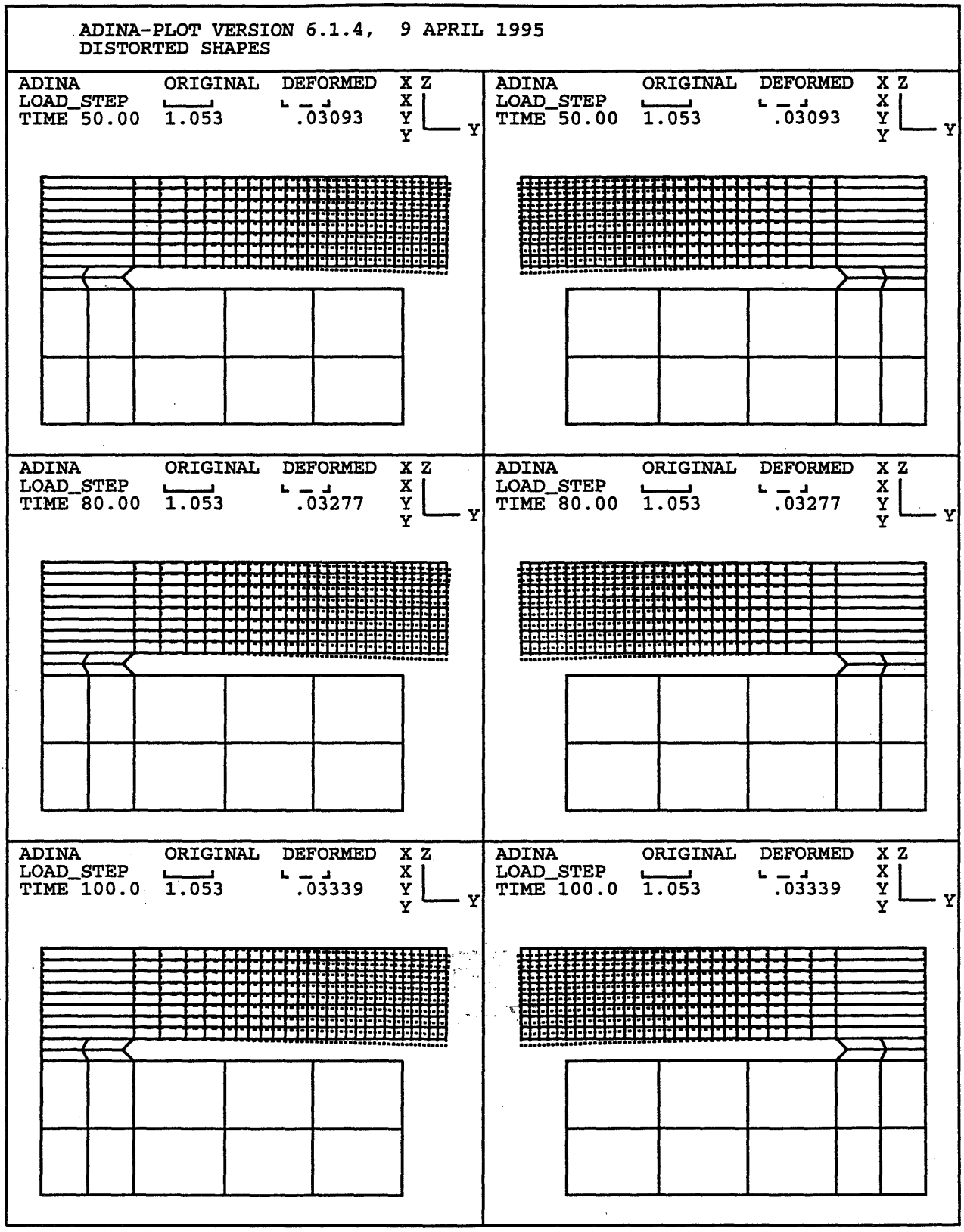

Figure 3.40. Distorted shapes of Specimen 6
at 50.0, 80.0, and 100.0 seconds

Figures 3.41 through 3.44 show the transient movement of Specimen 7 as caculated in the ADINA program.

From Figure 3.41, it can be seen that during the welding the measurement points moved downward until they reached their corresponding peak values. The peak values of the measurement point at 20 mm from the side edge is smaller in magnitude than that of the measurement point at 7 mm from the side edge. The whole distortion picture of the specimen during the welding is shown in Figure 3.42. This figure shows that during the welding the specimen bent downward like reverse wide V shape.

Then, after the welding was finished, the measurement points moved upward until they reached their final corresponding upward positions. The final upward position of the measurement point at 20 mm from the side edge is larger than that of the measurement point at 7 mm from the side edge. The whole distortion picture of the specimen after the welding are shown in Figures 3.43 and 3.44. These figures show that after the welding the specimen bent upward creating final wide V shape.

Compared to distortion behavior of a similar no-slit specimen previously analytically investigated by Goktug [11], the distortion of Specimen 7 is similar but smaller in magnitude. In other words, the effect of a slit in this type of specimen is only to decrease the magnitude of distortion.

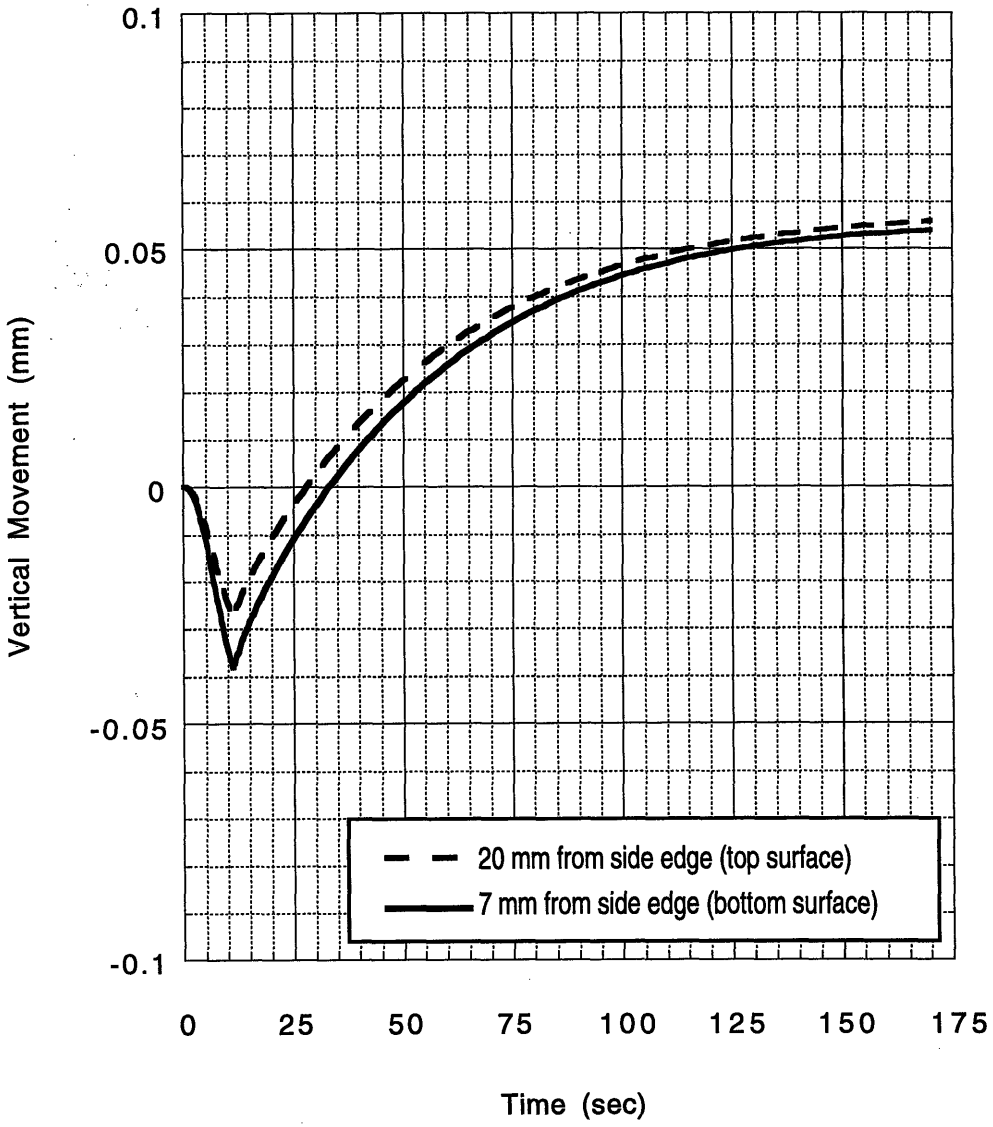

Figure 3.41. Vertical movement at the measurement points of Specimen 7 as calculated by ADINA

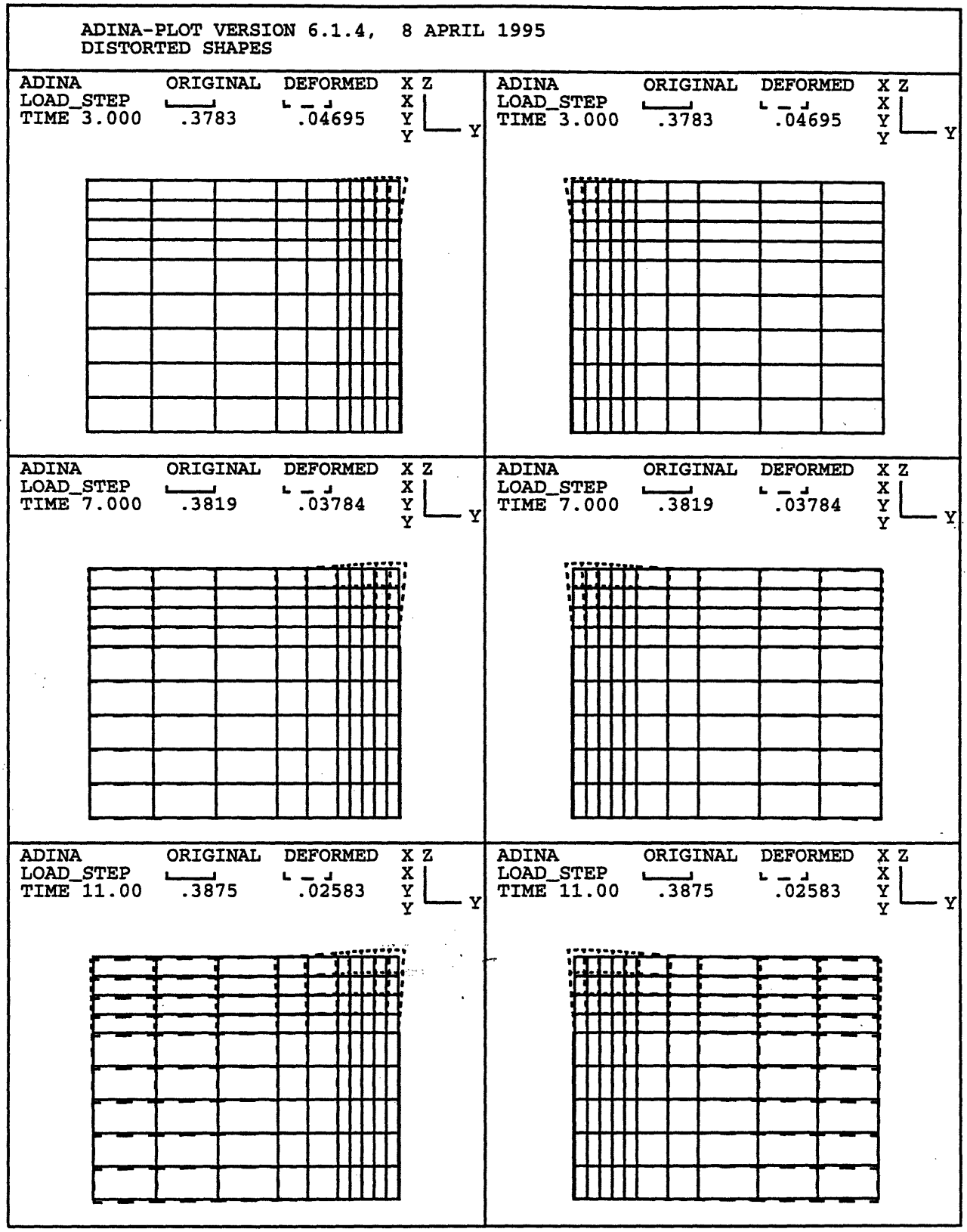

Figure 3.42. Distorted shapes of Specimen 7
at 3.0, 7.0, and 11.0 seconds

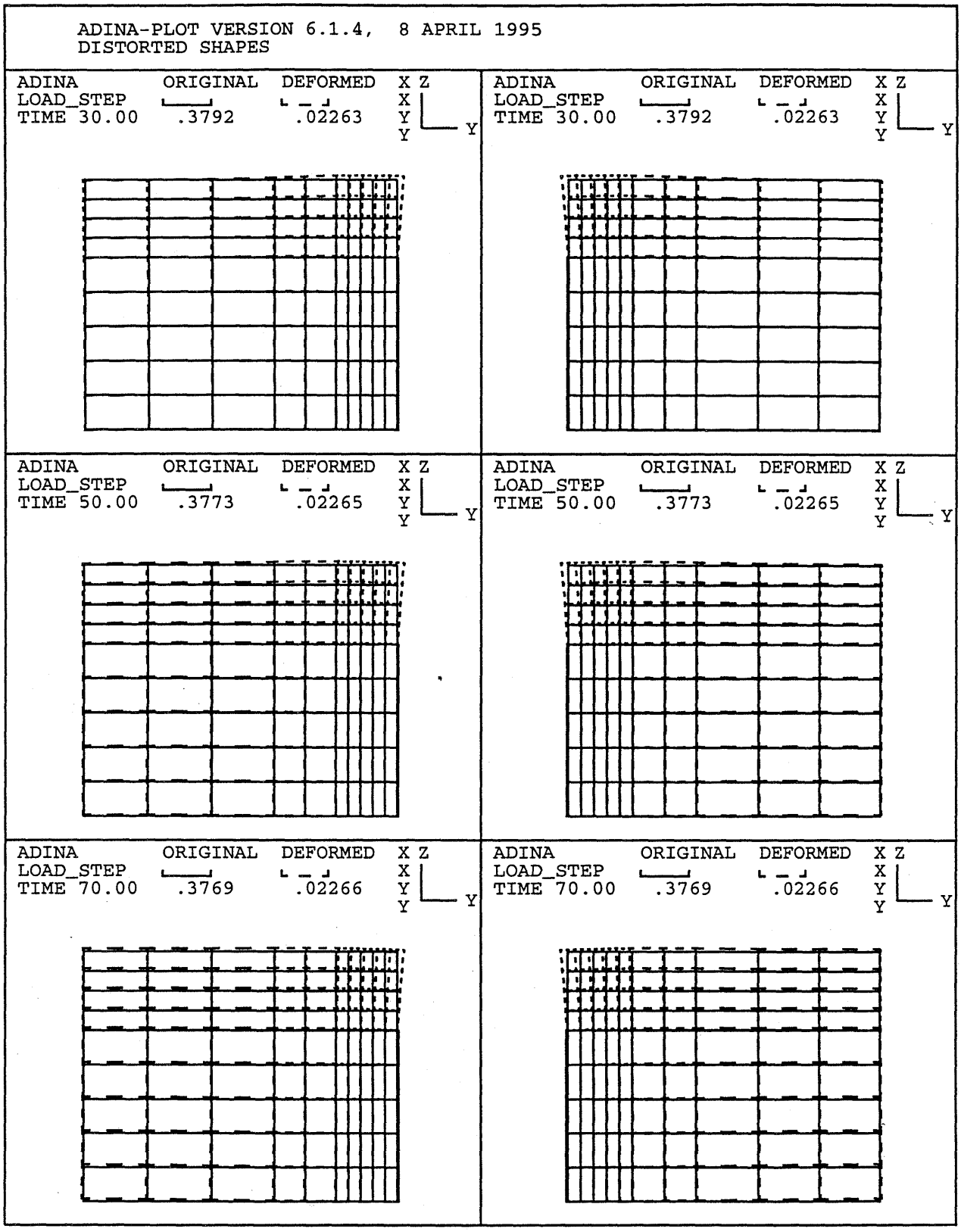

Figure 3.43. Distorted shapes of Specimen 7
at 30.0, 50.0, and 70.0 seconds

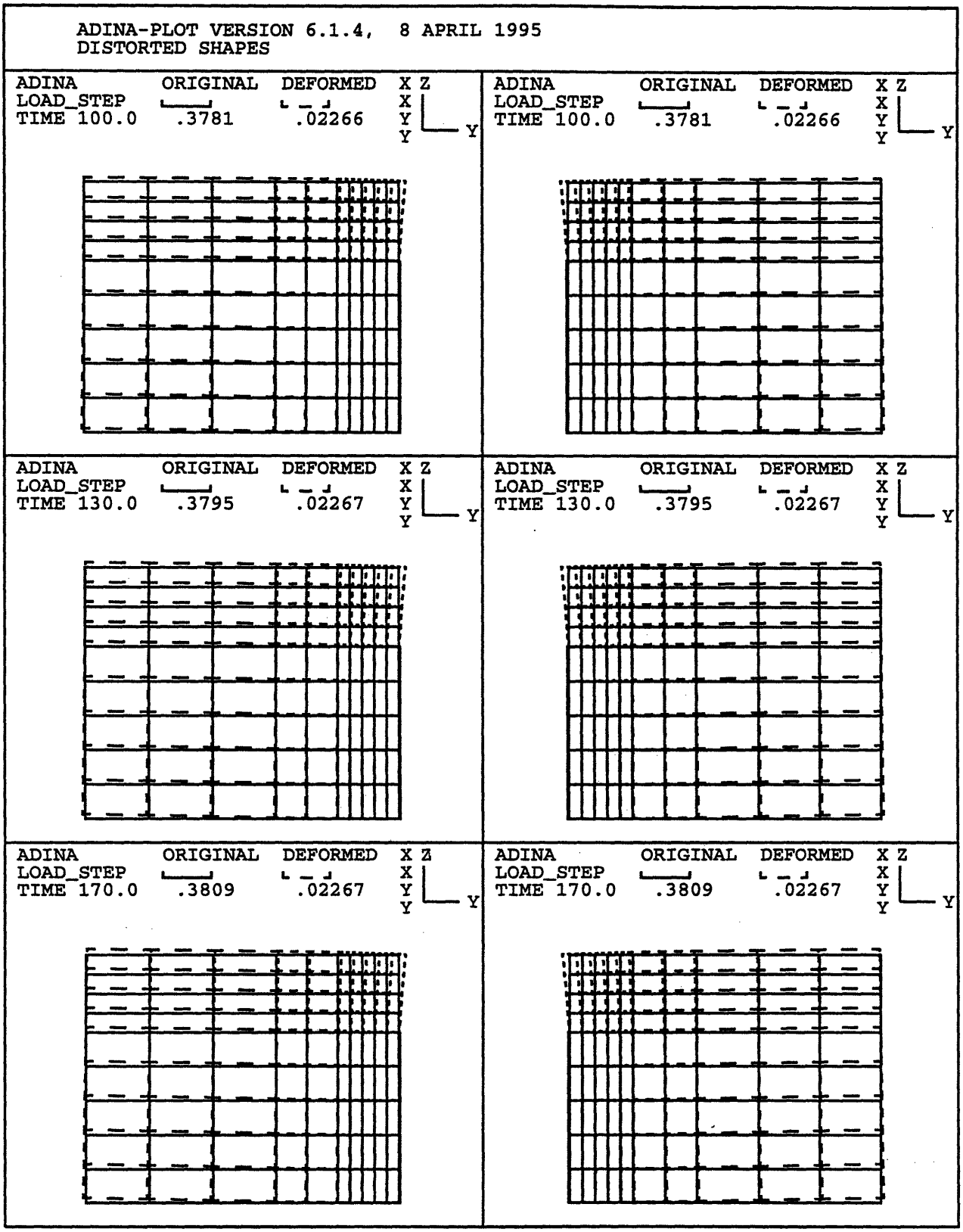

Figure 3.44. Distorted shapes of Specimen 7
at 100.0, 130.0, and 170.0 seconds

Chapter 4

Comparisons between Experimental and Analytical Results

The finite element calculation of the distortion of the specimens is dependable. By using the experimental equipment described in Chapter 2 of the thesis, the distortion data obtained from the real distortion measurement of the specimens can be assumed to be 100% correct and can be used as the reference for the distortion of the specimens. Therefore, since the distortion obtained from the finite element calculation correlates with the distortion obtained from the real measurement, the finite element calculation of the distortion of the specimens is accurate.

Shown in Figures 4.1 and 4.2 are the distortion of Specimens 3, 4, 5, and 6 obtained from respectively the real measurement and the finite element calculation at 6.8 cm from the weld point.

Shown in Figures 4.3 and 4.4 are the distortion of Specimens 3, 4, 5, and 6 obtained from respectively the real measurement and the finite element calculation at 12.8 cm from the weld point.

Shown in Figures 4.5 and 4.6 are the distortion of Specimen 7 obtained from respectively the real measurement and the finite element calculation at 20 mm from the side edge (top surface).

Shown in Figures 4.7 and 4.8 are the distortion of Specimen 7 obtained from respectively the real measurement and the finite element calculation at 7 mm from the side edge (bottom surface).

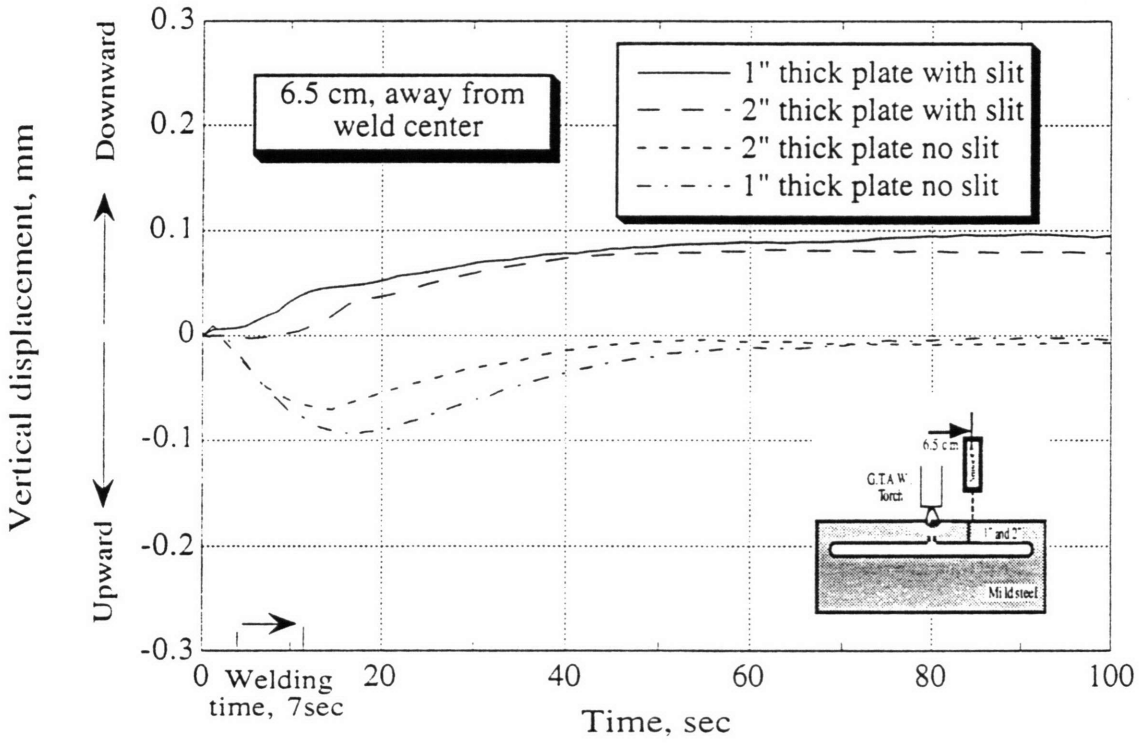

Figure 4.1. The distortion of Specimens 3, 4, 5, and 6 from the real measurement

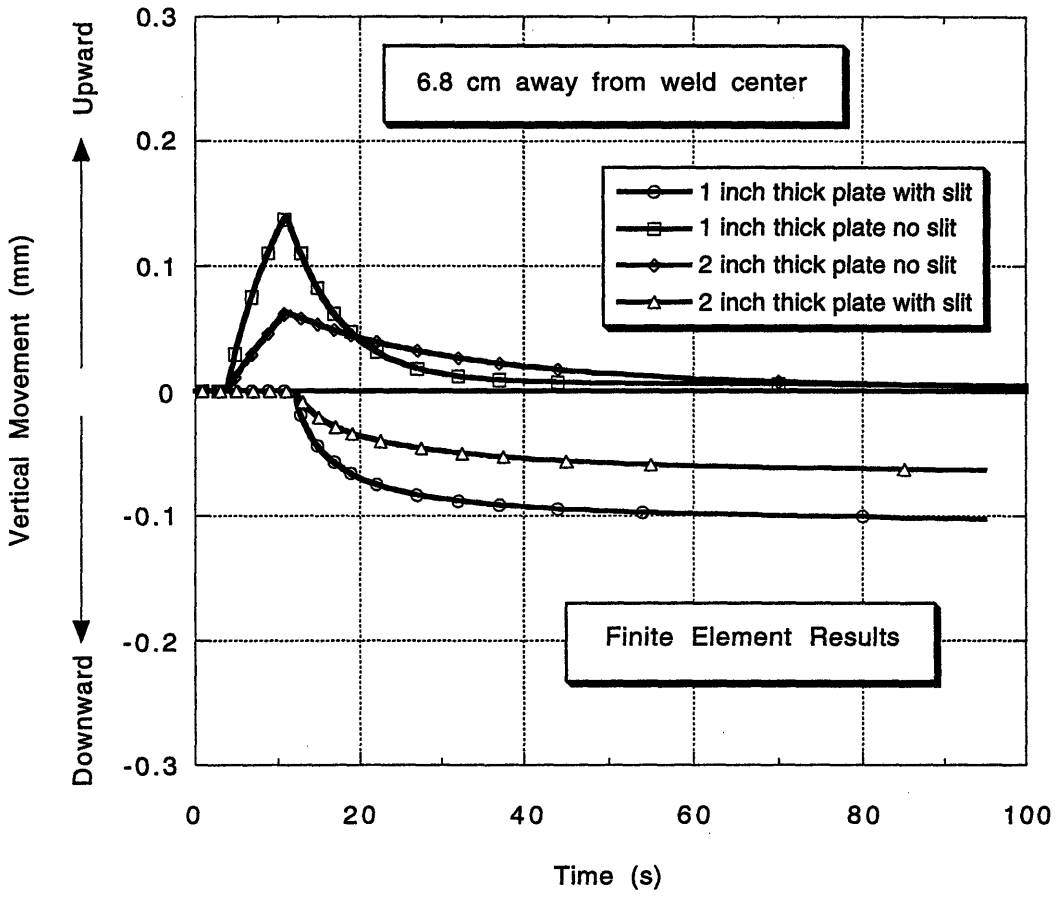

Figure 4.2. The distortion of Specimens 3, 4, 5, and 6 from the finite element calculation

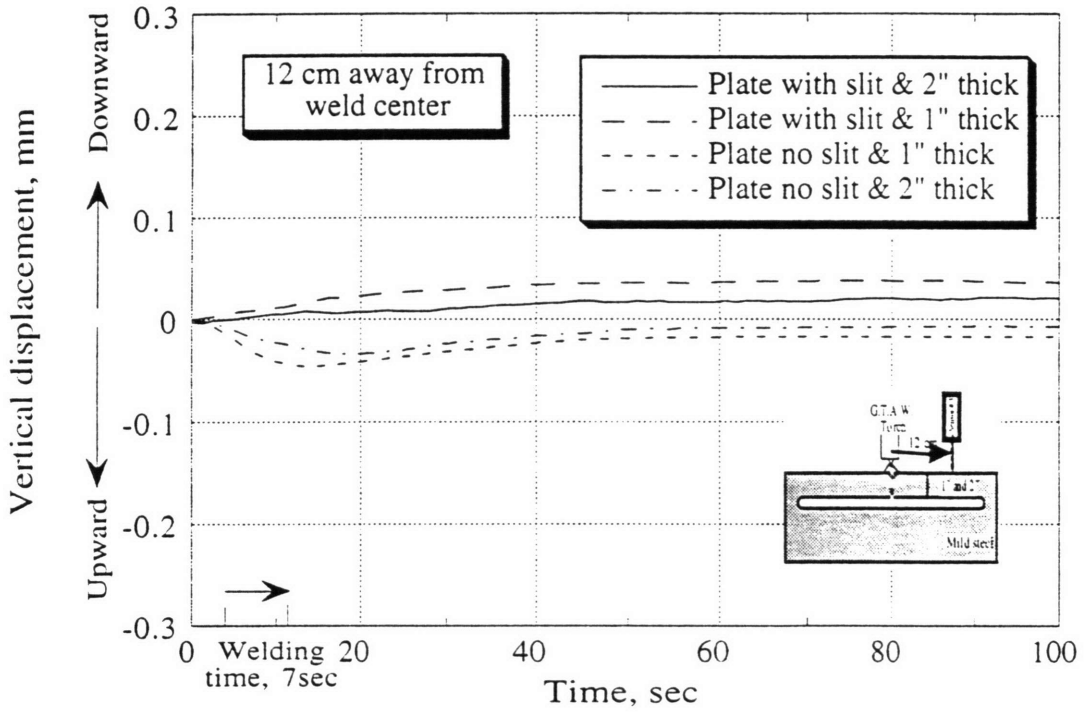

Figure 4.3. The distortion of Specimens 3, 4, 5, and 6 from the real measurement

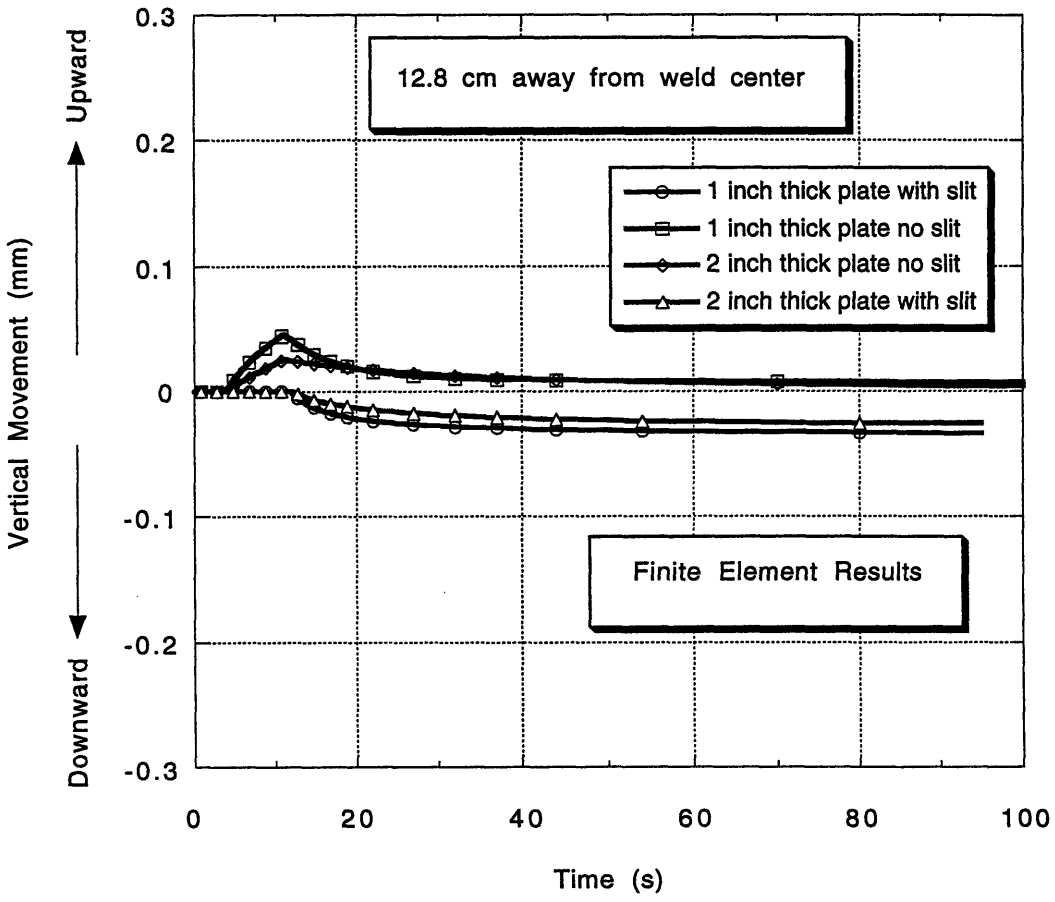

Figure 4.4. The distortion of Specimens 3, 4, 5, and 6 calculated in the finite element programs

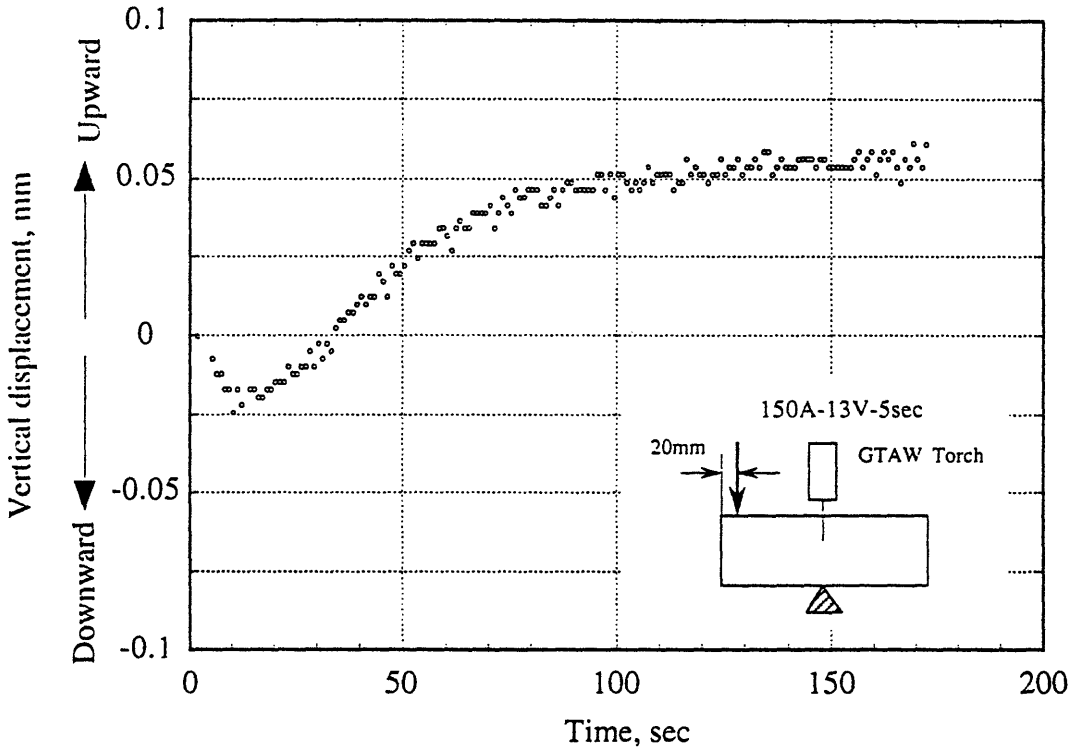

Figure 4.5. The distortion of Specimen 7 obtained from the real measurement

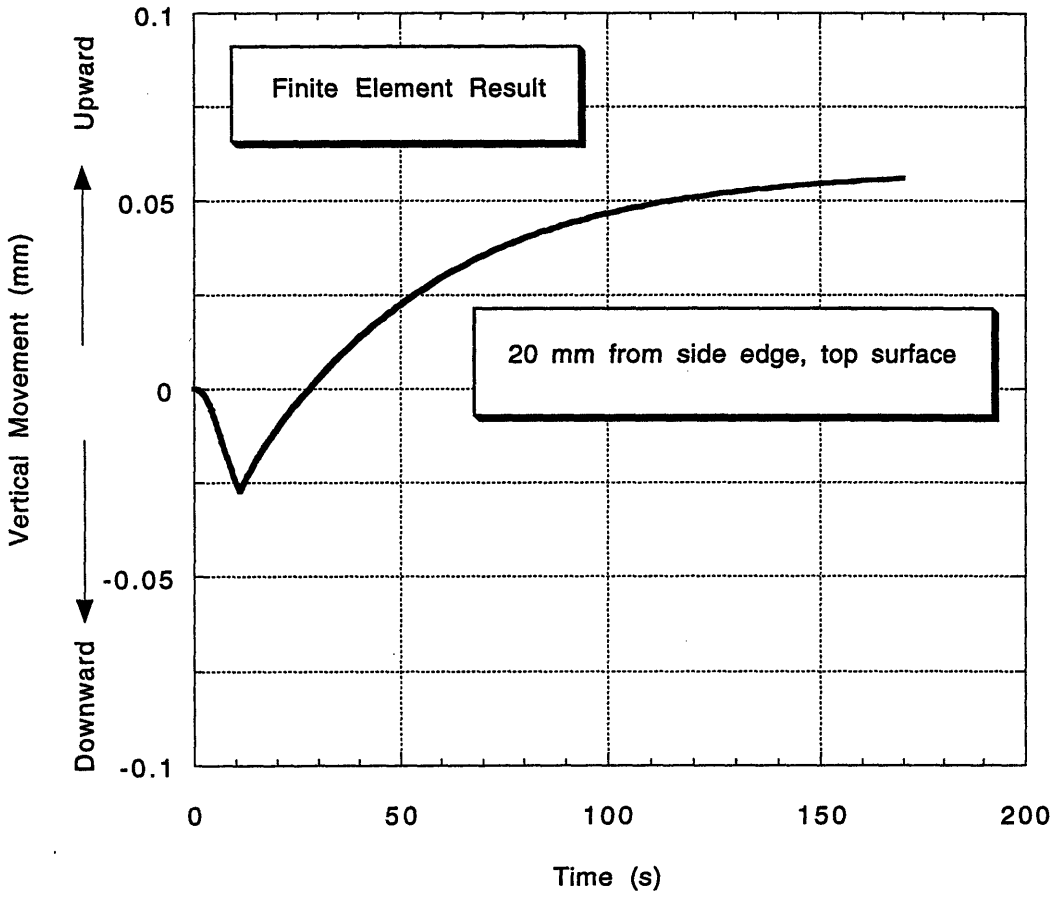

Figure 4.6. The distortion of Specimen 7 calculated in the finite element programs

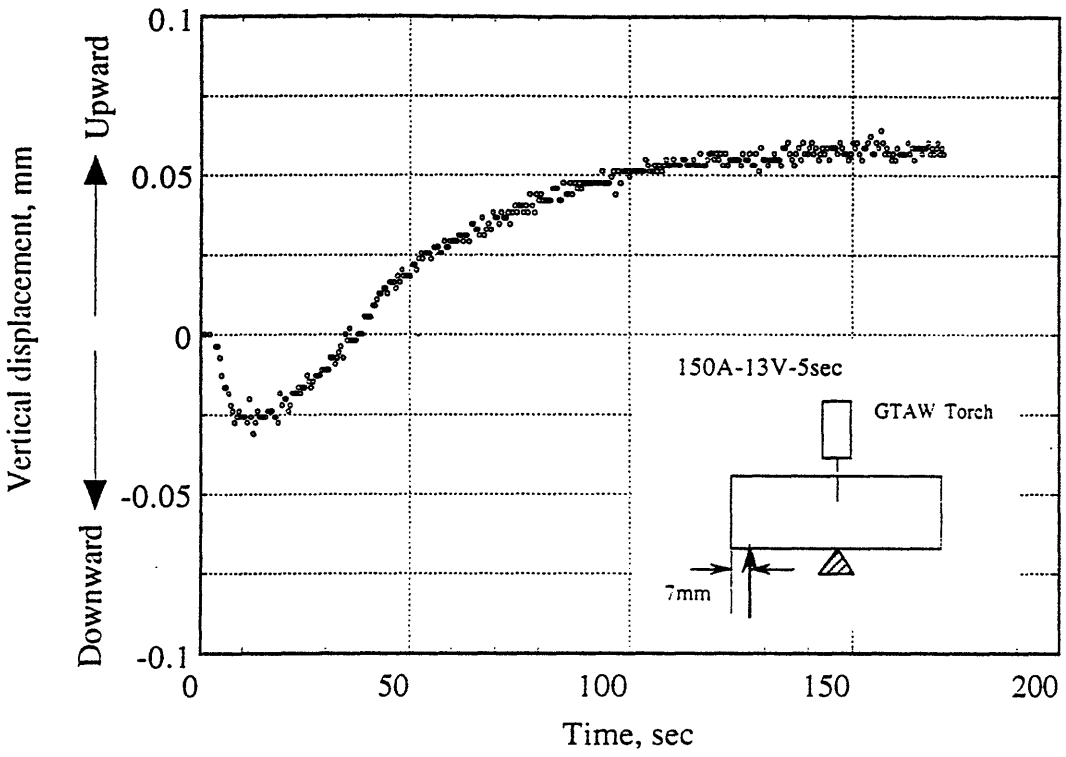

Figure 4.7. The distortion of Specimen 7 obtained from the real measurement

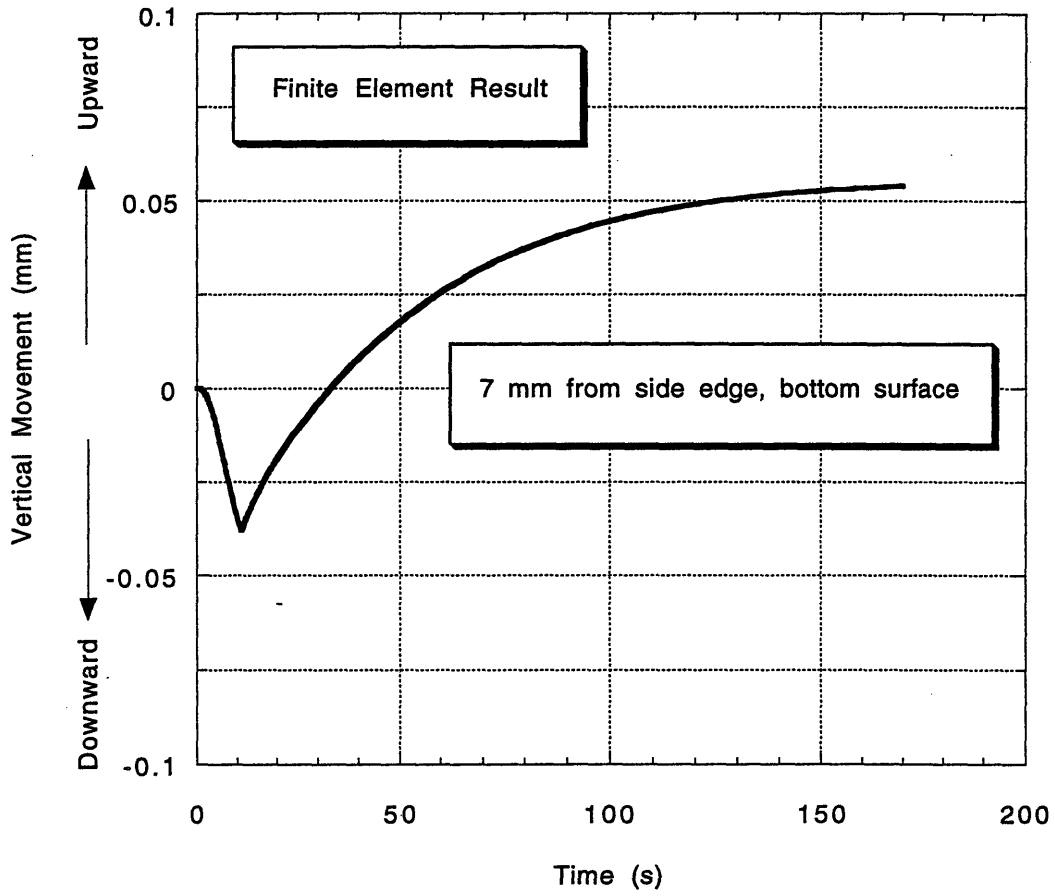

Figure 4.8. The distortion of Specimen 7 calculated in the finite element programs

Chapter 5

Summary and Discussion of Results

Due to the localized heat occurring when a welding arc applied to a welded structure, temperatures in the vicinity of the welded area are higher than the temperatures in other areas of the structure. As a consequence, the metal in the vicinity of the welded area expands more than the metal in the other areas of the structure. In other words, incompatible strains are being created in the welded structure. This means that distortion has occurred in the welded structure. In addition to the distortion, a distribution of thermal stresses also has been created in the welded structure. This whole process happens so fast that the distortion appears to occur as soon as the welding is applied. The distortion continues to occur after the welding. In general, the distortion during welding is very different from the distortion after welding. For example, during bead-on-edge welding of a rectangular plate, as described in the introduction section of this thesis, the rectangular plate bends downward. Then, after welding, the plate bends upward. Another example is the distortion described in connection with Specimen 7. During welding, the plate bent downward. Then, after the welding, the plate bent upward. Since the material of the welded structure behaves non-elastically during the course of the distortion, the distortion remains in the welded structure long after the welding.

There are many factors that affect the distortion creation in a welded structure. The first factor is how the welded structure is constrained. Simply, an object that is constrained cannot move as easily as an object that is not constrained. The same thing happens in welded structures. At one extreme, a welded structure that is not constrained at all distorts in all possible directions, while a welded structure that is totally constrained does not distort at all.

Between these extremes, it is generally observed that as the degree of constraint increases, the distortion decreases, and vice versa. Unfortunately, as the degree of constraint increases, more residual stress will be created in the welded structure. This is because the constraint only limits the distortion of the welded structure. Since the distortion cannot proceed due to the constraint, a thermal stress distribution is created in the welded structure. The thermal stress will remain in the welded structure as the residual stress. For this reason, welded structures are not totally constrained during the welding. This can significantly reduce distortion, but also limit the opportunity for residual stress to occur.

The second factor affecting distortion is size of the welded structure. As the size increases, the distortion decreases. In other words, in terms of the distortion, the size of the welded structure acts as a constraint. One demonstration of this can be seen comparing the results of tests using Specimens 3 and 4. The distortion in Specimen 4 was less than the distortion in Specimen 3. The size of Specimen 3 was smaller than the size of Specimen 4. Further, the distortion in Specimen 6 was less than the distortion in Specimen 5, for the same reason

The third factor in distortion is the material of the welded structure, particularly the physical and mechanical properties of the welded structure. Thermal conductivity, coefficient of thermal expansion, yield stress, Young's modulus, strain hardening parameter, and Poisson's ratio, affect the creation of distortion created. These material properties proved to be very important inputs when predicting distortion using the ADINA-T and ADINA welding simulation programs. In fact, the ADINA-T and ADINA programs cannot be run without these inputs. Simply, the distortion in a "weak" welded structure is greater than the distortion in a "strong" welded structure.

The fourth factor is amount of non-uniform heat input from the welding arc. As the amount of heat input increases, the amount of distortion also increases, and vice versa. One way to increase or decrease the amount of heat input is by increasing or decreasing the welding time respectively, if the other welding parameters are fixed. The fact that the duration of the heat input affects distortion, correlates directly to existing data proving that the non-uniform heat input of the welding arc is the primary cause of the distortion. Unfortunately, to create a sound welded joint, the amount of the heat input must be above a certain value.

The last factor considered here is the use of a slit. As shown in Figures 3.27, 3.28, 3.29, 3.35, 3.36, and 3.37, during and after the welding, the distortion of Specimen 3 is very different from the distortion of Specimen 5. Specimen 3 moved upward during welding and then downward after welding. Specimen 5 expanded into the slit during welding and then downward after welding. Specimen 3 was identical to Specimen 5, except that Specimen 3 had no slit and Specimen 5 had a slit. Therefore, it can be concluded that the slit was one reason for the difference in the distortion behavior between Specimen 3 and Specimen 5.

In some cases, a slit also reduces the amount of distortion during and after welding. Compare the distortion behaviors of Specimen 7, which has a slit, with the similar but slit-free stainless steel plate investigated by Goktug [11]. The general shapes of the distortion curves for both specimens are similar. However, the amount of distortion on Specimen 7 is smaller in magnitude than that of Goktug's slit-free stainless steel plate.

There are two methods that can be used to observe the distortion behavior of a welded structure during and after welding. They are experimental and analytical methods. In this study, six high frequency laser sensors produced by KEYENCE Corporation, Japan, were used to measure the distortion

behaviors of the specimens during and after welding. In addition, finite element programs developed by ADINA, Inc. were used to simulate the distortion behaviors of the same specimens. Since the results obtained from the real measurements consistently agree with those obtained from the finite element programs, it can be concluded that the finite element programs, i.e. the ADINA-T and ADINA programs, are reasonably dependable computer programs to simulate the distortion behaviors of the specimens.

Finally, there are several important points that need to be mentioned about the distortion simulation using the finite element programs. First, heat input from GTA welding can be accurately modeled by assuming Gaussian's distribution. Second, physical and mechanical properties of the specimens, including thermal conductivity, specific heat, thermal expansion coefficient, yield stress, Young's modulus, strain hardening parameter, and Poisson's ratio, are temperature dependent. Third, two-dimensional plane-stress models can be used to model the specimens and get the transient distortion behaviors accurately. Also, the behaviors related to the slits in the specimens during and after welding, can be simulated by using the available element birth option in the finite element programs.

Chapter 6

References

1. ADINA R&D, Inc., *ADINA-IN for ADINA-T User's Manual*, Report ARD 92-5, Watertown, Massachusetts, December 1992.

2. ADINA R&D, Inc., *ADINA-IN: User's Manual*, Report ARD 87-4, Watretown, Massachusetts, December 1987.

3. ADINA R&D, Inc, *ADINA-PLOT: User's Manual*, Report ARD 87-7, Watertown, Massachusetts, December 1987.

4. ADINA R&D, Inc., *ADINA Theory and Modeling Guide*, Report ARD 87-8, Watertown, Massachusetts, December 1987.

5. ADINA R&D, Inc., *ADINA Verification Manual-Nonlinear Problems*, Report ARD 87-10, Watertown, Massachusetts, December 1987.

6. Bathe, K. J., *Finite Element Procedures in Engineering Analysis*, Prentice-Hall, Inc., Englewood Cliffs, Nj, 1982.

7. Bathe, K. J, and Khoshgoftaar, M. R., *Finite Element Formulation and Solution of Nonlinear Heat Transfer*, Journal of Nuclear Engineering and Design, 51, pp. 389-401, 1979.

8. Chang, I. H., *Analysis and Control of Root Gap during Butt Welding*, Ph.D. Thesis, MIT, January 1988.

9. Christensen, N., Davies, V., and Gjermundsen, K., *Distribution of Heat Around Finite Moving Sources.* Technical Report CA-91-508-EVC-378, US Army, September 1959.

10. Christensen, N., Davies, V., and Gjermundsen, K., *The Distribution of Temperature in Arc Welding*, British Welding Journal, 12(1), pp. 54-75, 1965.

11. Goktug, G., *Real-Time Non-Contact Measurement and Analysis for the Control of Distortion during Welding*, Ph.D. Thesis, MIT, June 1994.

12. *Laser Displacement Sensors, LB-1000 Series*, Instruction Manual, Keyence Corporation, Osaka, Japan, 1992.

13. Leinhard, J. H., *A Heat Transfer Textbook*, Prentice-Hall, Inc., Englewood Cliffs, New Jersey, 1987.

14. Masubuchi, K., *Analysis of Welded Structures - Residual Stresses, Distortion, and Their Consequences*, Pergamon Press, 1980.

15. Miyachi, H., *Control of Thermal Stresses Acting on Tack Welds during Butt Welding*, Ph.D. Thesis, MIT, February 1989.

16. Park, S. W., *In-Process Control of Distortion during Aluminum Welding*, M.S. Thesis, MIT, August 1988.

17. Rykalin, N. N., *Calculation of Heat Processes in Welding.* Lecture presented before the AWS, April 1961.

18. Rykalin, N. N., and Nikolaev, A., *Welding Arc Heat Flow.* Welding in the world, pp. 112-132, September 1971.

19. Vitooraporn, C., *Experimental and Analytical Study on reduction of Residual Stresses and Distortion during Welding in High Strength Steel.* Ph.D. Thesis, MIT, 1986.

20. Wilson, E. L., Bathe, K. J., and Peterson, F. E., *Finite Element Analysis of Linear and Non-Linear Heat Transfer*, Journal of Nuclear Engineering and Design, 29, pp. 110-124, 1974.